Electrocatalysis of Degradation Products of V-type Nerve Agents at Single-Walled Carbon Nanotube Basal Plane Pyrolytic Graphite Modified Electrodes

by

Jeseelan Pillay

Submitted in fulfilment of the requirements for the degree of

Master of Science

In the Faculty of Natural and Agricultural Sciences,
University of Pretoria

June 2007

Supervisor: Dr. K. I. Ozoemena

DECLARATION

I declare that the dissertation, which I hereby submit for the degree Magister Scientiae in the Faculty of Natural and Agricultural Sciences at the University of Pretoria, is my own work and has not previously been submitted by me for a degree at this or any other tertiary institution.

_____

JESEELAN PILLAY

s26518504

DEDICATION

To my dad, Mr. Perumal Pillay for his unconditional love, encouragement,

support and being a pillar of strength in any decision I have made in life.

ACKNOWLEDGEMENTS

I will remain eternally grateful to my inspirational supervisor Dr. K. I. Ozoemena for his uncompromising guidance and I would like to express my sincere gratitude to him for making it possible for me to continue my studies at a Master of Science level. It has been a privilege to work alongside one of the leading academics in South Africa who has greatly sparked my enthusiasm to continue research in the field of electrochemistry.

I would like to thank my girlfriend, Nitasha, for her support during my transition from Grahamstown to Pretoria. I appreciate her thoughtfulness in accepting my decision to relocate in pursuit of my MSc. degree.

I wish to extend my appreciation to Mr. Chris Van der Merwe and Mr. Andre Botha of The Central Laboratory for Microscopy and Microanalysis at the University of Pretoria as well as Dr. Alistair Douglas of Mintek (AuTEK Nanotechnology Laboratory) for carrying out the TEM and SEM experiments. Thank you, National Research Foundation (NRF) for the financial assistance and the head of the chemistry department at the University of Pretoria, Prof. I. Cukrowski for accepting my application for MSc, and Prof. T. Nyokong for her guidance and for donating the phthalocyanines used in this project. I wish to give a substantial amount of credit to an extremely accommodating technician, Mr. Gerrard Pretorius, the mechanical maestro at the University of Pretoria, for fabricating electrodes to my specifications during my research project. Finally, I wish to acknowledge several colleagues for constructive criticism as well as the concerns raised by referees of the published works from this thesis.

ABSTRACT

Electrocatalysis of degradation products of V-type nerve agents at single-walled carbon nanotube basal plane pyrolytic graphite modified electrodes

by

Jeseelan Pillay

Supervisor: Dr. K. I. Ozoemena

Submitted in fulfilment of the requirements for the degree of Master of Science, Department of Chemistry, University of Pretoria, Pretoria

O-ethyl S-2-diisopropylaminoethyl methylphosphonothiolate (VX) and O-isobutyl-S-2-diethylaminoethyl methylphosphonothioate (R-VX), are considered chemical warfare agents due to their strong acetylcholinesterase-inhibiting properties. Subsequent to terrorist use of these V-type nerve agents in both Japan and the United States of America (the September 11, 2001 attacks) and the limited capability of anti-terrorist groups to detect such weapons, there has been an increased obligation by the Chemical Weapons Convection for specific detection and identification methods for VX and R-VX. Chemical and/or enzymatic hydrolysis yields sulfhydryl mimic products, diethylaminoethanethiol (DEAET) and dimethylaminoethanethiol (DMAET).

This thesis investigates the electrocatalytic parameters of DEAET and DMAET using basal plane pyrolytic graphite electrodes (BPPGEs) modified with: (a) single-wall carbon nanotube (BPPGE-SWCNT); (b) SWCNT functionalised

with cobalt (II) tetra-aminophthalocyanine by **(i)** physical (BPPGE-SWCNT-CoTAPc$_{(mix)}$), **(ii)** chemical (BPPGE-SWCNT-CoTAPc$_{(cov)}$) and **(iii)** electrochemical adsorption (BPPGE-SWCNT-CoTAPc$_{(ads)}$) processes; (c) nickel powder (BPPGE-Ni); (d) BPPGE-Ni decorated with SWCNT (BPPGE-Ni-SWCNT), and (e) SWCNT functionalised with nickel (II) tetra-aminophthalocyanine (BPPGE-SWCNT-*poly*-NiTAPc).

Electrochemical studies (performed by voltammetric and electrochemical impedance spectroscopic techniques) revealed that the SWCNT and SWCNT-CoTAPc$_{(mix)}$ films showed comparable electrocatalytic responses towards the detection of DEAET and DMAET whereas competitive electrochemical behaviour was seen between SWCNT and SWCNT-NiTAPc modified BPPGEs. Using the BPPGE-SWCNT-CoTAPc$_{(mix)}$, the estimated catalytic rate constants (k) and diffusion coefficients (D) were higher for DEAET than for the DMAET. Also, the detection limits of approximately 8.0 and 3.0μM for DMAET and DEAET were obtained with sensitivities of $5.0×10^{-2}$ and $6.0×10^{-2}AM^{-1}$ for DMAET and DEAET, respectively. Unlike BPPGE-SWCNT-CoTAPc$_{(mix)}$ that detected the two sulfhydryls at slightly different potentials, BPPGE-SWCNT did not.

The BPPGE-Ni gave enhanced Faradaic response for the redox probe ($[Fe(CN)_6]^{3-/4-}$) and also displayed enhanced electrocatalytic behaviour towards the detection of DMAET and DEAET with high sensitivity (~$23x10^{-3}$ AM^{-1}) and low detection limits (4.0 – 9.0 μM range). In comparison to other electrodes reported in the literature, BPPGE-Ni exhibits more promising features required for a simple, highly sensitive, fast and less expensive electrode for the detection

of the hydrolysis products of V-type nerve agents in aqueous solution. The efficient response of the BPPGE-Ni is attributed to the high microscopic surface area of the nickel powder. The poor response of the BPPGE-Ni-SWCNT suggests that the nickel impurity in SWCNT did not show any detectable impact on the heterogeneous electron transfer kinetics of SWCNT.

Unlike the nickel powder, SWCNT and CoTAPc-SWCNT, the NiTAPc-SWCNT hybrid did not show significant electrocatalysis towards the detection of the sulfhydryls. It is interesting, however, to observe for the first time that SWCNT induced crystallinity on the electropolymer of NiTAPc, and that such electropolymer exhibit charge-storage /-transfer properties that greatly enhance the electrochemical response of nitric oxide.

TABLE OF CONTENTS

LIST OF ABBREVIATIONS

Ag|AgCl	=	Silver|silver Chloride Reference Electrode
BPPGE	=	Basal Plane Pyrolytic Graphite Electrode
CA	=	Chronoamperometry
CE	=	Counter Electrode
CME	=	Chemically Modified Electrode
CNT	=	Carbon Nanotube
CoTAPc	=	Cobalt (II) Tetraamino-phthalocyanine
CPE	=	Constant Phase Angle Element
CV	=	Cyclic Voltammetry
CVD	=	Chemical Vapour Decomposition
DEAET	=	Diethylaminoethanethiol
DIPAET	=	Diisopropylaminoethanethiol
DMAET	=	Dimethylaminoethanethiol
DMF	=	*N,N*-Dimethylformamide
DOPAC	=	3,4-Dihydroxy Phenylacetic-Acid
EDX	=	Energy-Dispersive X-Ray
EIS	=	Electrochemical Impedance Spectroscopy
EPPG	=	Edge Plane Pyrolytic Graphite
ESCA	=	Electron Spectroscopy for Chemical Analysis
GCE	=	Glassy Carbon Electrode
HOPG	=	Highly Ordered Pyrolytic Graphite

IR	=	Infra-Red
IUPAC	=	International Union of Pure and Applied Chemistry
KCl	=	Potassium Chloride
LoD	=	Limit of Detection
MPc	=	Metallophthalocyanine
MTAPc	=	Metallotetraamino-phthalocyanine
MWCNT	=	Multi-Walled Carbon Nanotube
NaCl	=	Sodium Chloride
Ni	=	Nickel
NiTAPc	=	Nickel(II) Tetraamino-Phthalocyanine
OPCWAs	=	Organophosphates Based Chemical Warfare Agents
PBS	=	Phosphate Buffer Solutions
Pc	=	Phthalocyanine
R_{ct}	=	Charge Transfer Resistance
RE	=	Reference Electrode
R_s	=	Solution Resistance
R-VX	=	O-isobutyl-S-(2-diethylaminoethyl) Methylphosphonothioate
SEM	=	Scanning Electron Microscopy
SWCNT	=	Single-Walled Carbon Nanotube
SWV	=	Square Wave Voltammetry

TBABF$_4$	=	Tetrabutylammonium Tetrafluoroborate
TEM	=	Transmission Electron Microscopy
UV-vis	=	Ultraviolet-visible
VX	=	*O*-ethyl-*S*-(2-diisopropylaminoethyl) Methylphosphonothioate
WE	=	Working Electrode
Z_w	=	Warburg Impedance

LIST OF FIGURES

LIST OF SCHEMES

LIST OF TABLES

CHAPTER ONE

INTRODUCTION

1.1 GENERAL OVERVIEW

The ability to measure accurately molecules of environmental, industrial, pharmaceutical, clinical and biomedical importance is crucial to the understanding of the various roles they play in human systems. The use of analytical methods such as chromatography and spectroscopy for the detection and measurement of pollutants are difficult and time-consuming. Electrochemical sensors however, hold an outstanding ability among analytical devices available for environmental applications because of their simplicity and low-cost, hence the need to design and fabricate smart and highly selective electrochemical sensing devices is of immense importance. The success of electrochemical sensing depends on the type of electrode used, the electrocatalysts used to modify the electrode or sensor as well as the construction technique (which determines its stability or shelf life and reliability).

This project describes the electrocatalytic behaviour of single-walled carbon nanotube (SWCNT) – basal plane pyrolytic graphite electrode (BPPGE) modified with tetraamino-phthalocyanine complexes of cobalt (CoTAPc), nickel (NiTAPc) and nickel powder towards the detection of sulfhydryl degradation products of V-type nerve agents, notably diethylaminoethanethiol (DEAET) and dimethylaminoethanethiol (DMAET).

Aim of Thesis:
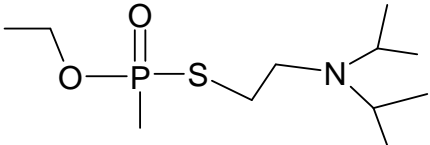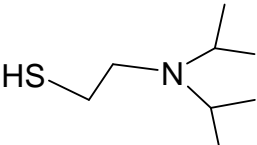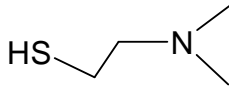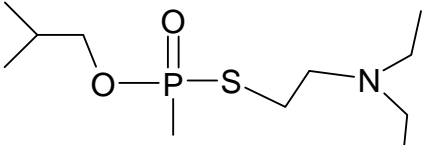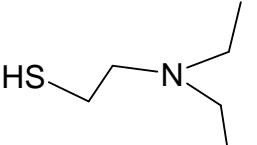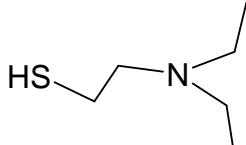
i.   To characterize single-walled carbon nanotube integrated to redox-active CoTAPc and NiTAPc using spectroscopic, microscopic and electrochemical techniques.

ii. To modify basal plane pyrolytic graphite electrode (BPPGE) with (i) SWCNT, (ii) SWCNT-CoTAPc, (iii) SWCNT-NiTAPc and (iv) nickel powder (Ni), and establish their electrochemical properties.

iii. To investigate the electrocatalytic ability of modified electrodes towards the detection of the degradation products of V-type nerve agents, notably DEAET and DMAET.

In this introductory section, a general overview of the degradation products of V-type nerve agents, electrochemical techniques, carbon nanotube (CNT) and metallophthalocyanine (MPc) as catalysts and electrode modifier will be given. In chapter two the procedure adopted for the experiment is provided. Chapter three discusses the results obtained.

1.2   THIOL-CONTAINING HYDROLYSIS PRODUCTS OF V-TYPE NERVE AGENTS

Organophosphates based chemical warfare agents (OPCWAs), especially those of the V-type nerve agents and their sulfhydryl hydrolysis products [1,2] (Table 1.1) are becoming a major global concern.

TABLE 1.1: Molecular structures of "V"-type nerve agents and their corresponding hydrolysis products.

OPCWAs (V-type nerve agents)	Actual hydrolysis product	Hydrolysis product mimics studied in this work
VX	DIPAET	DMAET
R-VX	DEAET	DEAET

The serious threat which they pose to society has resulted in the need for their fast detection in the environment. These nerve agents have been described as the poor man's atomic bomb which is used by terrorists in the development of

chemical weapons. Upon chemical or enzymatic hydrolysis, the V-type nerve agents, VX [*O*-ethyl-*S*-(2-diisopropylaminoethyl)methylphosphonothioate] and its Russian analogue R-VX [*O*-isobutyl-*S*-(2-diethylaminoethyl)methylphosphonothioate] generate sulfhydryl moieties such as the diisopropylaminoethanethiol (DIPAET), DEAET and DMAET [1,2]. These sulfhydryl degradation products are far more stable in the environment than their parent V-type nerve agents, meaning that they can be easily utilized as reliable indicators of the presence of their parent nerve agents.

Electrocatalytic detection of these agents is rarely supported [3, 4]. I am not aware of the use of basal plane pyrolytic graphite modified electrodes for their detection. This lack of literature motivated me to study the electrocatalytic detection of DEAET and DMAET using BPPGE modified with (i) SWCNT, (ii) SWCNT-CoTAPc, (iii) SWCNT-NiTAPc and (iv) nickel powder (Ni) in aqueous solutions.

1.3 ELECTROCHEMISTRY : AN OVERVIEW

Electrochemistry is the study of chemical reactions used to produce electric power or, alternatively, the use of electricity to effect chemical processes or systems [5,6]. Hence, electrochemistry can be defined as the relationship between electricity and chemistry, namely the measurements of electric quantities, such as current, potential, and charge, and their relationship to chemical parameters. The use of electrochemistry for analytical purposes has found a wide range of applications in industrial quality control, biomedical analysis and environmental monitoring [6].

Unlike many chemical measurements, which involve homogenous bulk solutions, the fundamental electrochemical reactions are heterogeneous in nature as they take place at interfaces, usually electrode-solution boundaries. The electrode creates a phase boundary that differentiates otherwise identical solute molecules; those at a distance from the electrode, and those close enough to the surface of the electrode to participate in the electron transfer process [5,6].

The work described in this thesis employed three electroanalytical techniques, Cyclic voltammetry (CV), Square wave voltammetry (SWV) and Chronoamperometry (CA). A closer look at electrode processes and these three techniques follows:

All current-measuring (voltammetric / amperometric) techniques make use of a three-electrode electrochemical cell (Figure 1.1) [7-10].
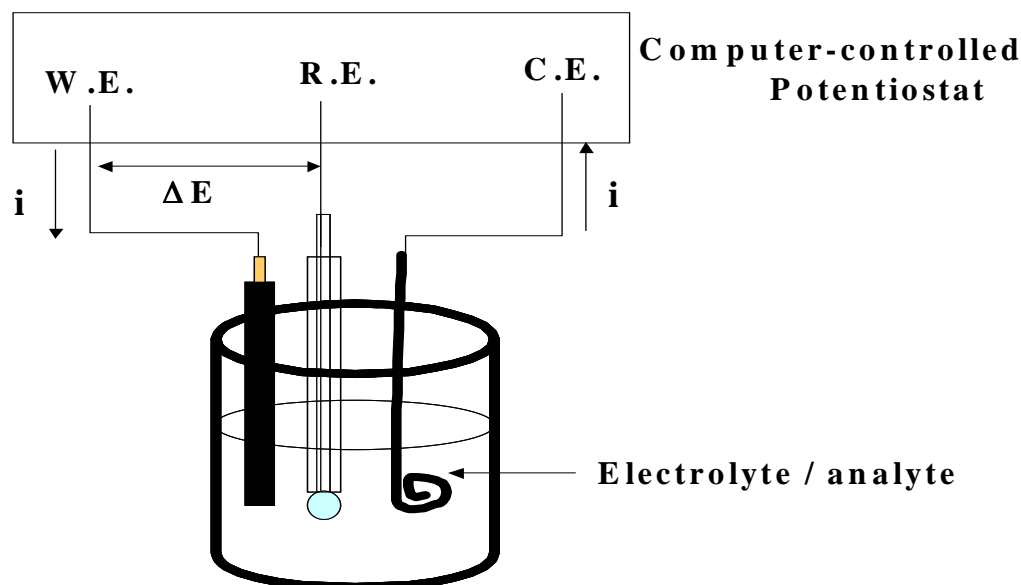
Figure 1.1: A representation of a conventional three-electrode cell.

The working (or indicator) electrode, W.E., is where the electrochemical reaction being studied takes place. A reference electrode, R.E., and a counter electrode C.E., complete the electric circuit. The best reference electrode is one whose potential does not shift from equilibrium (i.e. non polarisable). Therefore, to minimize its polarization, reference electrode with very large surface area is used [5].

There are several reference electrodes employed in electroanalytical experiments, silver|silver chloride (Ag|AgCl) being the most common. It consists of a piece of silver wire anodized with silver chloride in a glass tube. The wire is

in contact with the concentrated potassium chloride (KCl) or sodium chloride (NaCl) solution. A semi-permeable salt-bridge protects the electrode from the bulk of the solution [11]. Counter electrodes are commonly platinum wire, loops, gauze or foil. Working electrodes are commonly carbon and inert materials, particularly platinum or gold.

1.3.1 Mass Transport Processes

The fundamental movement of charged or neutral species in an electrochemical cell to the electrode surface is facilitated by three processes namely: diffusion, migration or convection [5-10].

Diffusion is mass transport resulting from the spontaneous movement of analyte species from regions of high concentrations to lower ones.

Migration refers to movement of charged particles under the influence of an electric field. However the addition of a large excess of easily ionisable salt (supporting electrolyte) eliminates the contribution of migration to mass transport of the target analyte [5].

Finally ***convection*** is a mass transport due to the movement of the solution as a whole which is assisted by means of stirring the solution, solution flow or rotation and/or vibration of the electrode.

1.3.2 Cyclic Voltammetry

Cyclic voltammetry (popularly referred to as CV) depicted in Figure 1.2 is the most extensively used electrochemical technique and is used to study

electrochemical reactions as well as to provide information on the reversibility and kinetics of such reactions [12]. During a cyclic voltammetry experiment, the potential of an electrode is scanned linearly from an initial potential to a final potential and then back to the initial potential. The potential at which the peak current occurs is known as the peak potential (E_p) where the redox species has been depleted at the electrode surface and the current is diffusion limited. The magnitude of the Faradaic current (I_{pa} - anodic peak current) or (I_{pc} - cathodic peak current), gives an indication of the rate at which electrons are being transferred between the redox species and the electrode. Cyclic voltammetric processes could be reversible, quasi-reversible and irreversible.
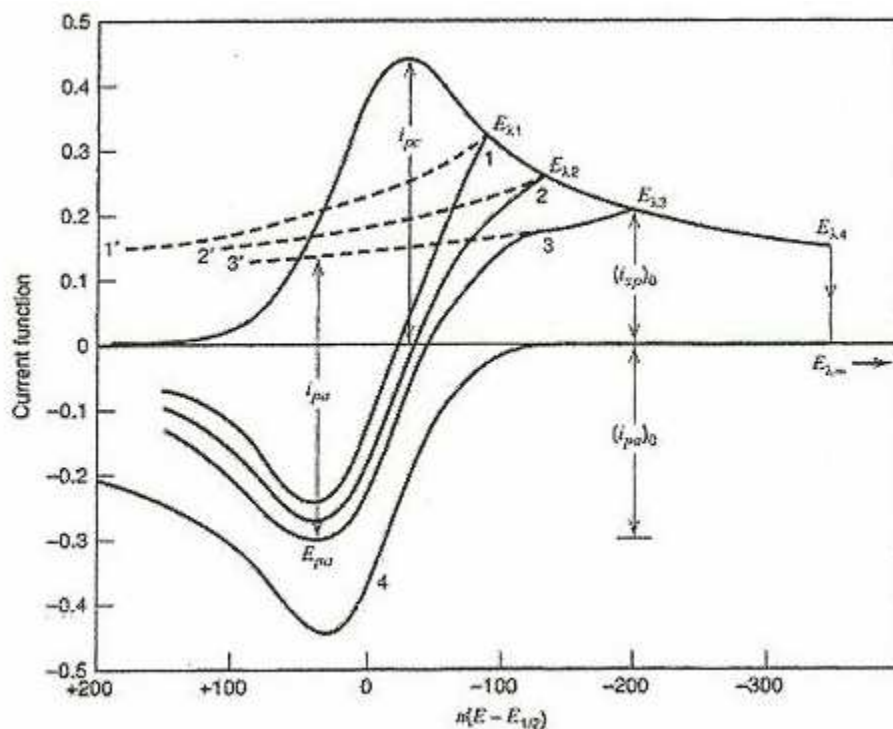
Figure 1.2:   Typical Cyclic Voltammogram for a reversible process [10].

Reversible Process

A reversible process is one in which the electron transfer process is rapid, and the electroactive oxidised (or reduced) species in the forward scan is in equilibrium with the electroactive reduced (oxidised) species in the reverse scan (equation 1.1).

$$\text{Red} \rightleftharpoons \text{Ox} + ne^- \qquad\qquad \textbf{1.1}$$
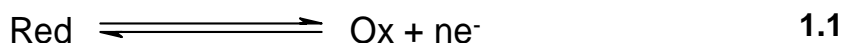
Figure 1.2 shows a typical CV for a reversible process. The electroactive species are stable and so the magnitudes of I_{pc} and I_{pa} are equal and proportional to the concentrations of the active species. $\Delta E(E_{pa} - E_{pc})$ should be independent of the scan rate (ν) but in practice ΔE increases slightly with increasing ν, this is due to the solution resistance (R_S) between the reference and working electrodes [13,14]. Theoretically, the potential difference between the oxidation and reduction peaks is 59 mV for one-electron reversible redox reactions. However, in practice, ΔE is sometimes found in the 60-100 mV range.

Reversibility is a direct and straight forward means of probing the stability of an electroactive species. An unstable species reacts as it is formed and hence produces no current wave in the reverse scan whereas a stable species remains in the vicinity of the electrodes surface and produces a current wave of opposite polarity to the forward scan. Larger differences or asymmetric reduction and oxidation peaks are an indication of irreversible reactions. Irreversibility is a result of slow exchange between the redox species and the working electrode [13].

At 25°C, the peak current is given by the Randles-Sevcik equation [6,10]:

$$i_p = (2.69 \times 10^5) n^{3/2} AC (Dv)^{1/2}$$ **1.2**

where, i_p = peak current (A)

  n = number of electrons transferred

  A = electrode area (cm^2)

  C = concentration (mol cm^{-3})

  D = diffusion coefficient (cm^2 s^{-1})

  v = scan rate (Vs^{-1})

These parameters make CV most suitable for characterization and mechanistic studies of redox reactions at electrodes.

A linear plot of i_p vs. $v^{1/2}$ indicates that the currents are controlled by planar diffusion to the electrode surface [13]. The ratio of anodic to cathodic currents (i_{pa}/i_{pc}) is equal for a totally reversible process and deviation from this is indicative of a chemical reaction involving either one or both of the redox species. The potential where the current is half of its limiting value is known as the half-wave potential ($E_{1/2}$) (also called equilibrium potential, E°′) which is the average of the two peak potentials, represented by equation 1.3.

$$E_{1/2}(or E^{\circ'}) = \frac{E_{pa} + E_{pc}}{2}$$ **1.3**

where E_{pa} and E_{pc} are the anodic and cathodic peak potentials, respectively.

The separation between two peak potentials, ΔE_p for a reversible couple is given by equation 1.4 and can be used to obtain the number of electrons transferred.

$$\Delta E = E_{pa} - E_{pc} = 2.303\frac{RT}{nF} \qquad \textbf{1.4}$$

ΔE_p is independent of the scan rate, and at $25°C$ equation 1.4 can be simplified to equation 1.5:

$$\Delta E_p = 2.303\frac{RT}{nF} = \frac{0.059V}{n} \qquad \textbf{1.5}$$

At appropriate conditions (i.e. at $25°C$, first cycle voltammogram) the standard rate constant (k) for the heterogeneous electron transfer process can be estimated [5,15].

Irreversible Process

For an irreversible process, only forward oxidation (reduction) peak is observed but at times with a weak reverse reduction (oxidation) peak as a result of slow electron exchange or slow chemical reactions at the electrode surface [11]. The peak current, i_p for irreversible process is given by equation 1.6:

$$i_p = (2.99 \times 10^5) n [(1-\alpha)n]^{1/2} Ac(Dv)^{1/2} \qquad \textbf{1.6}$$

where α is the coefficient of electron transfer, the rest of the symbols are defined above in equation 1.2. For a totally irreversible system, ΔE_p is calculated from equation 1.7:

$$\Delta E_p = E^{o'} - \frac{RT}{\alpha nF}\left[0.78 - \ln\frac{k}{D^{1/2}} \ln\left(\frac{\alpha nF}{RT}\right)^{1/2}\right] \qquad \textbf{1.7}$$

where all symbols are defined above. At $25°C$, E_p and $E_{1/2}$ differ by 0.048/αn.

Quasi-Reversible Process

Unlike the reversible process in which the current is purely mass-transport controlled, currents due to quasi-reversible process are controlled by a mixture of mass transport and charge transfer kinetics [6,16]. The process occurs when the relative rate of electron transfer with respect to that of mass transport is insufficient to maintain Nernst equilibrium at the electrode surface. For quasi-reversible process, i_p increases with $v^{1/2}$ but not in a linear relationship and $\Delta E > 0.059/n$ V increases with increasing v [10]. The slight differences in three cyclic voltammetric processes are summarized in Table 1.2.

TABLE 1.2: The diagnostic criteria for reversible, irreversible and quasi-reversible cyclic voltammetric processes [10,11,13-16]

Parameter	Cyclic Voltammetry Process		
	Reversible	*Irreversible*	*Quasi-reversible*
E_p	Independent of ν	Shifts cathodically by 30/αn mV for a 10-fold increase in V	Shifts with ν
$E_{pc} - E_{pa}$	~ 59/n mV at 25°C and independent of ν	_	May approach 60/n mV at low ν but increases as ν increases
$i_p / \nu^{1/2}$	Constant	Constant	Virtually independent of ν
i_{pa} / i_{pc}	Equals 1 and independent of ν	No current on the reverse side	Equals 1 only for $\alpha = 0.5$

1.3.3 Square Wave Voltammetry

Square wave voltammetry (SWV) is a differential technique developed in the early 1950's by Barker and Jenkins [17], which depends on excitation functions where a potential waveform composed of a constant, large amplitude square wave modulation is overlaid on a base staircase potential [18]. During each square wave cycle, the current is sampled twice, at the end of the forward and reverse scans. The difference between the forward (i_f) and reverse current (i_r), are plotted against the average potential of each waveform cycle. In this technique, the peak potential occurs at the $E_{1/2}$ of the redox couple because the current function is symmetrical around the half-wave potential [19]. The scan rate of a square wave voltammetry experiment is given by the equation 1.8:

$$v = f.\Delta E_s \qquad\qquad\qquad\qquad \textbf{1.8}$$

where f is the square wave frequency (Hz) and ΔE_s is the potential step size.

The major advantage of this electrochemical technique includes the use of faster scan rates compared to conventional differential pulse voltammetry, ability to reject capacitive charging currents and excellent sensitivity.

1.3.4 Chronoamperometry

Chronoamperometry (CA) is the simplest most short-lived amperometric method where the current is recorded as a function of time. This uncomplicated potential step wave form (Figure 1.3) monitors the current response following the

electrode potential being stepped from an initial electrode potential at which the oxidized (reduced) species is stable in solution, to the first step potential where a redox reaction occurs forming the reduced (oxidized) species and held at this value for the first step time in a single potential experiment. In a double potential step experiment, the potential is stepped again after the first step time and now changed to the second step potential, and it is then held at this value for the second step time.
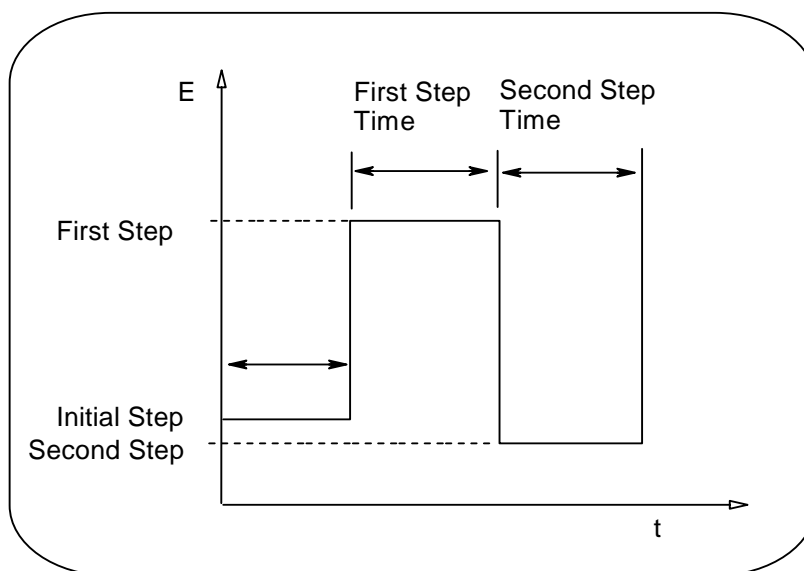
Figure 1.3:   Simple Potential wave form for chronoamperometry

The analysis of chronoamperometry (CA) data is based on the Cottrell equation, 1.9 [20-22]. A plot of i versus $t^{-1/2}$ is often referred to as the Cottrell plot which defines the current-time dependence for linear diffusion control and can be used to calculate the diffusion coefficient (D) resulting from the slope of the plot.

$$i = nFACD^{1/2}\pi^{-1/2}t^{-1/2}$$ **1.9**

where n = number of electrons transferred /molecule

F = Faraday's constant (96 485 C mol^{-1})

A = electrode area (cm^2)

D = diffusion coefficient (cm^{2}s^{-1})

C = concentration (mol cm^{-3})

t = time (s)

At intermediate times of chronoamperometric measurements the catalytic rate constant (k) can be determination using the established equation 1.10 [10,20-22]:

$$\frac{I_{cat}}{I_L} = \pi^{1/2}\left(kC_o t\right)^{1/2}$$ **1.10**

where I_{cat} and I_L are the currents of the electrode in the presence and absence of the analytes, respectively; k and t are the catalytic rate constant (M^{-1}.s^{-1}) and time elapsed (s), respectively; and C_o is the bulk concentration of analytes. The catalytic rate constant can be determined from the slope of the plot of I_{cat}/I_L versus $t^{1/2}$.

1.3.5 Electrocatalysis Using Voltammetry

Electrocatalysis using voltammetric techniques is characterized by current enhancement and/or a potential shift to lower values in the case of CV and SWV. Scheme 1.1 shows the basic mechanisms through which electrocatalytic reactions operate at electrodes modified with a catalyst (such as SWCNT, MPc or Ni as studied in this project).
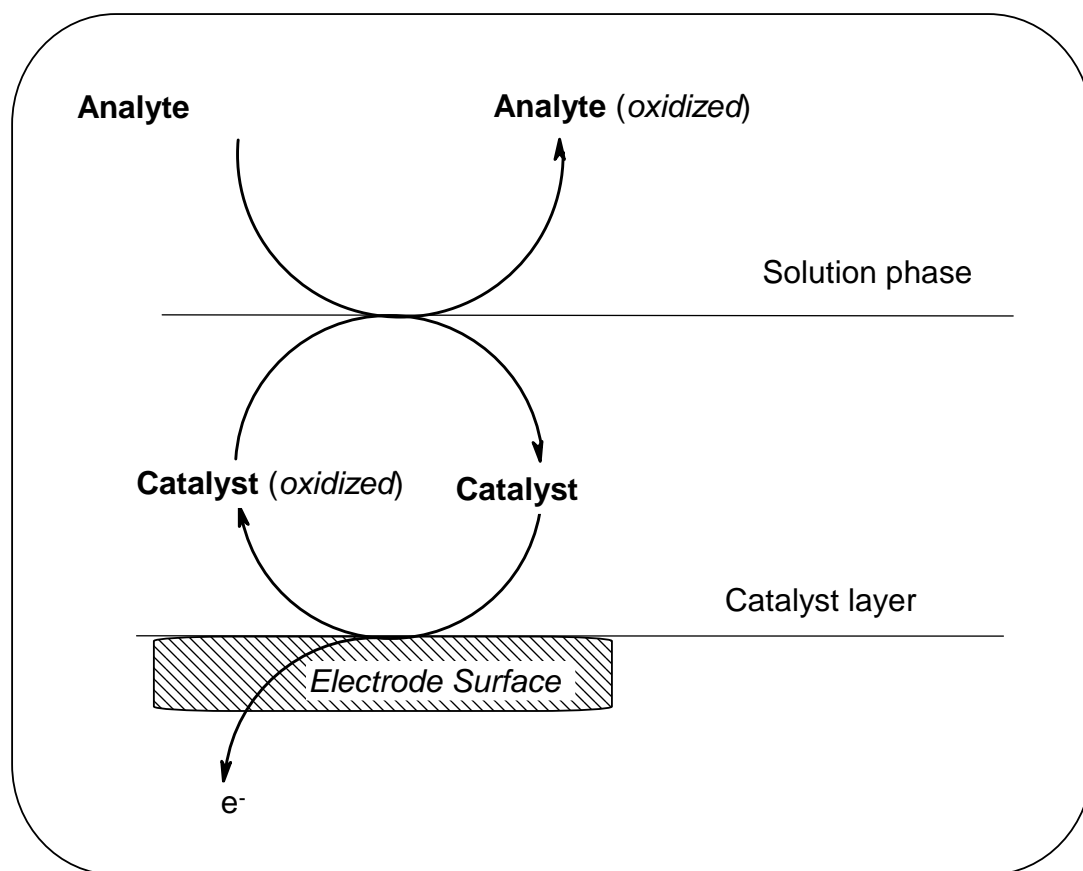
Scheme 1.1: Generalized schematic representation of electrocatalysis at an electrode modified with a catalyst.

The catalyst is first oxidized, which then interacts with the analyte leading to the formation of the oxidized analyte and regeneration of the catalyst [23-28].

Electrocatalysis amplifies the detection signal of an analyte resulting in faster electrode reactions at a lower potential in comparison to the bare (unmodified) electrode. Lowering of detection potentials minimizes interferences from co-existing electroactive species. Chemically modifying the electrodes improves their electrocatalytic current necessary for sensitive detection of target analytes using cyclic voltammetry, square wave voltammetry or chronoamperometry.

1.3.6 Electrochemical Impedance Spectroscopy

Electrochemical Impedance Spectroscopy (EIS) is a powerful method used for investigating electrochemical properties of modified electrodes or systems and their interfaces [29]. EIS measurements can be used to investigate the complex electrochemical behaviour of the modified BPPGEs. EIS serves as an effective technique for interrogating the kinetics at interfaces and to distinguish between the various mechanisms that govern charge transfer [3, 29,-31].

Impedance (or complex resistance) is measured by applying a sinusoidal potential $V(t)$, of small amplitude to an electrochemical cell and measuring resultant sinusoidal current $I(t)$, through the cell [29,32-34]. The applied sinusoidal potential and resulting sinusoidal current are represented as a function of time. These measurements are done over a suitable frequency range and the results can be related to the physical and chemical properties of the material [10,29,32-35]. The relationship is shown in equation 1.11:

$$Z = \frac{V(t)}{I(t)} \qquad\qquad \textbf{1.11}$$

where $V(t)$ is the sinusoidal applied voltage at time t, $V(t) = V_o \sin \omega t$ where V_o is the maximum potential amplitude, ω is the radial frequency (in rad.s^{-1}) and can be related to frequency f (Hz) as $\omega = 2\pi f$. At the same frequency as the applied sinusoidal potential the current response $I(t)$ is also sinusoidal but with a shift in phase, $I(t) = I_o \sin(\omega t + \theta)$, where I_o is the maximum current applied and θ represents the phase shift by which the voltage lags the current [10,29,32]. The impedance is a vector quantity with magnitude and direction. The magnitude of impedance is $Z(V/I)$ and the direction is represented by the phase angle, θ illustrated in Figure 1.4. The complex notation of impedance is shown in equation 1.12:

$$Z = Z' + jZ'' = Z_{real} + jZ_{imaginary} \qquad\qquad \textbf{1.12}$$

where Z' and Z'' are the real and imaginary parts of the impedance, respectively and j is a complex number [29].
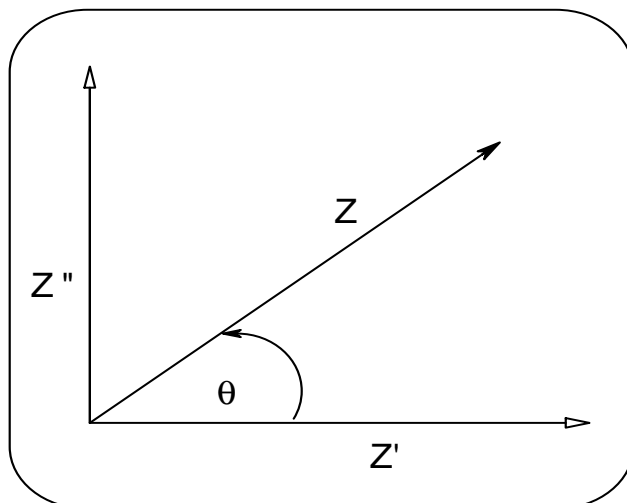
Figure 1.4: Vector representation of real Z' and imaginary Z'' parts of impedance (Z) [29,32].

Data representation of EIS

Electrical equivalent circuits are used for the analysis of the impedance data, and within the circuit, simple electric elements such as resistance (R) and capacitance (C) are connected to model the electrochemical processes [29,32]. The resistance in the equivalent circuit represents the electrical conductivity of the electrolyte and the constant phase element (CPE) caused by the charge which is in excess at the electrode-electrolyte interface. Randles equivalent circuit represented in Figure 1.5 is the most widely used circuit to fit electrochemical data. The Randles equivalent circuit shows the solution or electrolyte resistance, R_S connected in series to the parallel combination of charge transfer resistance, R_{CT} and the CPE. In other systems the reaction rate might be controlled by transport phenomenon and this effect needs to be taken into consideration, the measured impedance can be explained by the component that depends on the conditions of the transport or diffusion of electroactive

species [29,32,35]. This component is called the Warburg impedance (Z_W) and is connected in series to the charge transfer resistance.
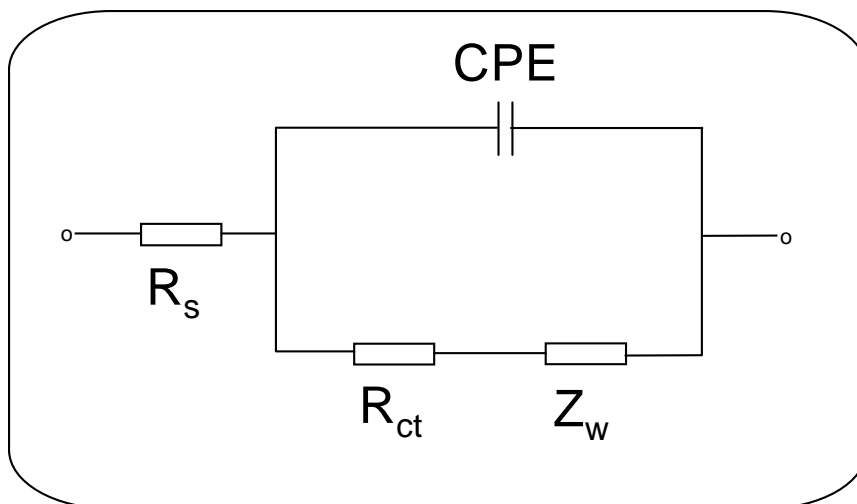
Figure 1.5: Randles circuit representing and electrochemical system.

Impedance data can be graphically represented by either the Nyquist or Bode plot [29,32,35]. A typical Nyquist plot exemplified in Figure 1.6(a) shows the plot of the imaginary part (Z'') versus the real part (Z') of the impedance data. The corresponding Bode plot represented in Figure 1.6(b) gives the frequency information of the measured impedance. Bode data representation is the plot of the phase angle (θ) and the logarithm of impedance magnitude ($\log Z$) versus the logarithm of the frequency ($\log f$).
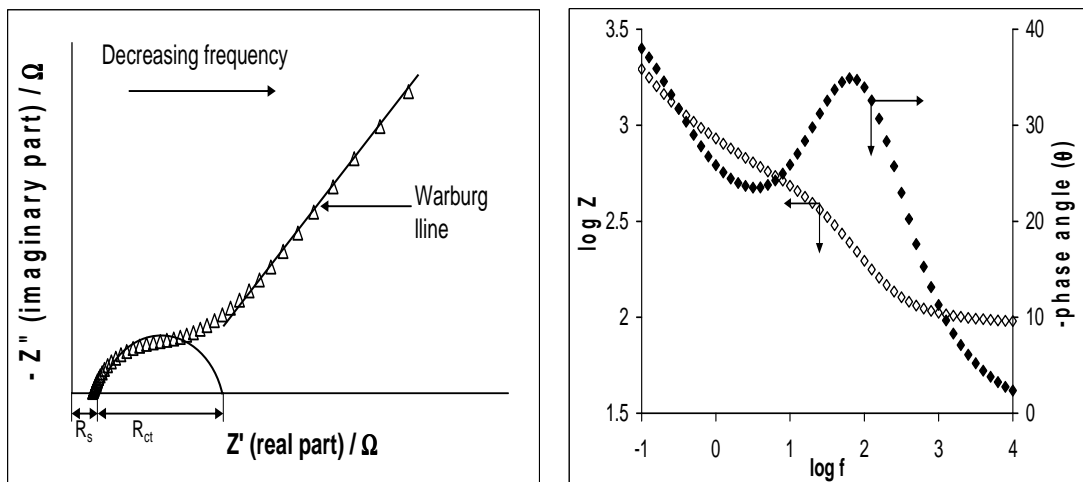
(a)   (b)

Figure 1.6:   Nyquist (a) and the corresponding Bode plot (b) for the Randles equivalent circuit.

Electrochemical impedance spectroscopy offers many advantages over other techniques, these include: (i) the use of low amplitude-sinusoidal voltage (~5mV) which makes the system remain at equilibrium, (ii) rapid acquisition of data such as ohmic resistance, capacitance, film conductivity, as well as charge or electron transfer at the electrode-film interface, (iii) accurate, repeatable measurements can be acquired, (iv) high adaptability of this technique to different applications and (v) the characterizing of interfacial properties in the absence of a redox reaction.

The following section briefly describes the various methods reported in literature for the fabrication of electrochemically modified basal plane graphite electrodes.

1.4 MODIFIED ELECTRODES

According to International Union of Pure and Applied Chemistry (IUPAC) [36], a chemically modified electrode (CME) can be defined as "an electrode made of a conducting or semi-conducting material that is coated with a film of a chemical modifier and that by means of Faradaic (charge transfer) reactions or interfacial potential differences (no net charge transfer) exhibits chemical, electrochemical, and/or optical properties of a film." In other words, the attachment of specific molecule to the surface of an electrode imparts on the electrode some chemical, electrochemical or desirable properties not available at the unmodified electrode [37-39].

1.4.1 General Methods of Electrode Modification

Electrode surfaces are modified using the following methods:

Chemisorption

In this method, the chemical film is strongly and ideally irreversibly adsorbed (chemisorbed) onto the electrode surface [39-41]. Electrode modification using self assembled monolayer falls into this category.

Covalent Bonding

This method employs a linking agent (e.g. an organosilane) to covalently attach one of several monomolecular layers of the chemical modifier to the electrode surface [42, 43].

Composite

The composite electrode is prepared by a simple impregnation of the bulk electrode material with a chemical modifier such as an MPc catalyst. A good example is the popular carbon paste electrode. [44].

Dip-dry Coating

The electrode is immersed in a solution of the polymer, modifier or catalyst for a period sufficient for spontaneous film formation to occur by adsorption. Thereafter the electrode is withdrawn from solution and the solvent is allowed to dry off [45].

Drop-dry Coating

A few drops of the polymer, modifier or catalyst solution are applied onto the electrode surface and left to stand to allow the solvent to dry out [46].

Spin-Coating

This method involves evaporating a drop of polymer, modifier or catalyst solution from an electrode surface by high speed rotations using centrifugal force. For example, oxide xerogel film electrodes prepared by spin-coating a viscous gel on an indium tin oxide substrate [47].

__Electrodeposition__

In this method, the electrode surface is immersed in a concentrated solution ($\sim 10^{-3}$ mol/L) of the polymer, modifier or catalyst followed by repetitive voltammetric scans. The first and second scans are similar, subsequent scans decrease with the peak current. For example, electrochemical deposition of poly(*o*-toluidine) on activated carbon fabric [48].

__Electropolymerization__

In this technique the electrode is immersed in a polymer, modifier or catalyst solution and layers of the electropolymerized material builds on the electrode surface. Generally, the peak current increases with each voltammetric scan such that there is a noticeable difference between the first and final scans indicating the presence of the polymerized material. For example, electropolymerization of aniline on polyaniline modified platinum electrodes [49].

1.4.2 Basal Plane Pyrolytic Graphite Electrode

Basal plane pyrolytic graphite electrodes are fabricated from highly ordered pyrolytic graphite (HOPG). The basal plane pyrolytic graphite electrode comprises of parallel graphite layers with an interspacing of 3.35 Å [50] as illustrated in Figure 1.7.
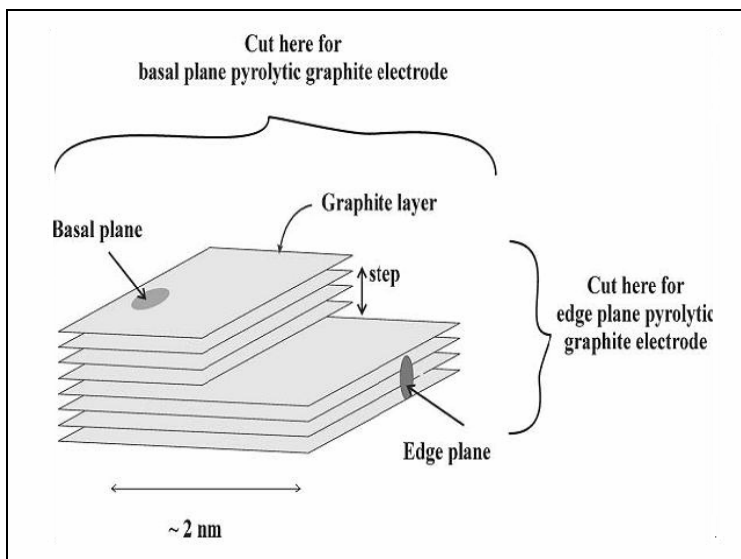
Figure 1.7: Edge plane and Basal plane pyrolytic graphite electrodes fabricated from highly ordered pyrolytic graphite [50].

Electroanalysts are continuously seeking new electrocatalytic surfaces so as to achieve modified electrode surfaces that serve as electrocatalytic platforms. Numerous experiments have been reported using carbon nanotube modified glassy carbon electrodes [51,52]. However, carbon nanotube modified basal plane pyrolytic graphite electrode has been reported to be superior due to the two distinct possible reactive sites of the CNT. These sites are the edge plane like defects found at the open ended tube and the basal plane like sites found on the side walls of the CNT [50, 53]. As a result of the nature of the chemical bonding in graphite, it is reported that basal plane exhibits kinetics which shows irreversible voltammetric behaviour [54].

1.4.3 Carbon Nanotube Modified Electrodes

Historical Perspective

In 1991, a Japanese electron microscopist, Sumio Iijima reported [55] the discovery of a new type of finite carbon structure, consisting of needle-like tubes known as carbon nanotubes (CNTs), whilst investigating material deposited on the cathode during the arc-evaporation synthesis of fullerenes. The carbon nanotubes are fullerene related structures which consist of graphite cylinders closed at either end. Further investigation using transmission electron microscopy revealed that each needle comprised of coaxial tubes of graphite sheets. Iijima also noted from high resolution micrographs, the appearance of the same number of lattice fringes from both sides of a needle concluding that it had a seamless and tubular structure. It was no more than two years after the primary discovery of multi-walled carbon nanotube (MWCNT) in the soot of the arc-discharge method, that Iijima and Ichihashi [56] discovered single-walled carbon nanotube using metal catalysts in the very same manner (Figure 1.8 (a)). Smalley and co-workers [57] in 1996 reported the synthesis of bundles of aligned SWCNT using laser-ablation techniques (Figure 1.8 (b)) whilst Yacaman *et al*. [58] accounted for the catalytic growth (Figure 1.8 (c)) of CNT by chemical vapour decomposition (CVD). During the manufacturing process of SWCNT small amounts of cobalt, nickel or iron are introduced as catalysts in the production process [59].

(a)

(b)

(c)
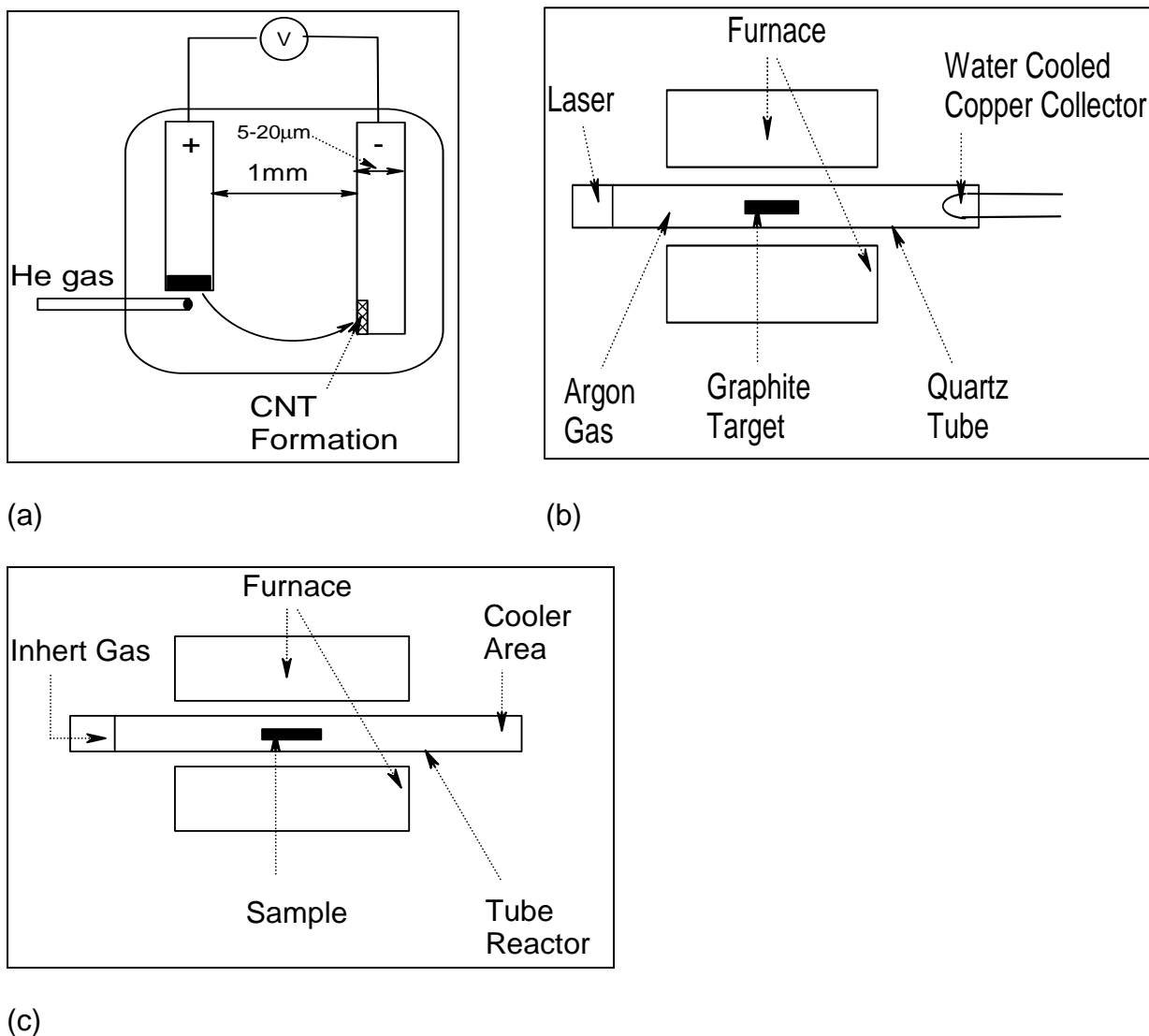
Figure 1.8: Experimental arrangement for synthesizing carbon nanotubes via. (a) Arc-discharge (b) Laser-evaporation (c) Catalytic Growth by decomposition of Hydrocarbon gas [59].

Ebbesen and Ajayan [60] proved that by varying the arc-discharge conditions nanotubes could then be produced in bulk quantities. CNTs are generally assigned into two classes: Single-walled carbon nanotube (an

individual cylinder of 1-2 nm diameter) depicted in Figure 1.9 (a) which is essentially a single graphite sheet rolled into a seamless tube capped at each end by half-spherical fullerene structures [50] and the multi-walled nanotube represented in Figure 1.9 (b) which comprises of numerous concentric tubes fitted one inside the other [61,62]. The number of tubes range from 2-50 graphite cylindrical sheets, with the tubes separated by a distance of 0.34 nm and the innermost tube having a diameter of 2 nm [55].
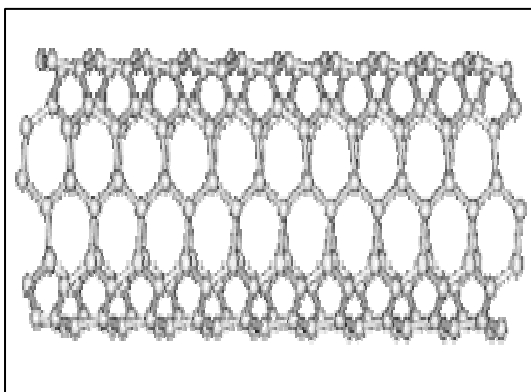
(a)   (b)

Figure 1.9: Illustration of (a) single-walled carbon nanotube and (b) multi-walled carbon nanotube [62].

The central aspect of this report will concentrate on SWCNT which has received immense interest over the last decade and are continued to be investigated as viable electrochemical materials because of their unique properties over the less expensive MWCNT. SWCNT possess certain special features over the MWCNT which include smaller size, larger specific area [63], stronger inter-tube attraction and adsorptive properties. In addition its

characteristic curve-shaped surface enables bonding of supramolecular complexes via non-covalent or hydrophobic interactions [64].

Structure

On each tube, built from sp^2 carbon units, the arrangement of the carbon-atom hexagons are in a helical fashion with respect to the needle axis [55]. The structures of carbon nanotubes shown in Figure 1.10 are determined by the manner in which the graphite sheet are rolled about the T vector represented in Figure 1.11. The graphite sheet rolled about the T vector parallel to C-C bonds of the carbon hexagons leads to the formation of the armchair structure (i), whereas zigzag (ii) and chiral (iii) structures are as a result of the T vector having different orientations except parallel to the C-C bonds [57,59]. This implies that chirality of the tubes is dependent on the direction in which the graphite sheet is rolled in respect to the T vector.

(i)

(ii)

(iii)
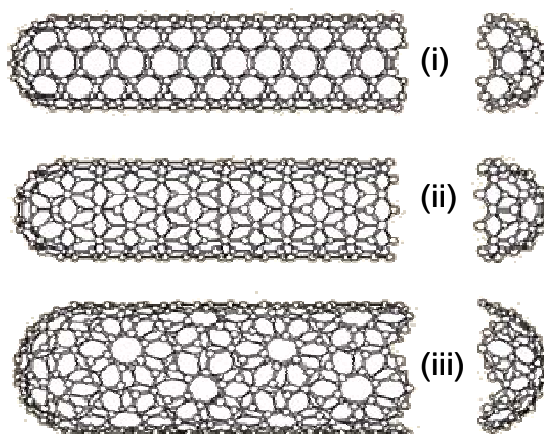
Figure 1.10:   Illustration of (i) armchair (ii), zigzag and (iii) chiral structures of carbon nanotubes [59].
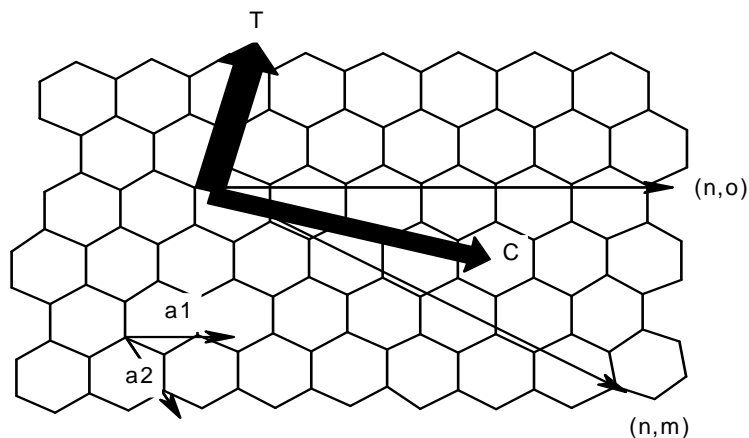
Figure 1.11: Representation of the helical arrangement of an unrolled graphite carbon tube [60].

Properties

The immense interest shown by researchers in carbon nanotubes, can be attributed to its unique properties such as high electrical conductivity, adsorption properties, high surface area, tremendous mechanical strength and good chemical stability so as to produce ideal nanomaterials for the development of nanoelectronic devices [65-67], drug delivery [54,68,69], and are ideal for constructing high-performance electrochemical sensors [70,71]. A few of the above mentioned properties will be considered separately.

Applications

CNTs have been studied for several potential applications [59], owing to their remarkable properties [72]. Oxygen reduction reaction is important for fuel cells and MWCNTs have the ability to electro-catalyze this reaction [73]. Electrochemically, SWCNT intercalated with lithium have shown to be an

excellent materials for potential development of batteries [74]. As a result of SWCNT having extraordinarily high and reversible hydrogen adsorption, it has attracted much consideration in the possibility of being used as high-capacity hydrogen storage media [75]. It is anticipated that CNTs may be used as central elements of electronic devices including field-effect transistors, single-electron transistors and rectifying diodes [76] and for logic circuits [77]. The fabrication of electrochemical sensors will be discussed in more detail.

Electrochemical sensors represent a subclass of chemical sensors in which the electrode used meets the size, cost and power requirements. The capability of CNT based electrodes to function as electrocatalysts permit them to operate as electrochemical sensors [61]. In 1996, Britto and co-workers [78] first reported a high degree of reversibility in the electrochemical oxidation of dopamine upon using carbon nanotube modified glassy carbon electrodes. A few years later [79] they used MWCNT microelectrodes in the study of electrocatalytic reduction of dissolved oxygen. The reported results confirmed that carbon nanotube modified electrodes were more effective as electrochemical sensors in electrochemical reactions than unmodified carbon electrodes. In 1997 Davis *et al.*[80] immobilized cytochrome C and azurin proteins on nanotubes to demonstrate the ability of carbon nanotube modified electrodes to act as biosensing devices. In 1999 Campbell *et al.*[81] used SWCNT attached to sharpened platinum wires to design a novel microelectrode to analyze biological systems. Wang *et al.*[82] recently reported the ability of SWCNT modified electrodes to act as a sensor for the detection of 3,4-dihydroxy phenylacetic acid

(DOPAC). Carbon nanotube modified electrodes have received enormous attention as electrochemical sensors, over the last decade and are continued to be investigated by electroanalysts for further applications.

Attachment of CNTs to metallophthalocyanine (to be discussed in the following section) improves the chemical properties of the CNT-MPc complexes [83,84]. There are strong π–π interactions between highly π-conjunctive and hydrophobic sidewalls (consisting of sp^2 carbons and open ends bearing oxygen-containing moieties) of CNT and the 18 π-electron phthalocyanine organic macrocycle system. Amino-substituted metallophthalocyanine complexes can be covalently linked to CNTs (via amide bond formation [83,84]) while unsubstituted MPc complexes are non-covalently adsorbed onto CNTs (via π–π interactions [85]). It is possible that facile co-ordination of these two remarkable π-electron species may well revolutionize their applications as electrocatalysts and in the fabrication of high-performance electrochemical sensors. Thus, in this project SWCNT and MPc are studied.

1.4.4 Metallophthalocyanine Modified Electrodes

Historical Perspective

Phthalocyanine (Pc) complexes represent a unique group of organic functional materials that have four fused benzo rings [86-94]. The discovery of Pc in the early 1900s was during a large scale preparation of phthalimide from phthalic anhydride at the Grangemouth plant of Scottish Dyes [89,90]. Traditionally, they have been used as dyes and pigments due to their intense blue-green colour.

Structure and Synthesis

The framework of the two-dimensional 18-π electron conjugated Phthalocyanine molecule are 16 carbons and 8 nitrogen atoms in which more than 70 different metals and non-metals can be incorporated [91]. Metallophthalocyanines illustrated in Figure 1.12 (a) are exploited in a wide range of applications as a result of their unique physical and chemical properties [91].

MPc synthesis is aimed at introducing a central metal ion or different substituents at the Pc ring as represented in Figure 1.12 (b), and can be synthesized from phthalic anhydride, phthalonitrile [92], o-cyanobenzamide [93] and synthesis of octasubstituted MPc from substituted phthalonitrile [94]. In this study, cobalt (II) tetra-aminophthalocyanine and nickel (II) tetra-aminophthalocyanine will be examined in further detail.

(a)   (b)
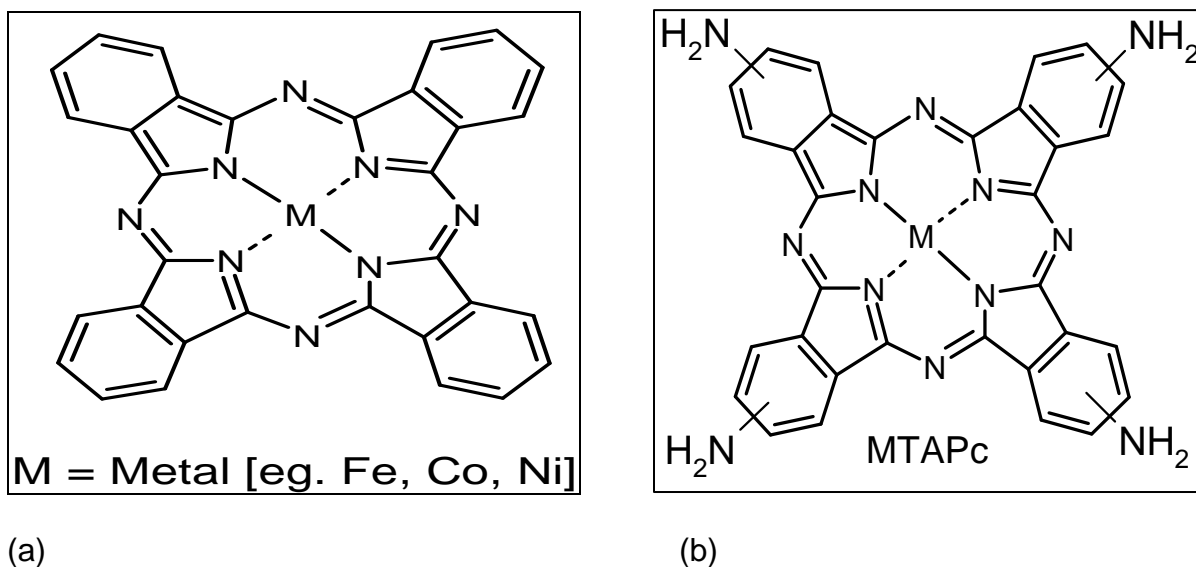
Figure 1.12: The geometric Structure of (a) Metallophthalocyanine and (b) Metallo-tetraaminophthalocyanine (MTAPc) complex, where M = transition metals. For example: Co, Ni or Fe.

Applications

Over the years, transition MPc complexes (notably cobalt phthalocyanines) have continued to establish themselves as excellent electrocatalysts for several organic and inorganic analytes [95-99] and have recently been reviewed by Ozoemena and Nyokong [100]. MPc complexes have the ability to retain their molecular structure and stability upon addition or removal of electrons [101] which enables them to exhibit electrocatalytic activity towards redox reactions especially in the design of electrochemical sensors. So, theoretically speaking, the integration of the electrocatalytic MTAPc complex and the conductive SWCNT will afford the fabrication of a remarkable electrochemical sensor. The adhesion of the CNT onto the frequently used glassy carbon electrode (GCE) is difficult and fraught with problems such as irreproducibility

[54], therefore the use of BPPGE or edge plane pyrolytic graphite electrode (EPPG) should be preferred because of the inherent ability of these electrodes to interact with CNTs via π–π interactions [102]. Although, multi-walled carbon nanotube metallophthalocyanine has recently been studied by Siswana *et al.* [103] for the detection of amitrole, this work presents the first use of SWCNT-MPc modified electrodes towards the detection of degradation products of V-type nerve agents.

1.4.5 Nickel Modified Electrodes

Historical Perspective

Nickel is a silvery white, conductor of heat and electricity [104]. This transitional metal is the 28th element on the periodic table.

Applications

Electrodes modified with nickel particles [105-109] and nickel-CNTs [108] have been reported as viable electrochemical sensors and electrocatalysts. Previous reports established that the electrocatalysis usually observed at multi-walled carbon nanotube based electrodes are due to the presence of metal (iron particles) impurities [110]. Although no such report is available for the single-walled carbon nanotube, to attribute or completely rule out the possible influence of metal impurities in the electrocatalytic behaviour of SWCNT, it is important to establish which metal(s) is/are present in the SWCNT being employed in this project. As will be discussed latter, energy-dispersive X-ray (EDX) proved that

nickel particles impurities are the main impurities in the SWCNT being used for this work. Nickel is used as a catalyst in the production of CNTs and this could be a possible justification for the presence of these impurities [59,111].

1.5 MICROSCOPIC TECHNIQUES

The following microscopic techniques were used in this work to characterize the electrodes and confirm the presence of suspected or unknown structures.

1.5.1 Scanning Electron Microscopy

Scanning Electron Microscopy (SEM) is a technique used to scan the dry surfaces of a material where one is only interested in the surface detail [112]. The operation of the SEM is as follows: At the top of a SEM column an electron gun generates a beam of electrons which are attracted through the anode, condensed (condenser lens) and focused (objective lens) as a fine point onto the sample. These electrons are collected by a secondary detector or a backscatter detector. The secondary electron detector produces a clear and focused topographical image of the sample whereas the backscatter electron detector reflects an elemental composition of the sample and is used for energy dispersive X-ray analysis [112,113].

1.5.2 Energy Dispersive X-Ray

Energy dispersive X-ray sometimes referred to as an electron spectroscopy for chemical analysis (ESCA) is an electron spectroscopic method for the determination of elemental and chemical composition of the materials on metal surfaces [114-117]. The presence of the desired elements in the film can be confirmed using the EDX spectra and evaluation of atomic compositions

[114,115]. EDX is based on the photoelectron effect [114-115] and this effect is illustrated in Figure 1.13, where the surface is irradiated with the photons. Upon measuring the energy lost as a result of secondary electrons being displaced from the primary beam the corresponding element to that energy loss may be determined. This occurs when an X-ray photon, characteristic of its own atom (element) is released when incoming primary electrons bombard target material electrons [117].

(a)   (b)
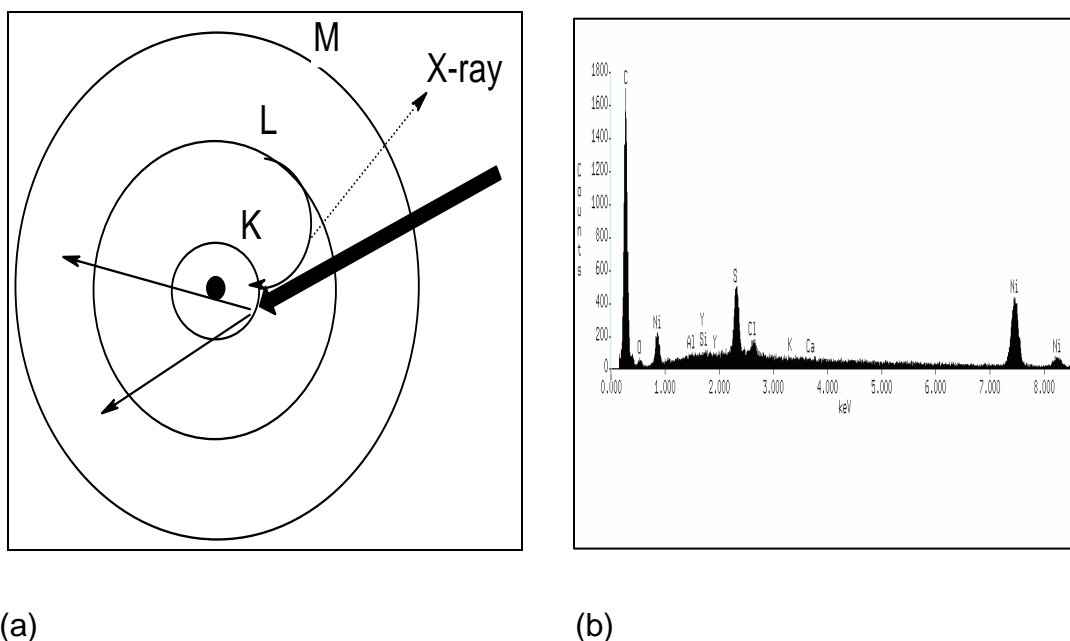
Figure 1.13:   A simple representation of the first three shells showing, (a) the formation of energy dispersive X-ray resulting in (b) a unique spectrum.

An atom has a conventional sequence of electrons known as 'electron shells' arranged around its nuclei as a result of electrical charge differences between them. The shells are, also conventionally, labeled K, L, M, N, O, P, and Q from innermost to outermost. Primary electrons strike the atom (Figure 1,13 (a)), and knock electrons out of their shell. As a result the atom is excited to

higher energy state and relaxes after the 'knocked out' electrons are replaced with outer shell electrons. Therefore, there is a difference in energy states where the excess energy can be released in the form of an X-ray, which carries this energy difference, and has a wavelength that is characteristic of the atomic species from which it came. This same process can occur with the L and M electrons and as a result leads to a large number of generated X-rays of differing wavelengths and hence a number of possible lines of X-rays available for analysis [114-115]. A spectrum (Figure 1.13 (b)) is an accumulation of an index of X-rays collected from a particular spot on the sample surface each X-ray generated from an element are characteristic of that particular element and can thus be used to identify elements that are truly present under the electron probe [114].

1.5.3 Transmission Electron Microscopy

Transmission Electron Microscopy (TEM) is a technique operated at a high resolution where the electron is transmitted through the sample owing to the interest in internal detail thus revealing the morphology (size, shape and arrangement of the particles), the crystallographic information (the atom arrangement) and the compositional information (the elemental composition) of the material examined [118-119]. The operation of a TEM is similar to that of a slide projector; however, it shines a beam of electrons, instead of light, generated from an electron gun. This stream of electrons is focused by a coherent beam that is restricted by a condenser aperture. The beam striking the sample

transmits portions of the sample which are focused by the objective lens into an image that is projected onto a screen. There are dark and light areas of the image representing the more densely packed section which allowed fewer electrons to pass through and the less densely packed section which allowed more electrons to pass through, respectively [118-119].

CHAPTER TWO

EXPERIMENTAL

2.1   MATERIALS AND REAGENTS

Single-walled carbon nanotubes were obtained from Aldrich, and converted to short and uncapped nanotubes bearing carboxylic functional group SWCNT-COOH following the established multi-step acid treatment procedures [120], simply referred to in this work as SWCNT. Cobalt phthalocyanine (CoPc) was obtained from Aldrich and used as supplied. Nickel (II) tetra-aminophthalocyanine and cobalt (II) tetra-aminophthalocyanine complexes were donated to our research group by Prof. Nyokong (Rhodes University). Both MTAPc complexes were synthesized and characterized according to established procedures [121]. The SWCNT-COOH and its CoTAPc hybrids obtained by physical attachment (herein referred to as SWCNT-CoTAPc$_{(mix)}$) and covalent bonding (i.e. SWCNT-CoTAPc$_{(cov)}$) were obtained and characterized as described in my BSc (Hons) project [122] and summarized in scheme 2.1.

Briefly, the SWCNT was first purified and cut into short and uncapped nanotubes bearing acidic functions (SWCNT-COOH) according to the multi-step procedures developed by Smalley and co-workers [120]. Following that procedure, SWCNT was first refluxed in 2.6M HNO_3, then underwent ultrasonicaton in a mixture of concentrated H_2SO_4 and HNO_3 (3:1, v/v) and finally heated and stirred in a mixture of concentrated H_2SO_4 and 30% aqueous H_2O_2 (4:1, v/v). IR [(KBr) V_{max} (cm^{-1})]: 3461 (O–H), 2922, 1616 (C=O). The newly formed SWCNT-COOH were converted to acyl chlorides moieties (SWCNT-COCl) by reacting it, at 70°C for 72 h, with excess thionyl chloride (SOCl$_2$) containing a catalytic amount of DMF. SWCNT-COCl (25 mg) was reacted with

0.15 g of CoTAPc in 25 ml of DMF mixed with several drops of pyridine at 100°C for 10 days [120, 122]. Excess CoTAPc was completely removed by washing with dry DMF giving a black solid product (SWCNT-CoTAPc$_{(cov)}$) (~0.4 mg) after centrifugation, thorough cleaning and vacuum-drying. IR [(KBr) V_{max} (cm^{-1})]: 3377 (N–H), 1576 (C=O).

SWCNT

i. 2.6M HNO$_3$, reflux, 48 h
ii. HNO$_3$ / H$_2$SO$_4$, sonication 24 h
iii. H$_2$SO$_4$ / H$_2$O$_2$, 60 min

SWCNT $-\!\!\!<\!\!{}^{O}_{OH}$

CoTAPc, DMF
ultrasonication, 1 h → **SWCNT-CoTAPc$_{(mix)}$**

(Route 1)

SOCl$_2$ / DMF
70 °C, 72 h

SWCNT $-\!\!\!<\!\!{}^{O}_{Cl}$

CoTAPc, DMF   10 days
Pyridine, 100 °C → **SWCNT-CoTAPc$_{(cov)}$**
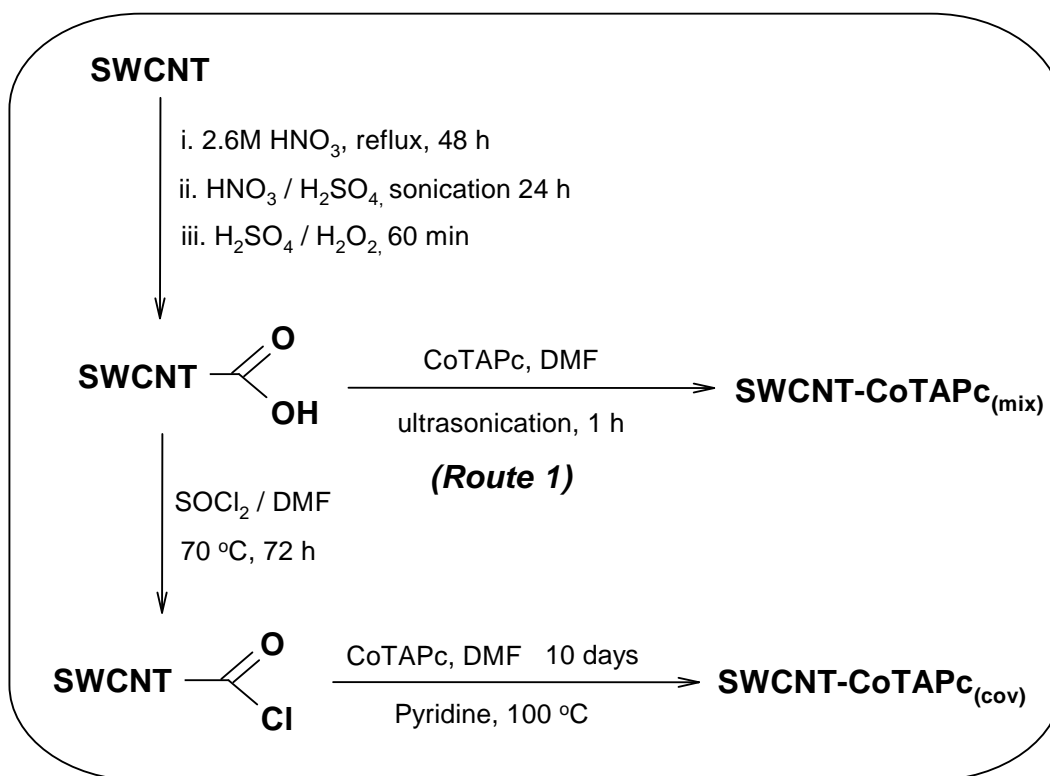
Scheme 2.1: Schematic representation for the synthesis of SWCNT-CoTAPc hybrids

Covalent coordination of the CoTAPc with SWCNT via amide-bond formation were carried out using (a) the established multi-step chemical procedures [84] involving the reaction of SWCNT-COCl and CoTAPc, and (b) a composite form of the SWCNT-CoTAPc system was obtained by simple

ultrasonication of a mixture of CoTAPc and SWCNT-COOH (1:1, w/w) in DMF at 1000 rpm for 1 h. The solution was then decanted, centrifuged, and vacuum-dried. The product is abbreviated as already mentioned as BPPGE-SWCNT-CoTAPc$_{(mix)}$. IR [(KBr) V_{max} (cm^{-1})]: 3420 (O–H, N–H), 1562 (C=O).

Nickel powder was obtained from Riedel-de-Haën and used as supplied. Basal plane pyrolytic graphite plate, (geometrical surface area of the electrode ~0.181cm^2), from which the BPPGE was fabricated was obtained from Le Carbone (Sussex, UK). The Norton carborundum paper (p1200C) used to clean the electrode was purchased from Saint-Gobain Abrasives (Saint-Gobain Abrasives (pty) Ltd., Isando, South Africa). DEAET and DMAET were obtained from Sigma. Tetrabutylammonium tetrafluoroborate (TBABF$_4$), used as an electrolyte, was obtained from Aldrich. Pyridine was obtained from SAARCHEM (South Africa). *N,N*-Dimethylformamide (DMF) was obtained from Sigma–Aldrich. Ultra pure water of resistivity 18.2 MΩ was obtained from a Milli-Q Water System (Millipore Corp., Bedford, MA, USA) and was used throughout for the preparation of solutions. Phosphate buffer solutions (PBS) at various pHs were prepared with appropriate amounts of K$_2$HPO$_4$ and KH$_2$PO$_4$, and the pH adjusted with 0.1 M H$_3$PO$_4$ or NaOH. All electrochemical experiments were performed with nitrogen-saturated phosphate buffer, except for the potassium ferricyanide solutions, which were prepared in 0.05M potassium chloride (all solutions nitrogen saturated as well). All other reagents were of analytical grades and were used as received from the suppliers without further purification.

2.2   EQUIPMENT

All electrochemical experiments were carried out using an Autolab Potentiostat PGSTAT 302 (Eco Chemie, Utrecht, Netherlands) driven by the General Purpose Electrochemical Systems data processing software (GPES, software version 4.9). Electrochemical impedance spectroscopy (EIS) measurements were performed with an Autolab FRA software between 1.0 Hz and 10 kHz using a 5 mV rms sinusoidal modulation with a solution of 1 mM of $K_4Fe(CN)_6$ and 1 mM $K_3Fe(CN)_6$ (1:1) mixture containing 0.1 M KCl, and at the $E_{1/2}$ of the $[Fe(CN)_6]^{3^-/4^-}$ (0.124 V vs. Ag|AgCl). A non-linear least squares (NNLS) method based on the EQUIVCRT programme developed by Boukamp [123] was used for fitting the obtained EIS data. Transmission electron microscopy (TEM) was performed with Multi-purpose TEM (Philips 301). Field emission scanning electron microscopy (FESEM) images were obtained on JSM-6000F (JEOL, Tokyo, Japan) and FESEM images obtained at the AuTEK Nanotechnology laboratory of MinTEK were carried out with FEI Nova NanoSEM 200 (Japan). Energy dispersive X-ray (EDX) images were obtained on JSM 5800 LV, Vantage 6, Analytical Systems with 130eV detector (JEOL, Tokyo, Japan). The diameters of the Ni particles, determined with Mastersizer 2000 ver. 2.00 (Malvern Instruments, UK), are in the 6.25 µm (10%), 17.33 µm (50%), 59.61 µm (90%) range. Bare or modified basal plane pyrolytic graphite (BPPGE) disk (d = 5 mm in Teflon) was used as the working electrode and was fabricated at the Chemistry department workshop of the University of Pretoria from BPPG plate. Electrical contact with the disk was maintained through an inserted copper wire

held in place with conducting silver varnish L 100 (Kemo_ Electronic, Germany). The working electrode was plane BPPGE disk or BPPGE modified with SWCNTs (BPPGE-SWCNT) or BPPGE modified an electrocatalytic modifier. A BAS nickel disk electrode (MF 2016, 3.0 mm Ø) was also used as the working electrode. Ag|AgCl wire and platinum wire were used as pseudo-reference and counter electrodes, respectively. A bench top pH / ISE ORION meter, model 420A, was used for pH measurements. All solutions were de-aerated by bubbling pure nitrogen (Afrox) prior to each electrochemical experiment. All experiments were performed at 25±1°C.

2.3   ELECTRODE MODIFICATION AND PRE-TREATMENT

The BPPGE surface was freshly prepared as reported by Compton's group [124] by gentle polishing on a p1200C Norton carborundum paper, followed by cleaning with the cellotape procedure of removing graphite layers and finally rinsing in acetone to remove any adhesive. The CoTAPc, NiTAPc and nickel powder modified electrodes are discussed below:

CoTAPc Based Electrodes

The CoTAPc- and CoPc- modified BPPGE-SWCNT was obtained by immersing a BPPGE-SWCNT (obtained by drop-dry method) in a solution of 1mM CoTAPc (or CoPc), in dry DMF containing 10 mM tetrabutylammonium tetraflurororoborate (TBABF$_4$) as the supporting electrolyte and repetitively scanned 50 times between -0.4 and 1.2V. The cobalt phthalocyanine modified

electrodes underwent electrosorption at 50 scans and are herein referred to as BPPGE-SWCNT-CoTAPc$_{(ads)}$. CoTAPc exhibits poor solubility in DMF, thus the CoTAPc-DMF solution was left for about 4 days in an air-tight container to allow for the complete dissolution of the CoTAPc. The BPPGE-SWCNT-CoTAPc$_{(ads)}$ was conditioned for electrocatalytic studies by repetitively scanning 20 times between -1.0 V and 1.0 V (vs. Ag|AgCl) in 0.1M phosphate buffer solutions until a stable cyclic votammogram was obtained.

Other modified BPPGEs (SWCNT-COOH, BPPGE-CoTAPc, BPPGE-SWCNT-CoTAPc$_{(cov)}$ and BPPGE-SWCNT-CoTAPc$_{(mix)}$) were obtained by placing a drop of the DMF solution of the required modifier onto the BPPGE surface and drying in an oven at 80℃. The modified electrodes were also conditioned for electrocatalytic studies using the same conditions and parameters used to condition BPPGE-SWCNT-CoTAPc$_{(ads)}$.

NiTAPc Based Electrodes

The NiTAPc- modified BPPGE-SWCNT was obtained by immersing a BPPGE-SWCNT (obtained by drop-dry method) in a solution of *ca.* 5 mM NiTAPc , in dry DMF containing 10 mM tetrabutylammonium tetrafluroroborate (TBABF$_4$) as the supporting electrolyte and scanned between 5 and 40 scans in a potential window of -0.4 to 1.2V. As will be discussed latter, the electropolymer obtained at scan number 7 (represented herein as BPPGE-SWCNT-*poly*-NiTAPc) was used for most of the experiment, unless otherwise stated. The BPPGE-*poly*-NiTAPc was obtained by repetitively scanning between -1.0 V and 1.0 V in 0.1M NaOH

until about the 20th scan a stable cyclic votammogram was obtained. The electropolymer was successfully transformed into the oxo-bridged derivatives, BPPGE-*poly*-Ni(OH)TAPc.

Nickel Powder Based Electrodes

Nickel powder modified BPPGE (BPPGE-Ni) was obtained by gently rubbing a freshly prepared BPPGE on a piece of quality filter paper containing 5 mg of nickel powder. BPPGE and BPPGE-Ni modified with SWCNT (i.e., BPGGE-SWCNT and BPPGE-Ni-SWCNT, respectively) were obtained by placing a 5 μl of a SWCNT-DMF solution (1 mg SWCNT / 1ml DMF solution) on the electrode surface and drying in oven at 80°C. The real surface areas of the electrodes were estimated as described [103] using the $[Fe(CN)_6]^{3-/4-}$ reversible electrochemistry and employing the Randles-Sevcik theory [6,10]. The areas were approximately, 0.192 cm^{-2} for the BPPGE-Ni, 0.194 cm^{-2} for the BPPGE-SWCNT and 0.190 cm^{-2} for the BPPGE-Ni-SWCNT. In the experimental conditions used for the BPPGE and the nickel disk electrode, no detectable reversible electrochemistry for the $[Fe(CN)_6]^{3-/4-}$ was observed, thus, all calculations were based on their geometric surface areas of 0.181 cm^{-2} for the BPPGE and 0.071 cm^{-2} for the nickel disk electrode.

CHAPTER THREE

RESULTS AND DISCUSSION

_____

*The following publications resulted from part of the research work presented in this thesis and they are not referenced further in this thesis:

1. K.I. Ozoemena, **J. Pillay** and T. Nyokong, "Preferential electrosorption of cobalt (II) tetra-aminophthalocyanine at single-wall carbon nanotubes immobilized on a basal plane pyrolytic graphite electrode", _Electrochem. Commun._ 8 (2006) 1391.

2. **J. Pillay** and K.I. Ozoemena, "Electrochemical properties of surface-confined films of single-walled carbon nanotubes functionalised with cobalt (II) tetra-aminophthalocyanine: Electrocatalysis of sulfhydryl degradation products of V-type nerve agents", _Electrochim. Acta_ 52 (2007) 3630.

3. **J. Pillay** and K.I. Ozoemena, "Single-walled carbon nanotube-induced crystallinity on the electropolymeric film of tetra-aminophthalocyaninatonickel (II) complex: Impact on the rate of heterogeneous electron transfer", _Chem. Phys. Lett._ 441 (2007) 72.

4. **J. Pillay** and K.I. Ozoemena, "Efficient electron transport across nickel powder modified basal plane pyrolytic graphite electrode: Sensitive detection of sulfhydryl degradation products of the V-type nerve agents", _Electrochem. Commun._ 2007 in press (doi:10.1016/j.elecom.2007.04.004)

3.1 SWCNT-CoTAPc Hybrid Electrode

3.1.1 Characterization

- ### *Spectroscopic Characterization*

The solubility of CoTAPc and SWCNT-CoTAPc$_{(cov)}$ were investigated. CoTAPc easily forms a precipitate in DMF while the SWCNT-CoTAPc systems, especially the SWCNT-CoTAPc$_{(cov)}$, did not form any detectable precipitate even after 6 months, thus suggesting an enhanced solubility of organic solvents due to the coordination with SWCNT-COOH. Similar results have been reported for MWCNT-MnTAPc [125]. The insolubility of SWCNT was evident from the precipitate formation subsequent to sonication in DMF whereas SWCNT-COOH was highly soluble once sonicated and no precipitate formed. Thus, it was possible to run the UV-visible spectra which are exemplified in Figure 3.1.
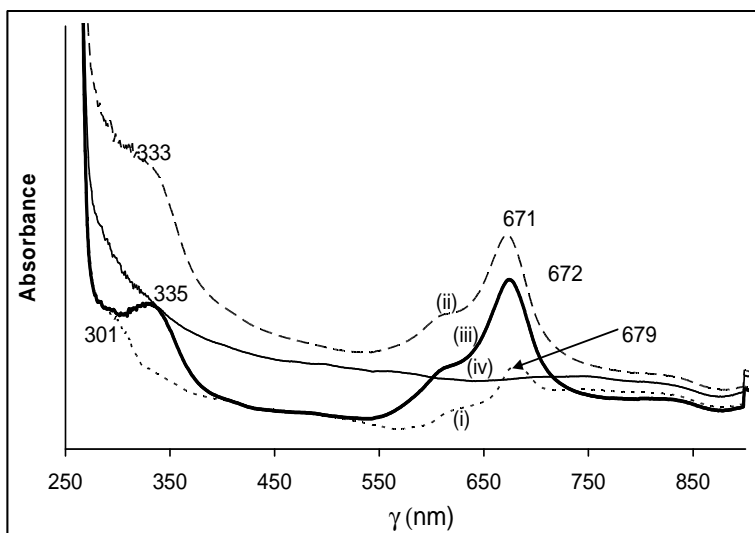
Figure 3.1: Ultra violet – Visible spectra depicting (i) CoTAPc, (ii) SWCNT-CoTAPc$_{(mix)}$, (iii) SWCNT-CoTAPc$_{(cov)}$ and (iv) SWCNT-COOH.

The Q and B bands occur at 679 nm and 301 nm respectively confirming the presence of CoTAPc [126]. The Q and B bands of the SWCNT-CoTAPc$_{(mix)}$ were exactly the same as that of the SWCNT-CoTAPc$_{(cov)}$. The Q and B bands occurred at 671/672 nm and 333/335 nm, respectively. The shifts in the wavelength of the Q and B bands confirm the mutual interaction of the two π-electron systems.

- *Scanning Electron Microscopy*

SEM images show in Figure 3.2 show the SEM images of the pristine SWCNT before (a) and after (b) shortening of the CNTs by harsh acid treatment.

(a) (b)
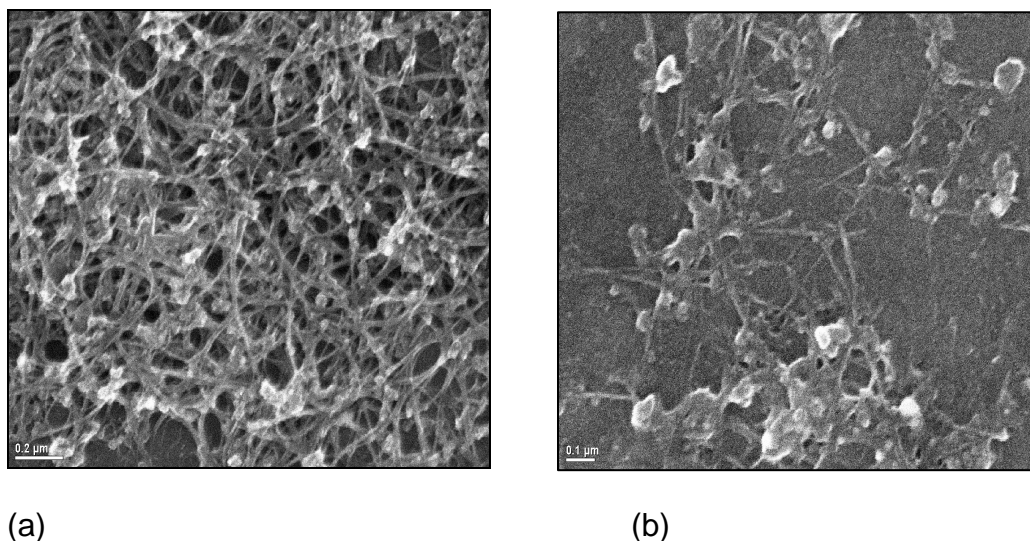
Figure 3.2: SEM images illustrating (a) SWCNT and (b) SWCNT-COOH.

- *Transmission Electron Microscopy*

The TEM images illustrated in Figure 3.3 confirms the conversion of the pristine SWCNT (a) to short nanotubes, bearing the carboxylic function confirmed by IR and EDX, SWCNT-COOH (b) which allows for possible covalent bonding

with phthalocyanine molecules. The dark spots attributed to carbonaceous impurities [127] are dramatically reduced after acid washing. The attachment of the acidified SWCNT to the cobalt (II) tetra-aminophthalocyanine complex (c) forming (d) SWCNT-CoTAPc complex clearly shows the acid-treated SWCNT entangled and protruding from the cobalt phthalocyanine complex, indicative of the strong interactions between these two π-electron species.

- ### *Energy Dispersive X-Ray*

Energy Dispersive X-Ray (EDX) profiles confirms the elemental compositions of the examined complexes. The EDX graphical report is illustrated in Figure 3.4. Certain features are immediately apparent when one compares the EDX of the pristine and acid-treated SWCNTs. First, unlike the pristine (a) SWCNT, the acid-treated (b) SWCNT showed presence of oxygen, confirming the successful introduction of the oxo-functionalities, mostly the –COOH groups onto the SWCNT. Second, the acid-treated SWCNT exhibited insignificant amount of the Ni impurities compared to the pristine SWCNT, confirming that the adopted procedure removed most of the Ni impurities.
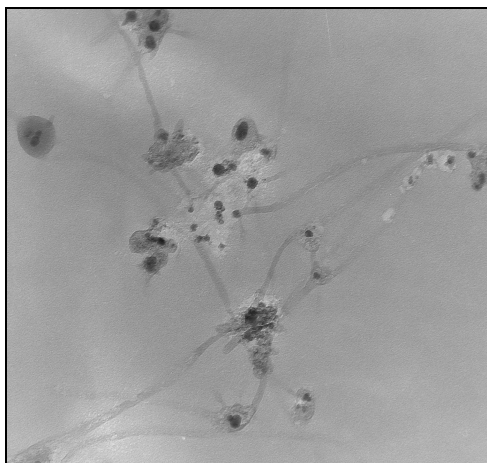
(a)
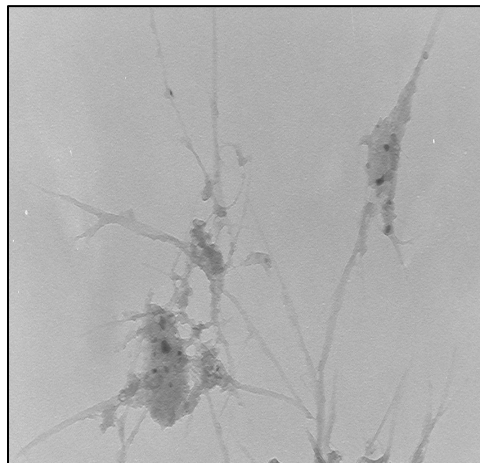
(b)
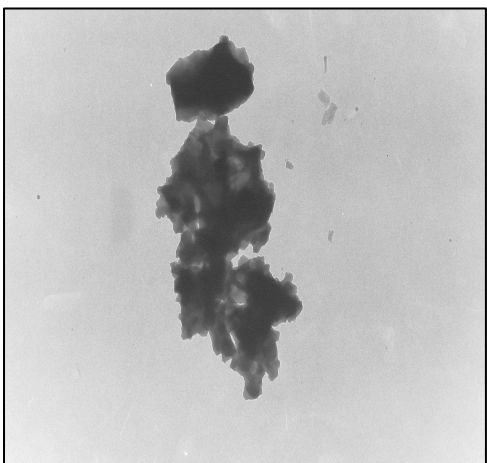
(c)
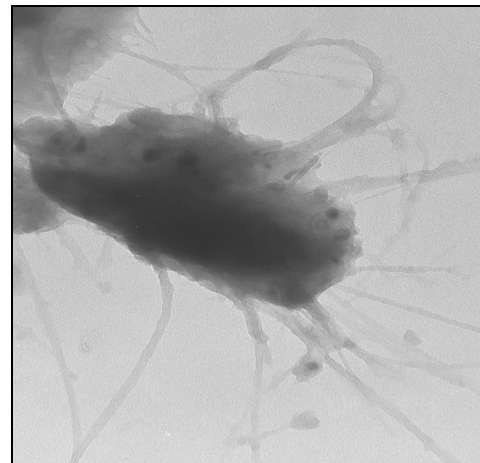
(d)

Figure 3.3: TEM images illustrating (a) SWCNT, (b) SWCNT-COOH, (c) CoTAPc and (d) SWCNT-CoTAPc$_{(mix)}$.

(a)

(b)

(c)

(d)
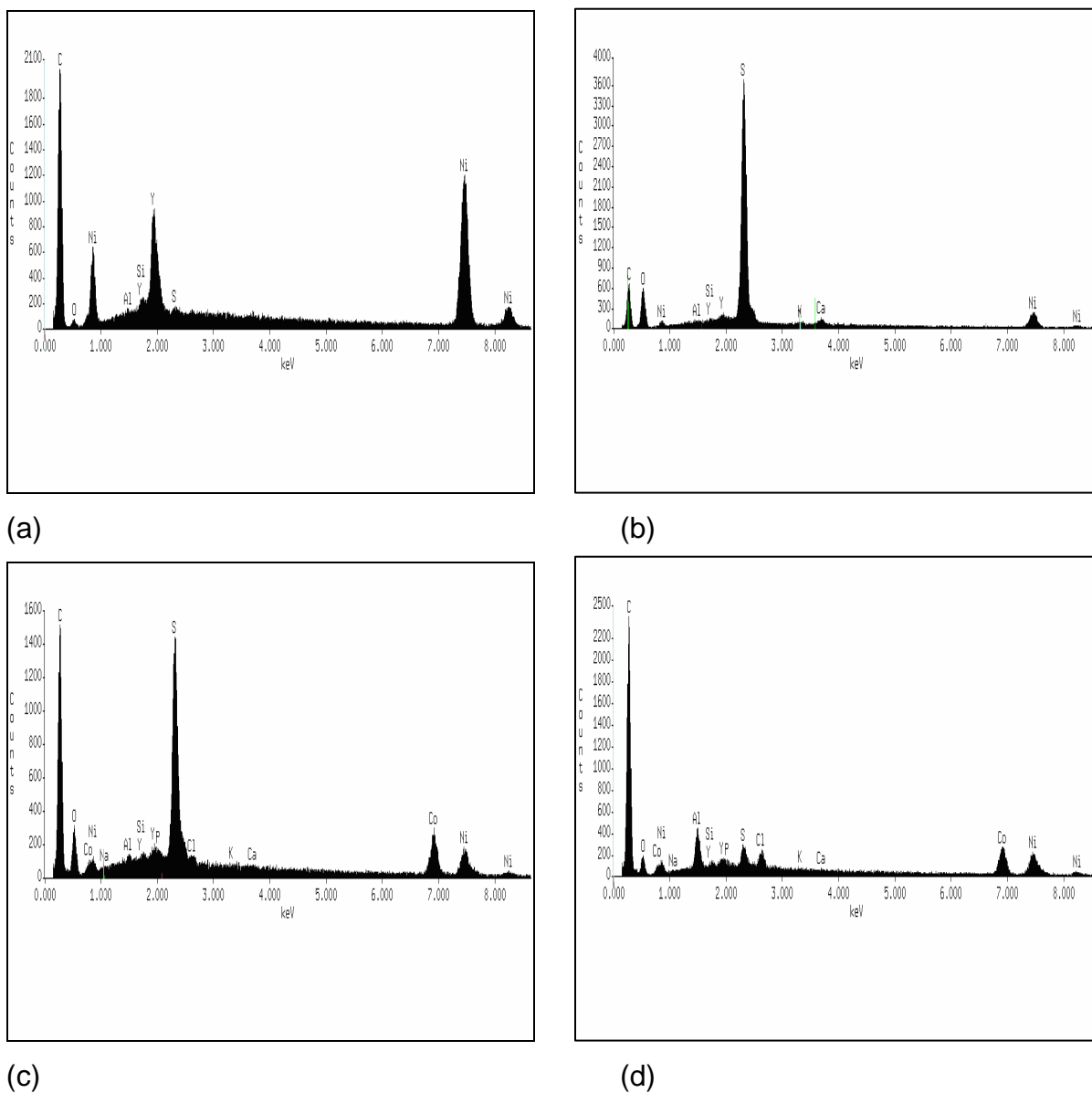
Figure 3.4: EDX profiles of (a) SWCNT, (b) SWCNT-COOH, (c) SWCNT-CoTAPc$_{(mix)}$ and (d) SWCNT-CoTAPc$_{(cov)}$.

The sulphur peak in the acid-treated SWCNT-COOH is the result of sulphuric acid solution used in the cutting and washing of the SWCNT. The representation of the (c) SWCNT-CoTAPc$_{(mix)}$ indicates a high sulphur content as

well as trace amounts of nickel which can be attributed to the presence of the SWCNT. The (d) SWCNT-CoTAPc$_{(cov)}$, however, does not show this elevated sulphur peak which implies that large amounts of sulphur are removed during the chemical synthesis of SWCNT-CoTAPc$_{(cov)}$ hence the protracted chemical synthesis does tend to prove advantageous over the more economical physical attachment of SWCNT and CoTAPc SWCNT-CoTAPc$_{(mix)}$.

A recent study by Compton's group [110] reported that the metal impurities in multi-walled carbon nanotube (MWCNT) are responsible for the catalytic nature of the MWCNT. The high nickel impurity content found in the SWCNT used in this work as well as previous other reports regarding the effect of nickel [105-109] particles on the electrocatalytic behaviour of CNT-based electrodes fuelled my curiosity to determine if these nickel impurities influence the behaviour of the SWCNT towards the electrocatalytic detection of the sulfhydryl degradation products of nerve agents. Thus, NiTAPc and nickel powder based electrodes were investigated as discussed in sections 3.2 and 3.3, respectively.

- ***Square Wave Voltammetric Studies***

SWCNT-CoTAPc$_{(mix)}$ and SWCNT-CoTAPc$_{(cov)}$ were found to be more soluble than CoTAPc in organic solvents, consistent with the previous observation for MnTAPc-MWCNT [125]. Figure 3.5 shows typical square wave voltammograms of solution electrochemistry of both SWCNT-CoTAPc$_{(mix)}$ (a) and CoTAPc (b). Both complexes did not show significant difference in terms of peak

potentials. However, due to the enhanced solubility, SWCNT-CoTAPc$_{(mix)}$ species showed well-resolved voltammograms compared to the CoTAPc. From the publicized electrochemistry of CoPc complexes [128], the redox processes IV (−0.31 V) and V (0.80V for CoTAPc-SWCNT and 0.90V for CoTAPc) are attributed to the central cobalt redox processes Co^{II}/Co^{I} and Co^{III}/Co^{II}, respectively, while other peaks I, II, III and VI are due to phthalocyanine ring processes. The enhancement of the Co^{III}/Co^{II} process is an indication that the SWCNT markedly promotes the electron transfer reaction of the CoTAPc in this solvent system.
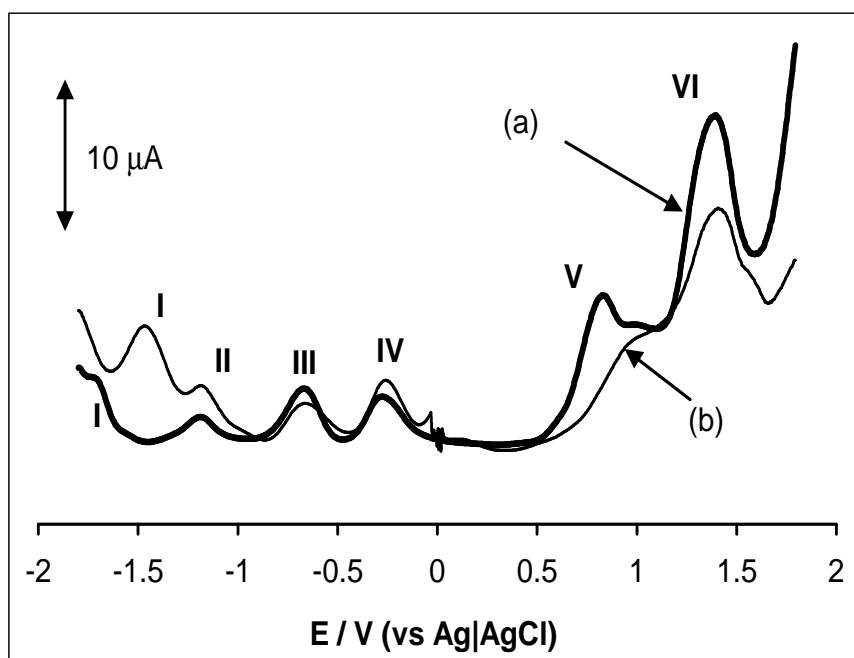
Figure 3.5:   Square wave voltammograms of (a) CoTAPc-SWCNT$_{(mix)}$ and (b) CoTAPc in DMF containing TBABF$_4$.

3.1.2 Modified Basal Plane Pyrolytic Graphite Electrodes

3.1.2.1   Electrosorption Behaviour and Aqueous Pre-treatment

Figure 3.6 represents typical voltammetric responses obtained during the continuous scanning of the DMF solutions of CoTAPc (a) and CoPc (b) containing $TBABF_4$. Figure 3.6 (a) illustrates the continuous decrease of both cathodic and anodic voltammetric waves from the first scan up until the 30th scan where the peaks (**I**) and (**III**) finally disappeared. This behaviour exhibited by CoTAPc is characteristic of an electrosorption process [129,130] and clearly suggest the continuous interaction or attachment of the CoTAPc onto the BPPGE-SWCNT forming the BPPGE-SWCNT-CoTAPc$_{(ads)}$.

(a)   (b)
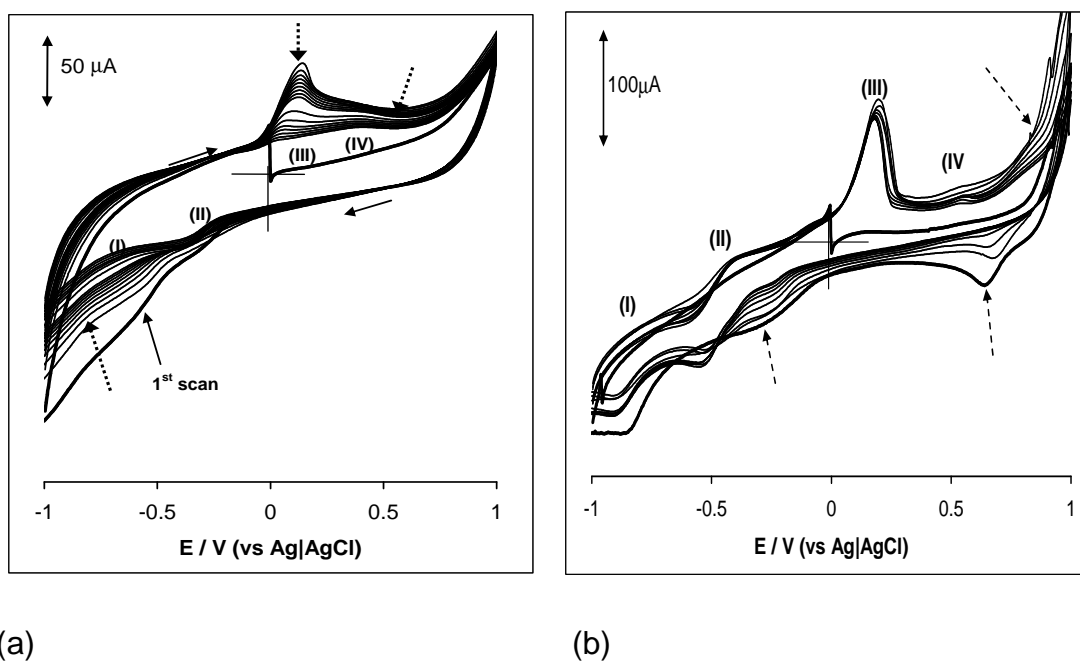
Figure 3.6:   Repetitive cyclic voltammetric profiles at 50 scans (1st and every 5th scan recorded, outer to inner) of (a) 1 mM CoTAPc and (b) 1mM CoPc in DMF containing $TBABF_4$ at a BPPGE-SWCNT. Scan rate = 50 mV/s. Broken arrows indicate the direction of voltammetric responses.

Electropolymerization process occurred (i.e., growth in anodic and cathodic peaks during experiments) only when CoTAPc was still dissolving in DMF. Thus, all electrochemical deposition experiments for CoTAPc were carried out only when the CoTAPc was completely solubilized in the DMF, in which case only electrosorption was observed. The final CV obtained after the completion of the electrosorption process was highly reproducible and electrochemically stable. This observation is interesting in that MTAPc complexes easily undergo electropolymerization onto surfaces of carbon electrodes [131-135] and BPPGE-MWCNT [103]. The preferential electrosorption of CoTAPc may be related to the special features of the SWCNTs over MWCNTs (previously mentioned in the introductory section 1.4.3). In fact, SWCNTs have characteristic curve-shaped surface that facilitates bonding of supramolecular complexes via non-covalent or hydrophobic interactions [63]. Thus, the reproducibility of the electrosorption trend may be the result of highly efficient or intense adsorption of the CoTAPc onto the SWCNT by $\pi-\pi$ interaction between the benzene rings of the phthalocyanine and the sidewalls of the immobilized SWCNT.

CoPc (i.e., without amino substituent as the CoTAPc) was employed in this study to provide some insights as to the possible influence of the $-NH_2$ functionality on the observed electrosorption process. Thus, the ill-resolved and weak electrosorption process for the CoPc in Figure 3.6 (b) suggests that with CoTAPc there might be some additional types of interaction involving the NH_2 functionality of the CoTAPc. The only explanation at this moment as to how such electrochemical process occurs, is possibly the involvement of electrochemical-

induced radical formation, radical–radical coupling, and/or bonding. From literature reports [131-135], peaks (**II**) and (**IV**) are attributable to Co^{II}/Co^{I} and Co^{III}/Co^{II} processes, respectively. Peaks (**I**) and (**III**) are due to the Pc ring processes. The total collapse of the peaks (**I**) and (**III**) during electrosorption is indicative of the involvement of the Pc rings rather than the cobalt centre.

During pre-treatment of the electrosorbed film in aqueous solution (Figure 3.7 (a)), there was a well defined continuous growth of a reversible redox couple (with peaks at +0.22 V and -0.12 V vs. Ag|AgCl) for the BPPGE-SWCNT-CoTAPc$_{(ads)}$, exhibiting peak current ratio (I_{pa}/I_{pc}) of 1:1, with a peak separation (ΔEp) of 0.34 V (vs. Ag|AgCl) and half-wave potential ($E_{1/2}$) of 0.05 V (vs. Ag|AgCl). The two waves were dependent on each other as none occurred without the other. Similar CV evolutions also occurred at a wide potential window with the Co^{III}/Co^{II} peak found at 0.4 V. This rarely observed behaviour could be ascribed to the rearrangement of electrosorbed CoTAPc film on the BPPGE-SWCNT surface. After the 20th scan, the CV remained stable and started to decrease, signifying the end of the rearrangement. Figure 3.7 (a) inset reveals a stable Co^{II}/Co^{I} redox couple (I). Figure 3.7 (b) compares the CVs obtained in PBS pH 4.4 for the bare (i), BPPGE-SWCNT (ii) and the BPPGE-SWCNT-CoTAPc$_{(ads)}$ (iii). As evident, the intrinsic redox processes of the SWCNT [136,137] are not properly resolved at the BPPGE. A similar CV evolution to that of the BPPGE-SWCNT-CoTAPc$_{(ads)}$ in the buffered aqueous solutions were also obtained for the BPPGE-SWCNT-CoTAPc$_{(mix)}$ and BPPGE-SWCNT-CoTAPc$_{(cov)}$ obtained by the drop-dry process. Therefore, it is reasonable to associate the

single redox couple obtained for the BPPGE-SWCNT-CoTAPc$_{(ads)}$, especially the broad cathodic peak, to be the consequence of the overlapped redox processes of the SWCNT, the phthalocyanine ring as well as the irreversible Co^{II}/Co^{I}.

(a)   (b)
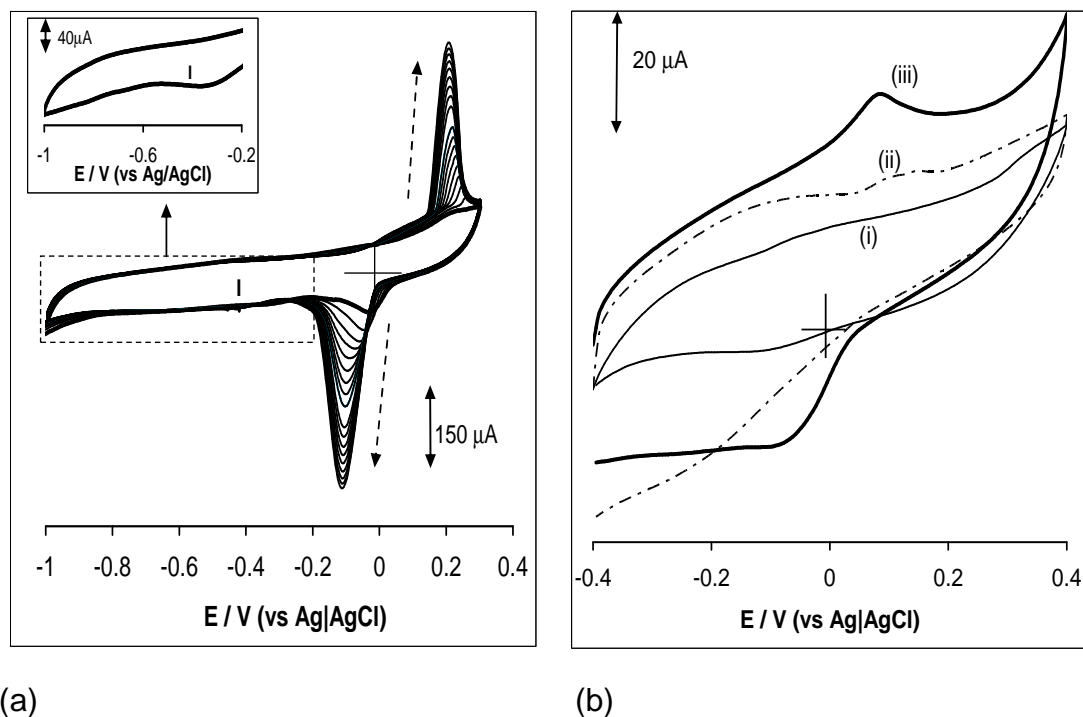
Figure 3.7: (a) Repetitive cyclic voltammetric profiles of a BPPGE-SWCNT-CoTAPc$_{(ads)}$ in PBS (pH 7.0), 1st to 20th scans (inner to outer voltammograms). Inset shows the Co^{II}/Co^{I} couple, and (b) the comparative CVs of: (i) bare BPPGE, (ii) BPPGE-SWCNT and (iii) BPPGE-SWCNT-CoTAPc$_{(ads)}$ in PBS (pH 4.4). Scan rate = 50 mV/s.

3.1.2.2   Surface Coverage

The surface coverage (Γ_{MPc} (mol cm^{-2})) of each of the three CoTAPc-based electrodes was estimated from this well-defined redox couple in pH 4.4 solutions from the background-corrected charge, Q, under the anodic peaks at 50mVs^{-1} using the following relationship of equation 3.1 [6]:

$$\Gamma_{MPc} = \frac{Q}{nFA}$$ **3.1**

where, *n* represents number of electrons transferred (assume≈1), *F* the Faraday constant (96,485 Cmol^{-1}), and *A* is the real surface area of the electrode. The surface coverage was found to be *ca.* 1.0×10^{-9} mol cm^{-2}, a magnitude higher than monolayer coverage, indicating that the obtained film is about a magnitude denser than a monolayer film.

3.1.2.3   pH Studies

The modified Nernst equation may be simplified as represented in equations 3.2 and 3.3 and used to determine the slope of the graph and hence indicate the number of electrons involved in the electron transfer process [138].

$$E = E^{o} + \left(2.303\frac{RT}{nF}\right)pH$$ **3.2**

$$E = E^{o'} + \left(\frac{0.0591}{n}\right)pH$$ **3.3**

where all the symbols are already defined above. The plot of E_p vs. pH illustrated in Figure 3.8 (investigated with BPPGE-SWCNT-CoTAPc using SWV at pH 4–9) resulted in a slightly higher slope (~70 mV/pH) than the theoretical value of ~59 mV/pH (indicating a one-to-one ratio of proton to electron), which might have been influenced by the overlapped redox processes mentioned above.
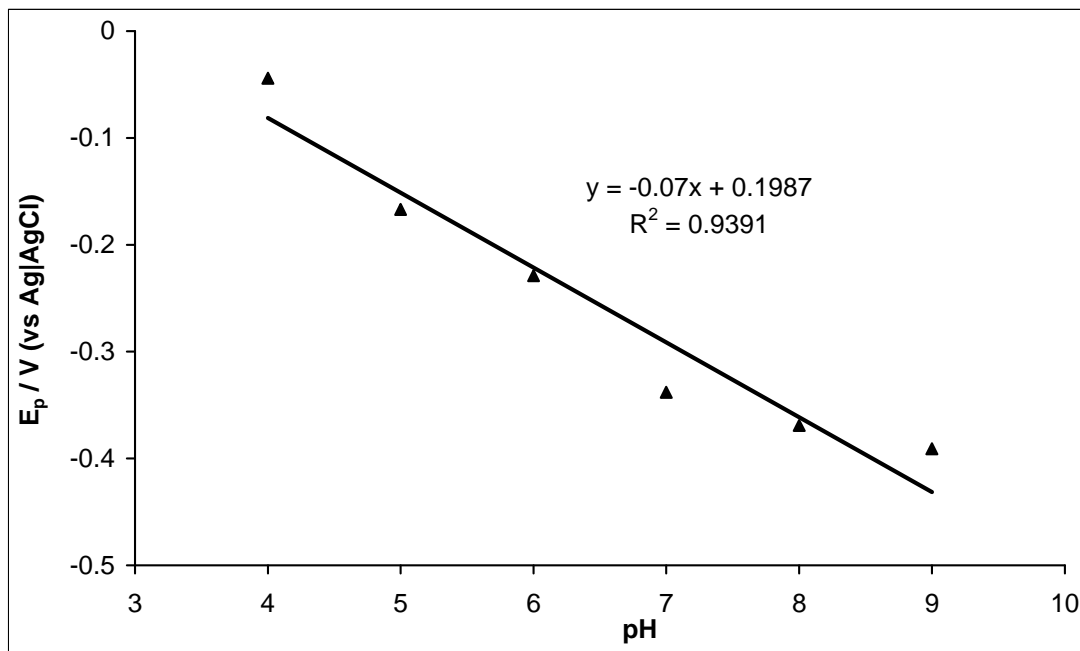
Figure 3.8: Plot of peak potential vs. pH for BPPGE-SWCNT-CoTAPc(mix).

3.1.2.4 Electrochemical Kinetics of the Electrosorbed CoTAPc

Figure 3.9 (a) shows an example of a typical CV evolution at varying rates (25–1500 mV/s) using the pre-treated BPPPGE-SWCNT-CoTAPc(ads). Similar CV trends were observed for the BPPGE-SWCNT-CoTAPc(mix) and BPPGE-SWCNT-CoTAPc(cov).

The redox currents resulted in a linear increase at low scan rates, expected for surface-immobilized redox species. At scan rates >100 mV/s, the cathodic peak became severely distorted, shifting to more negative potentials compared to the positive shifts recorded for the anodic wave at similar scan rates, suggesting irreversibility at high scan rates. Such irreversible electrode reaction follows the Laviron's theory [139, 140]:

$$E_{pa} = E^{\circ\prime} + \frac{RT}{(1-\alpha)nF} \ln \frac{RTk_s}{(1-\alpha)nF} - \frac{RT}{(1-\alpha)nF} \ln \nu \qquad \textbf{3.4}$$

$$E_{pc} = E^{\circ\prime} + \frac{RT}{\alpha nF} \ln \frac{RTk_s}{\alpha nF} - \frac{RT}{\alpha nF} \ln \nu \qquad \textbf{3.5}$$

where $E^{\circ\prime}$ (or $E_{1/2}$) is the formal potential, α is the electron transfer coefficient, k_s the standard rate constant of the surface reaction, and ν is the scan rate. R, T and F have their usual meanings.
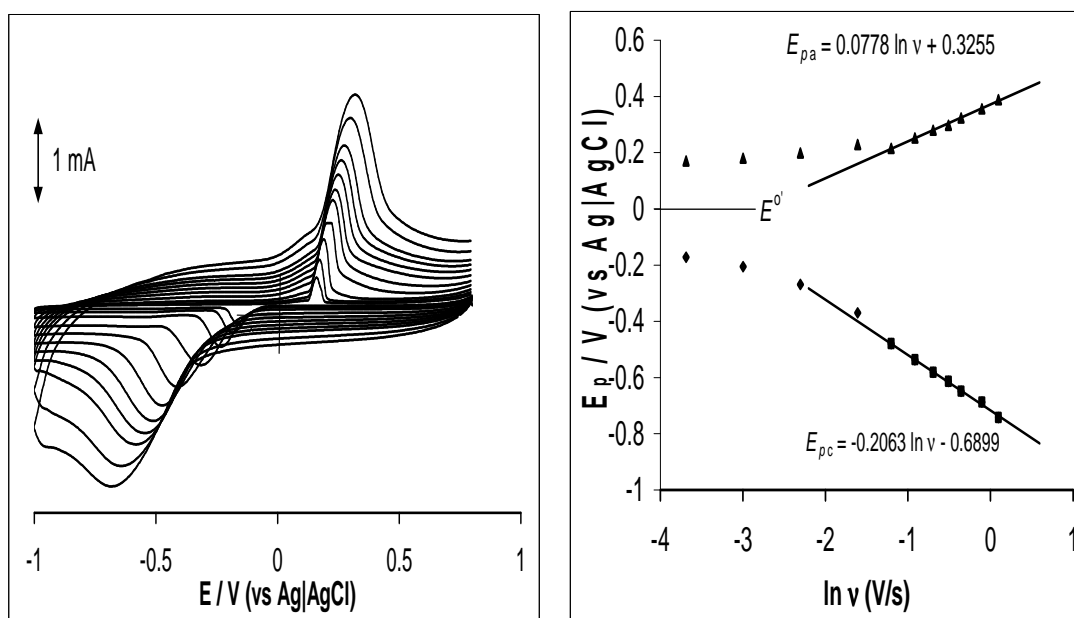
(a)   (b)

Figure 3.9: (a) Effect of varying scan rates (25–1500 mV/s inner to outer) of a BPPGE-SWCNT-CoTAPc$_{(ads)}$ in PBS (pH 4.4) and the corresponding plot (b) of E_p vs. ln ν.

Electrochemical kinetic studies were carried out in pH 4.4 solutions as a result of better electrochemical reversibility at pH 4.4 solution compared to pH ≥

7.4 solutions. At high scan rates, Figure 3.9 (b), the plots of E_p vs. ln ν (and $E° ≈$ 0V vs. Ag|AgCl) were linear. The straight line equations lines are:

- For the BPPPGE-SWCNT-CoTAPc$_{(ads)}$:

  $$E_{pa} = 0.0778 \ln v + 0.3255 \qquad\qquad \textbf{3.6}$$

  $$E_{pc} = -0.2063 \ln v - 0.6899 \qquad\qquad \textbf{3.7}$$

- For the BPPPGE-SWCNT-CoTAPc$_{(mix)}$:

  $$E_{pa} = 0.1312 \ln v + 0.3712 \qquad\qquad \textbf{3.8}$$

  $$E_{pc} = -0.1970 \ln v - 0.7171 \qquad\qquad \textbf{3.9}$$

- For the BPPPGE-SWCNT-CoTAPc$_{(cov)}$:

  $$E_{pa} = 0.0987 \ln v + 0.3497 \qquad\qquad \textbf{3.10}$$

  $$E_{pc} = -0.1883 \ln v - 0.6995 \qquad\qquad \textbf{3.11}$$

According to the respective equations above for, BPPPGE-SWCNT-CoTAPc$_{(ads)}$, BPPGE-SWCNT-CoTAPc$_{(mix)}$ and BPPGE-SWCNT-CoTAPc$_{(cov)}$ the anodic and cathodic parameters are calculated and tabulated below in Table 3.1. From the tabulated values of αn it was possible to estimate that the rate determining step of the reduction process was a single electron transfer reaction (n=1). The values also suggest that the rate-determining steps of the cathodic and anodic reactions are different. The small k_s value for the cathodic reaction is indicative of weak electron transfer process arising from the complications of the overlapped reactions. This behaviour where one redox wave exhibits higher peak current than its reverse wave is typical for CoPc and its complexes [141].

TABLE 3.1: Summary of the kinetic data for the CoTAPc modified BPPGE-SWCNT.

Electrode	Electrochemical Kinetic Parameters			
	Anodic		Cathodic	
	αn	k_s (s^{-1})	$(1-\alpha)n$	k_s (s^{-1})
BBPGE-SWCNT-CoTAPc$_{(ads)}$	0.125	0.169	0.33	832.2
BPPGE-SWCNT-CoTAPc$_{(mix)}$	0.130	0.130	0.20	129.0
BPPGE-SWCNT-CoTAPc$_{(cov)}$	0.140	0.130	0.26	350.0

[a.] *R^2 values for the straight line equation > 0.98*

3.1.2.5 Electrochemical Impedance Spectroscopy

Prior to EIS experiments (used to investigate the complex electrochemical behaviour of the modified BPPGEs [142,143]), CVs of the $[Fe(CN)_6]^{3-/4-}$ redox probe in 0.1M KCl were run using different electrodes. Such CV experiments serve as initial insights into the electron transfer processes at the modified electrodes. Figure 3.10 presents typical modified BPPGEs: (i) BPPGE-SWCNT-CoTAPc$_{(cov)}$, (ii) BPPGE-CoTAPc, (iii) BPPGE-SWCNT-CoTAPc$_{(mix)}$, (iv) BPPGE-SWCNT, (v) bare BPPGE and (vi) BPPGE-SWCNT-CoTAPc$_{(ads)}$.

Unlike the bare BPPGE, the modified BPPGEs gave well-defined redox peaks for the redox probe. The BPPGE modifiers act as redox mediators by enhancing the electronic communication between the BPPGE and the $[Fe(CN)_6]^{4-}/[Fe(CN)_6]^{3-}$ species. The ΔEp were estimated as 105, 105, 102, 128 and 105mV (versus Ag|AgCl) for the BPPGE-CoTAPc, BPPGE-SWCNT, BPPGE-SWCNT-CoTAPc$_{(mix)}$, BPPGE-SWCNT-CoTAPc$_{(cov)}$ and BPPGE-SWCNT-CoTAPc$_{(ads)}$ respectively. This result indicates a relatively faster electron

transfer process at the BPPGE-SWCNT-CoTAPc$_{(mix)}$ compared to other electrodes. The successful attachment of the CoTAPc film onto SWCNT is evident from the Co^{III}/Co^{II} redox couples (Figure 3.10 inset).
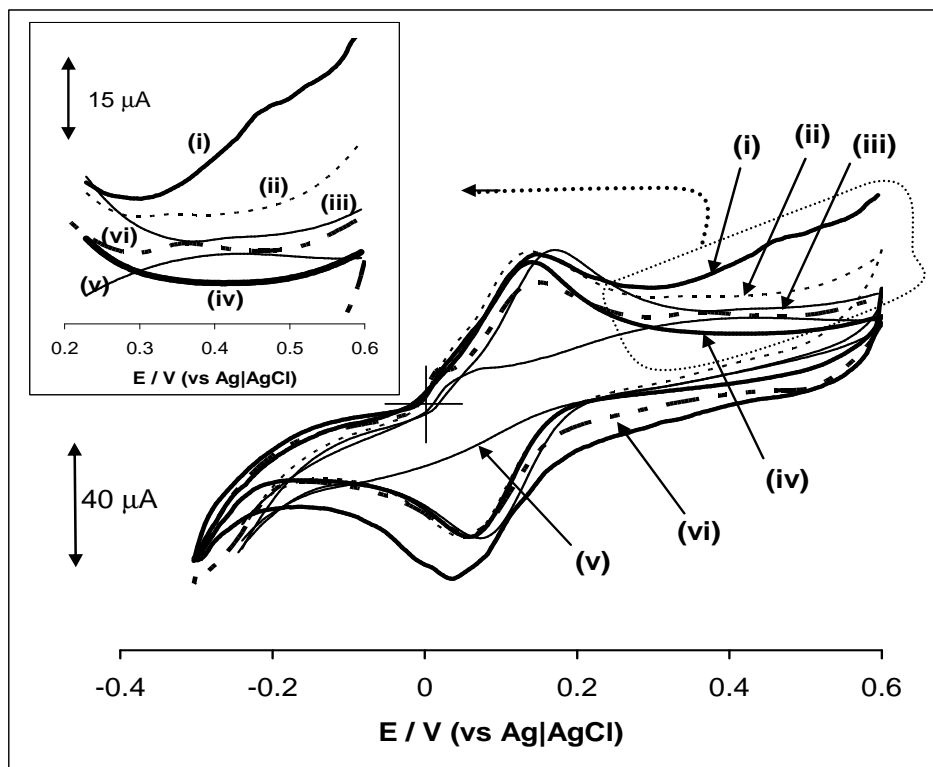
Figure 3.10: CV profiles of [Fe(CN)$_6$]$^{3-/4-}$ resulting from (i) BPPGE-SWCNT-CoTAPc$_{(cov)}$, (ii) BPPGE-CoTAPc, (iii) BPPGE-SWCNT-CoTAPc$_{(mix)}$, (iv) BPPGE-SWCNT, (v) bare BPPGE and (vi) BPPGE-SWCNT-CoTAPc$_{(ads)}$ in 0.1 M KCl containing equimolar mixture of K$_4$Fe(CN)$_6$ and K$_3$Fe(CN)$_6$. Scan rate, 25 mVs^{-1}. Expanded portion (inset) is meant to show the Co^{II}/Co^{III} redox couple of the CoTAPc-based electrodes.

The Ep for Co^{III}/Co^{II} are *ca.* 0.35, 0.43, 0.46, 0.45 and 0.37V (versus Ag|AgCl) for BPPGE-CoTAPc, BPPGE-SWCNT-CoTAPc$_{(mix)}$, BPPGE-SWCNT-CoTAPc$_{(cov)}$ and BPPGE-SWCNT-CoTAPc$_{(ads)}$, respectively. These Co^{III}/Co^{II} couples are irreversible. Irreversibility of the Co^{III}/Co^{II} process is characteristic of

adsorbed CoPc complexes [144]. The higher peak potential values of the SWCNT-CoTAPc electrodes compared to the CoTAPc electrode are consistent with the introduction of electron-withdrawing substituents to the MPc ring. Introduction of electron-withdrawing substituents to the MPc ring leads to a decrease of the average electron density of the total conjugated Pc system which in turn leads to difficult oxidation.

For further insights into the electron transfer at the modified BPPGEs, EIS experiments were carried out in the same conditions as for Figure 3.10 with potential fixed at $E_{1/2} = 0.13$V versus Ag|AgCl, which is the formal potential of $[Fe(CN)_6]^{3-/4-}$ obtained in Figure 3.10. The Nyquist plots (Figure 3.11 (i–vi)) exhibited the characteristic semicircles at high frequencies and a straight line at low frequencies, corresponding to kinetic and diffusion processes, respectively. Thus, the EIS data, were fitted using the Randles simple equivalent circuit of mixed kinetic and diffusion control shown in Figure 1.5.

Due to the inherent roughness of the BPPGE, the CPE [143] was used to explain the EIS data obtained in this work. The impedance of the CPE (Z_{CPE}) is a power-law dependent interfacial capacity given as equation 3.12 [32,35]:

$$Z_{CPE} = [Q(j\omega)^n]^{-1} \qquad\qquad \textbf{3.12}$$

where Q is the frequency-independent constant, ω is the radial frequency, and n is an exponent related to the depression angle. An n value of zero corresponds to a pure resistor; a unit value of n corresponds to a pure capacitor while a 0.5 value corresponds to Warburg impedance.
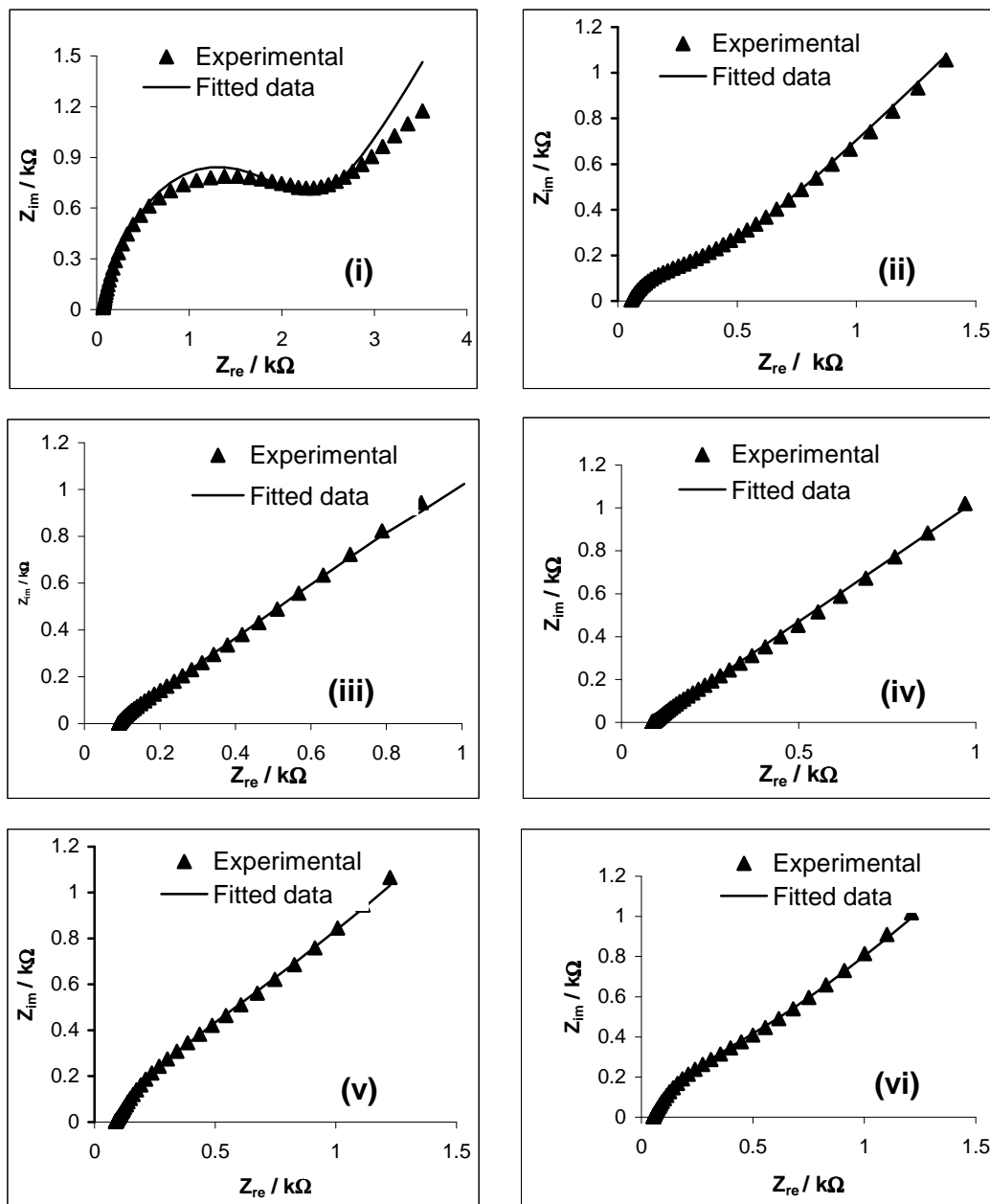
Figure 3.11: Nyquist plots resulting from (i) BPPGE-SWCNT-CoTAPc$_{(cov)}$, (ii) BPPGE-CoTAPc, (iii) BPPGE-SWCNT-CoTAPc$_{(mix)}$, (iv) BPPGE-SWCNT, (v) bare BPPGE and (vi) BPPGE-SWCNT-CoTAPc$_{(ads)}$ in 0.1MKCl containing equimolar mixture of $K_4Fe(CN)_6$ and $K_3Fe(CN)_6$.

As shown by the fitted lines in the Nyquist plots, the simple equivalent circuit model showed good agreement with the experimental results. Table 3.2 summarizes the obtained parameters for the equivalent circuit model.

The Z_w values, which correspond to the diffusion process of the oxidized and reduced species of the $[Fe(CN)_6]^{3-/4-}$ couple, are approximately of the same magnitude for all the electrodes. Ideally, Z_w and R_s should not be affected by the modification of the electrode surface [145]. The increase in R_s (~40%) observed in BPPGE-SWCNT, BPPGE-SWCNT-CoTAPc$_{(cov)}$ and BPPGESWCNT-CoTAPc$_{(mix)}$ is not fully understood at this time but may be related to the resistances induced by these films. An increase in Z_w was observed between the bare electrodes and the modified electrodes. A similar phenomenon was recently observed by Yang and Li [145] which was attributed to the differences between the electron transfer rate within the modifier and the interfacial rate of the electron transfer. The experimental Z_w variation could be as a result of this reason. The relatively higher CPE value for BPPGE-SWCNT-CoTAPc$_{(ads)}$ indicates that this type of electrodeposition offers a more uniform or homogenous film compared to the drop-dry method. The *n* values (<1.0) indicate that the electrodes are not true capacitors.

TABLE 3.2: Summary of estimated EIS parameters obtained for the electrodes (errors ≤0.3%).

Electrodes	R_s / Ω	R_{CT} / $k\Omega$	CPE / μF	Z_w / $\Omega s^{-1/2}$	n	k_{app} / cm s^{-1}
Bare BPPGE	64.30	2.16	0.68	6.35×10^{-4}	0.80	2.42×10^{-5}
BPPGE-CoTAPc	53.80	0.41	1.48	7.95×10^{-4}	0.69	12.90×10^{-5}
BPPGE-SWCNT	90.71	0.27	0.19	6.50×10^{-4}	0.73	19.22×10^{-5}
BPPGE-SWCNT-CoTAPc$_{(mix)}$	89.12	0.22	14.81	7.37×10^{-4}	0.72	23.6×10^{-5}
BPPGE-SWCNT-CoTAPc$_{(cov)}$	88.03	1.12	15.13	7.99×10^{-4}	0.71	4.68×10^{-5}
BPPGE-SWCNT-CoTAPc$_{(ads)}$	53.74	0.61	21.01	8.77×10^{-4}	0.77	8.35×10^{-5}

The apparent electron transfer rate constant k_{app}, was obtained from the following equation 3.13 [146]:

$$k_{app} = \frac{RT}{n^2 F^2 A R_{CT} C} \qquad\qquad \textbf{3.13}$$

where n = 1, which is the number of electron transferred for the redox couple $[Fe(CN)_6]^{3-/4-}$, A is the area of the respective electrodes, C is the concentrations of (mol cm^{-3}) of $[Fe(CN)_6]^{3-}$ and $[Fe(CN)_6]^{4-}$, $R_{CT,}$ R, T and F is defined above.

From Table 3.2, there is a significant decrease in the R_{CT} values for the modified electrodes compared to that of the bare BPPGE which confirm that the charge transfer processes on the modified electrodes for $[Fe(CN)_6]^{3-/4-}$ are easier than in the bare BPPGE. The weak CV response for BPPGE towards $[Fe(CN)_6]^{3-/4-}$ could be associated to its roughness and/or basal nature, thus the consequent high R_{CT} is not surprising. The R_{CT} values for the BPPGE-SWCNT and the BPPGE-SWCNT-CoTAPc$_{(ads)}$ are consistent with step-wise build-up of the layers on the BPPGEs.

From the Bode plots of phase angle versus log f (Figure 3.12), it is seen that the bare BPPGE showed well-defined symmetrical peak with a maximum value of ~54° at 158 Hz corresponding to the relaxation process of the BPPGE/solution interface. On modification of the BPPGE, this relaxation process shifts to different phase angles (*ca.* 34–42° range) and at lower frequencies (1.4–

6.4 Hz range). These shifts indicate that the reactions now occur at the surface of the modifying films rather than the bare BPPGE.

As reflected in their k_{app} and R_{CT} values, BPPGE-SWCNT and BPPGE-SWCNT-CoTAPc$_{(mix)}$ exhibited faster electron transfer processes towards $[Fe(CN)_6]^{3-/4-}$ compared to other electrodes investigated in this work. Thus, all subsequent studies, unless otherwise stated, were carried out with these two electrodes.
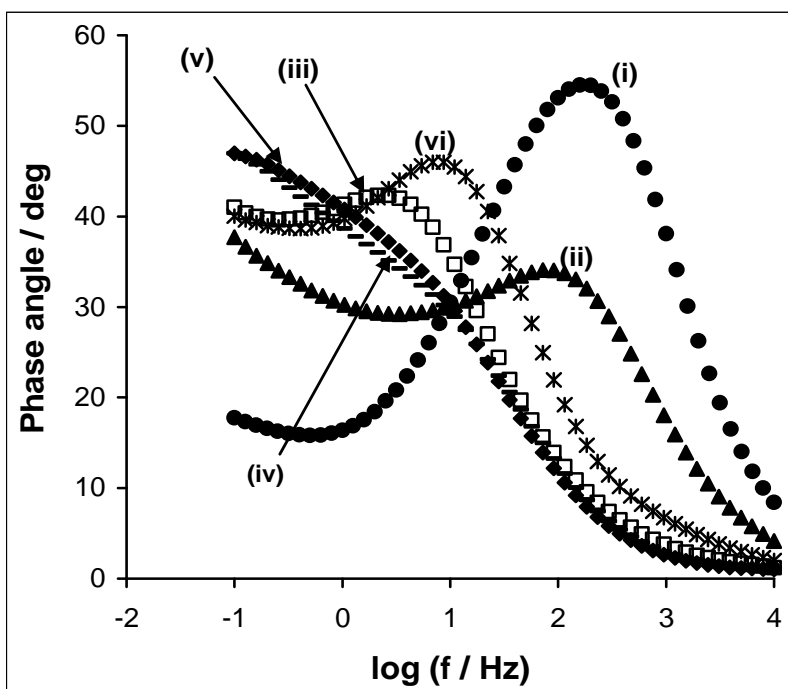
Figure 3.12: Bode plots of phase angle vs. logarithm of frequency for the (i) bare BPPGE, (ii) BPPGE-CoTAPc, (iii) BPPGE-SWCNT-CoTAPc$_{(cov)}$, (iv) BPPGE-SWCNT-CoTAPc$_{(mix)}$, (v) BPPGE-SWCNT and (vi) BPPGE-SWCNT-CoTAPc$_{(ads)}$ in 0.1M KCl containing equimolar mixture of $K_4Fe(CN)_6$ and $K_3Fe(CN)_6$.

3.1.3 Electrocatalysis of V-Type Nerve Agents Degradation Products at BPPGE-SWCNT-CoTAPc(mix)

3.1.3.1 pH Analysis

BPPGE-SWCNT-CoTAPc(mix) was used to ascertain the effect of different solution pHs on the catalytic detections of the DEAET and DMAET. Figure 3.13 shows an example of the cyclic voltammetric responses (i.e. peak potential and peak currents) obtained for DEAET (10^{-4} M) at different solution pHs (5.0–12.0). Similar voltammetric profiles were obtained for DMAET at the same pH range.

$$y = -0.0573x + 1.2355$$
$$R^2 = 0.9898$$
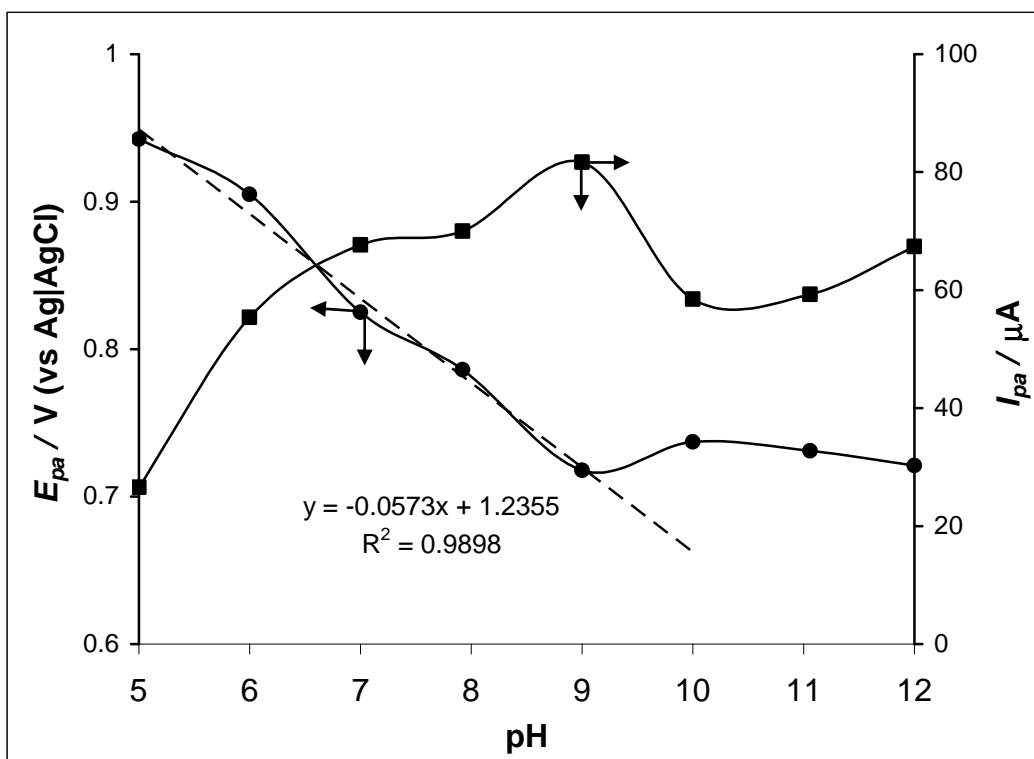
Figure 3.13: Plots of E_{pa} and I_{pa} vs. pH for DEAET (10^{-4} M) using BPPGE-SWCNT-CoTAPc(mix). Arrow directions indicate the respective axes for each of the plots. The broken line is the straight line plot for the E_{pa} vs. pH (pH 5–9) extracted from the E_{pa} vs. pH (pH 5–12) curve. Scan rate, 50mVs^{-1}.

- 75 -

For both analytes, no detectable catalytic current was observed at pH ≤ 5.0. However, in the pH 5.0–9.0 range, linear plots of Ep versus pH are obtained with slopes of ~59 mV/pH, indicating approximately equal electron and proton transfer process. Maximum catalytic currents were observed at equal or greater than pH 9.0 for both analytes. This behaviour is consistent with the pKa of DEAET reported as 8.3 at 25 $^{\circ}$C [147]. Thus, all subsequent studies here for DEAET and DMAET were performed at pH 9.3 PBS with some works done at the physiological pH 7.4 conditions.

3.1.3.2   Comparative Catalytic Responses of Different Electrodes

Figure 3.14 shows typical CVs obtained at different electrodes for the electrocatalytic detection of 10^{-4}M DMAET. BPPGE-SWCNT (v) gave slightly higher catalytic current at less potential (although with higher background current) when compared to other electrodes. Similar experiment with DEAET, using the same concentration as for DMAET, gave slightly higher (~10%) catalytic current response at less potential.

In general background-corrected catalytic current responses for both analytes follow this trend: BPPGESWCNT ≈ BPPGE-SWCNT-CoTAPc$_{(mix)}$ ≈ BPPGE-SWCNT-CoTAPc$_{(cov)}$ > BPPGE-CoTAPc > bare BPPGE.   BPPGE-SWCNT-CoTAPc$_{(ads)}$ gave similar catalytic current response to SWCNT. SWCNT is a well-known electron-acceptor [63, 125], CoTAPc is electron-donating (by virtue of the lone pair electrons on the –NH$_2$ substituent) and acts as a viable reaction centre. Therefore, BPPGE-SWCNT and CoTAPc modified BPPGE-

SWCNT exhibited catalytic response (enhanced current at less positive potential) while the other electrodes exhibited little or no detectable catalytic response for this analyte.
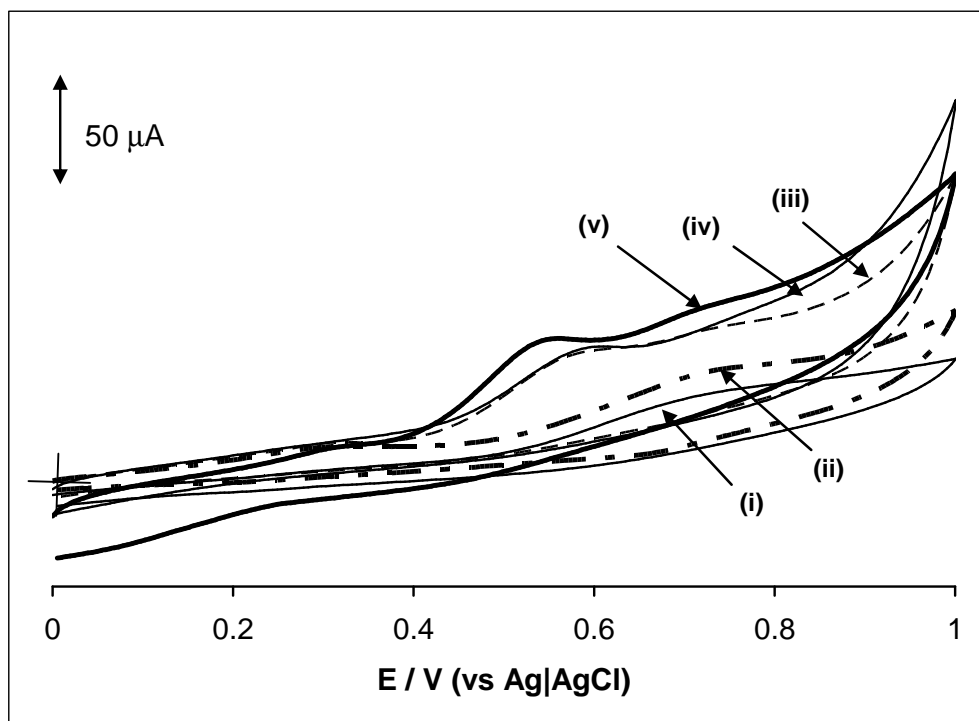
Figure 3.14: Typical comparative cyclic voltammograms for 10^{-4} M DMAET in pH 9.3 PBS at different electrodes: (i) bare BPPGE, (ii) BPPGE-CoTAPc, (iii) BPPGE-SWCNT-CoTAPc(mix), (iv) BPPGE-SWCNT-CoTAPc(cov) and (v) BPPGE-SWCNT. Scan rate = 50 mVs^{-1}.

The CV of DMAET with BPPGE-SWCNT showed two peaks, one at about 0.48 V, and the other at about 0.74 V. Such double oxidation peaks have been observed before for CNT-based electrodes during electrocatalytic detection of thiol-containing analytes [148]. Based on such reports, the first oxidation peak (at ~0.48 V) may be ascribed to be mediated by the quinone-like functional groups at the tube ends of the SWCNT, while the second oxidation peak (at ~0.74 V)

may be attributed to be mediated by the edge plane-like carbon at the SWCNT [149]. On BPPGE-SWCNT-CoTAPc$_{(mix)}$ (iii), the peak corresponding to DMAET oxidation was observed a lower potential (+0.58 V) with an enhanced current compared to the BPPGE-CoTAPc, indicating that SWCNT-CoTAPc$_{(mix)}$ greatly improves the electronic communication between the analyte and the bare BPPGE. The enhanced electrocatalytic activity in the presence of SWCNT is not surprising as electrodes modified with SWCNT have been known to exhibit better catalytic activity compared to their unmodified electrodes [148]. It is interesting to note that the SWCNT-CoTAPc based electrodes give similar current responses towards the catalytic detection of these V-type nerve agents, suggesting that the long synthetic processes for the production of SWCNT-CoTAPc$_{(cov)}$ can be avoided for this type of work.

The stability of the BPPGE-SWCNT-CoTAPc$_{(mix)}$ was investigated to determine its shelf life and significance to potential analytical utility. The decrease in catalytic current (Figure 3.15) subsequent to repetitive scans is an implication of electrode contamination. However, cleaning by continuous scanning (~10 times) restores the electrode to ~90% of its original activity (current response at a given DEAET or DMAET concentration). A similar mechanism to those reported [149-151] for the electrocatalytic oxidation of sulfhydryls using MPc-based electrodes could well apply to these two sulphdryl species, as shown below:

$$RSH + OH^- \rightarrow RS^- + H_2O \qquad\qquad \textbf{3.14}$$

$$RS^- + Co(II)TAPc \rightarrow [(SR) - Co(III)TAPc]^- \qquad\qquad \textbf{3.15}$$

$$[(SR) - Co(III)TAPc]^- \rightarrow [(SR) - Co(III)TAPc] + e^- \, (rds) \qquad\qquad \textbf{3.16}$$

$$[(SR) - Co(III)TAPc] \rightarrow Co(II)TAPc + RS^\bullet \qquad\qquad \textbf{3.17}$$

$$RS^\bullet + RS^\bullet \rightarrow RSSR(fast) \qquad\qquad \textbf{3.18}$$
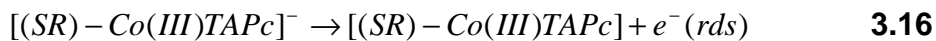
RSH denotes the sulfhydryl nerve-agent hydrolysis products (DEAET and DMAET), $RS^\bullet$ is thiyl radical, while RSSR is the disulphide products. DEAET is ionized in alkaline solution (equation 3.14) [147]. The ions formed interact with the Co(II)TAPc molecule which results in the oxidation of the Co(II)TAPc to Co(III)TAPc. The negatively charged complex is neutralized after the loss of an electron in the (equation 3.16) rate-determining step (rds). Reduction of the Co(III)TAPc allows for the generation of the thiyl radical and the subsequent regeneration of the Co(II)TAPc species. Thiyl radicals undergo fast reactions to form the disulphide product.
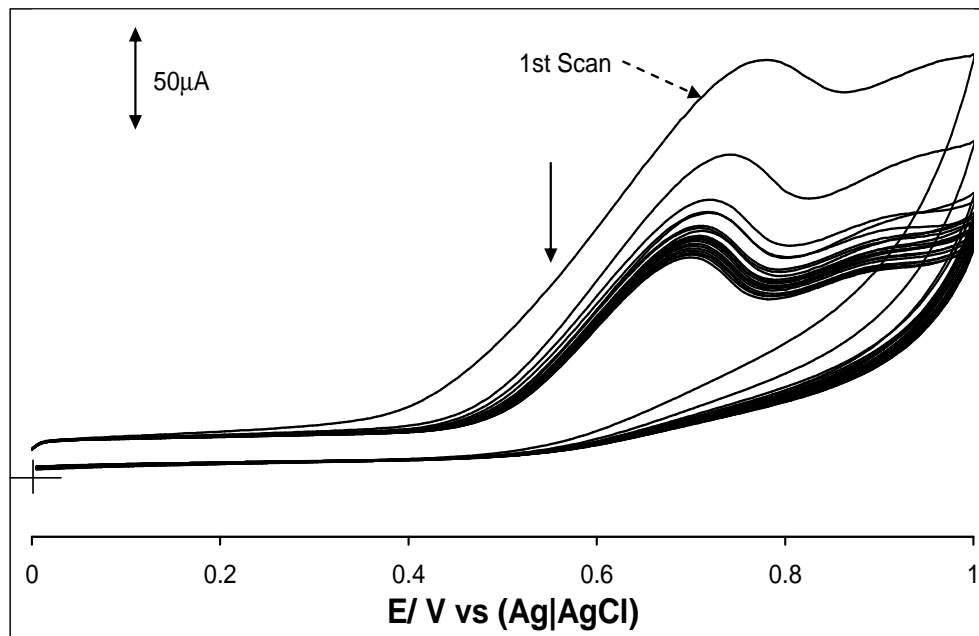
Figure 3.15: A typical CV of multiple scans of BPPGE-SWCNT-CoTAPc$_{(mix)}$ in 10^{-4} DMAET at 100 mV/s depicting an electrode poisoning effect.

3.1.3.3 Discrimination of DEAET and DMAET at SWCNT-CoTAPc Based Electrodes

Given its relatively higher sensitivity over cyclic voltammetry, SWV was used to probe the response of the two electrodes, BPPGE-SWCNT and BPPGE-SWCNT-CoTAPc$_{(mix)}$ towards the detection of DMAET and DEAET. As clearly evident in Figure 3.16, the SWCNT-CoTAPc$_{(mix)}$ film showed a better potential discrimination for the two sulfhydryls than the SWCNT film. BPPGE-SWCNT (a) detects both analytes at the same potential (*ca*. 0.55V versus Ag|AgCl) while the BPPGE-SWCNT-CoTAPc$_{(mix)}$ (b) provides a significant advantage, in that it shows detection at different potentials (*ca*. 0.64 and 0.73V versus Ag|AgCl for DEAET and DMAET, respectively).

(a)   (b)
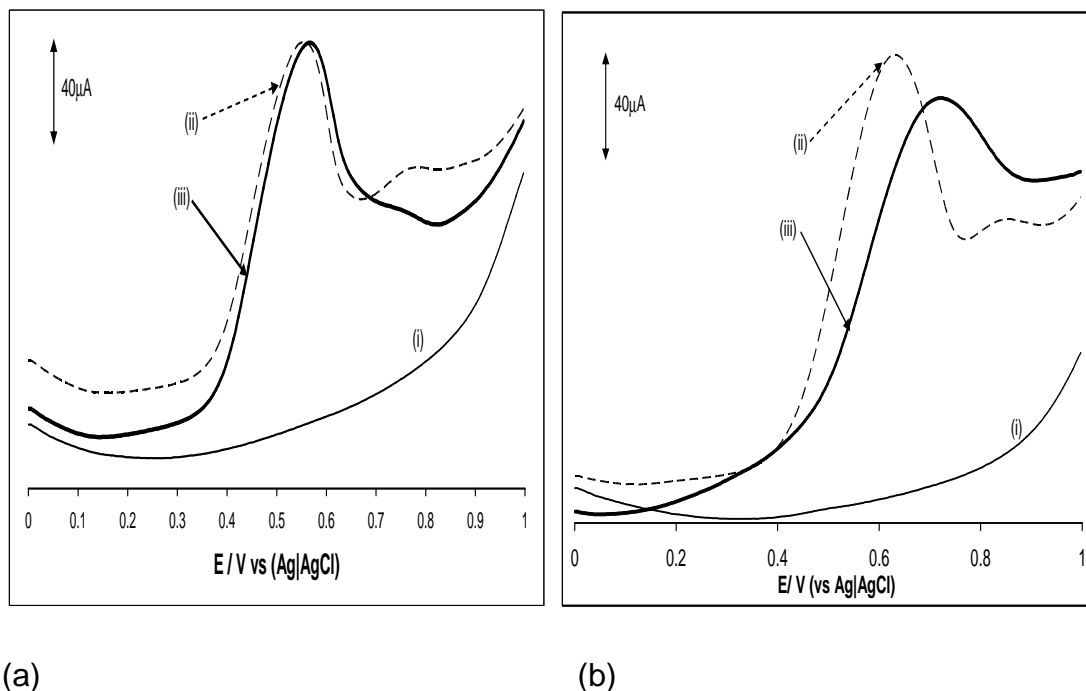
Figure 3.16:   Square wave voltammetric profiles for (a) BPPGE-SWCNT and (b) BPPGE-SWCNT-CoTAPc$_{(mix)}$ in (i) buffer, (ii) DEAET, and (iii) DMAET in pH 9.3 buffer solution. Concentration of individual analyte was maintained at 10^{-4} M.

All subsequent electrocatalysis experiments for these thiols were performed with the BPPGE-SWCNT-CoTAPc$_{(mix)}$. A plot of the peak current (I_p) against the square root of scan rate ($v^{1/2}$) using the Randles-Sevcik equation (equation 1.2) resulted in a straight line, which is an indication that the electrocatalytic oxidation of DEAET (equation 3.19) and DMAET (equation 3.20) are diffusion controlled reactions. The straight line equations are as follows:

- $DEAET : y = 9.7x10^{-6} + 4.26x10^{-5}$ **3.19**
  $R^2 = 96.21$

- $DMAET : y = 5.2x10^{-6} - 9.29x10^{-6}$ **3.20**
  $R^2 = 97.97$

However, at higher scan rates (300 –1200 mVs^{-1}) the I_p versus $\nu^{1/2}$ plot became non-linear, most likely due to the adsorption of these sulfhydryls on the surface of the electrodes. A plot of $I_{pa}/\nu^{1/2}$ versus ν (Figure 3.17) resulted in the characteristic shape that is typical for catalytic process of electrochemical reaction preceding chemical reaction (EC$_{cat}$) processes [152].
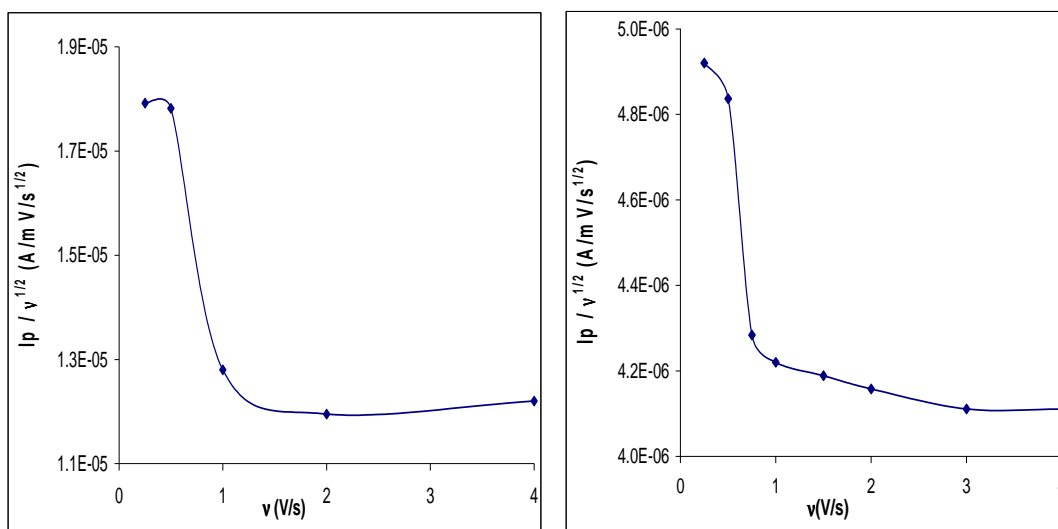
(a)   (b)

Figure 3.17:   Plot of $I_p/\nu^{1/2}$ vs. ν for 10^{-3}M (a) DEAET and (b) DMAET using BPPGE-SWCNT-CoTAPc$_{(mix)}$.

From equation 3.21 [10,152-155] plots of E_p vs. ½ log ν (Figure 3.18) were plotted for these irreversible diffusion controlled processes.

$$Ep = \frac{b}{2}\log\nu + const.\qquad\qquad\textbf{3.21}$$

where b = Tafel slope = 2.303 RT/ αnF, and all symbols are already defined above.

The value of the Tafel slope was calculated to be approximately 234 and 260 mVdecade^{-1} for DEAET and DMAET, respectively.
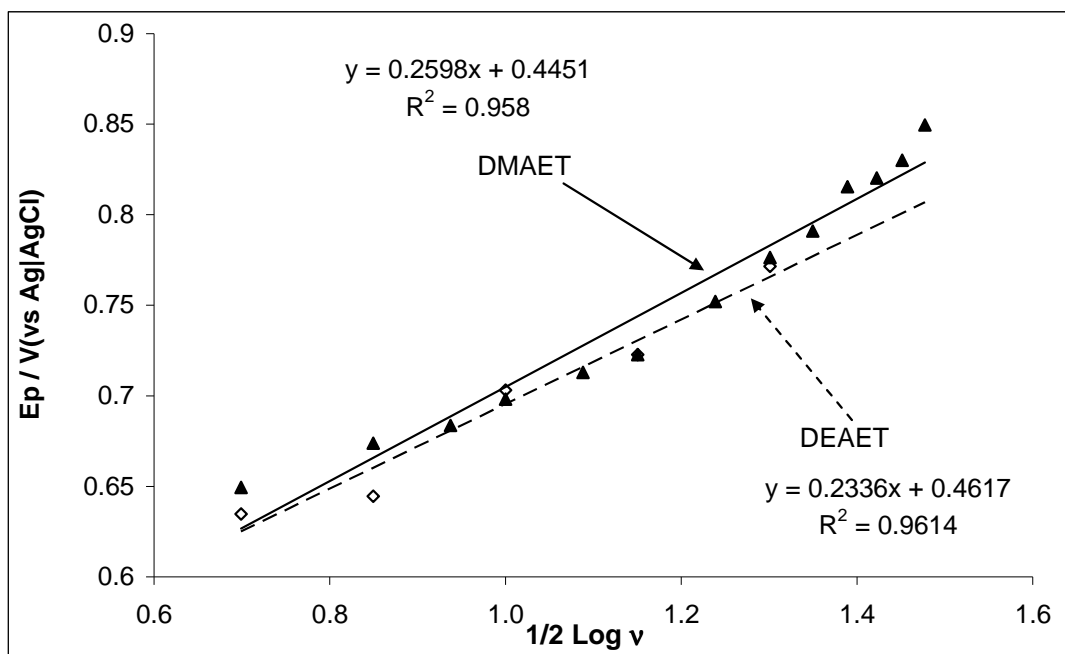
Figure 3.18: Plot of peak potential vs. ½ log scan rate for 10^{-3}M DEAET and DMAET using BPPGE-SWCNT-CoTAPc$_{(mix)}$.

Assuming an electrochemical transfer coefficient (*α*) < 0.5, these results indicate that the rate-determining step for the catalysis of these sulfhydryls involve one-electron transfer process. It is well established [156-158] that high Tafel slopes (> 120 mV/decade) as obtained in this study is the consequence of strong binding of reactants or intermediates on the electrode surfaces and/or reactions occurring within a porous electrode structure. Thus, the Tafel slopes obtained in this work can be attributed to the strong binding of these sulfhydryls

with the SWCNT-CoTAPc catalyst. Repetitive scanning experiments with these sulpydryls at constant concentration showed electrode poisoning. However, on rinsing the fouled electrode by 5 repetitive scans in buffer solution alone ~90% recovery was observed. This electrode fouling also agrees with binding of the analytes with the SWCNT-CoTAPc film.

3.1.3.4   Chronoamperometric Analysis

Based on the SWV results described above, chronoamperometric technique was employed for the analysis of DEAET (+640 mV) and DMAET (+730mV) using BPPGE-SWCNT-CoTAPc(mix) in pH 9.3 PBS. From the current responses of the BPPGE-SWCNT-CoTAPc(mix) and the changes in the analyte concentration, the limit of detection (LoD = 3.3s/m [159], where s is the standard deviation of the intercept and m the slope of the linear peak current vs. the concentration of DMAET or DEAET) and sensitivities, of these sulfhydryls were determined and tabulated in Table 3.3 below. All data were obtained with the same electrode, rinsing the electrode prior to immersing it in a new concentration. BPPGE-SWCNT-CoTAPc(mix) was used in determining the catalytic rate constants and diffusion coefficients of these analytes at constant concentration, using the established equation [10,160]:

$$\frac{I_{cat}}{I_d} = \gamma^{1/2}[\pi^{1/2}erf(\gamma^{1/2}) + \frac{\exp^{(-\gamma)}}{\gamma^{1/2}}] \qquad\qquad \textbf{3.22}$$

where, $\gamma = kCt$ is the argument of the error function and in cases where $\gamma > 1.5$, erf($\gamma^{1/2}$) is almost equal to unity and the equation 3.22 can be reduced to equation 1.10:

$$\frac{I_{cat}}{I_L} = \pi^{1/2}(kC_ot)^{1/2}$$

At intermediate times (0.5–2.2 s) of the chronoamperometric measurements (Figure 3.19) , the catalytic currents (I_{cat}) were dominated by the rate of the electrocatalysed oxidation of these nerve agents, thus the rate constants for the chemical reactions between the nerve agents and redox sites of surface immobilized SWCNT-CoTAPc$_{(mix)}$ were determined using equation 1.10. From the slopes of the plots of I_{cat}/I_L vs. $t^{1/2}$ for 10^{-3}M DMAET (Figure 3.20(a)) and DEAET, the values of the catalytic rate constants, k, were determined. From the Cottrell equation the diffusion coefficients, D, for DMAET (Figure 3.20(b)) and DEAET were determined. The values of the above mentioned analytical parameters are tabulated below in Table 3.3.
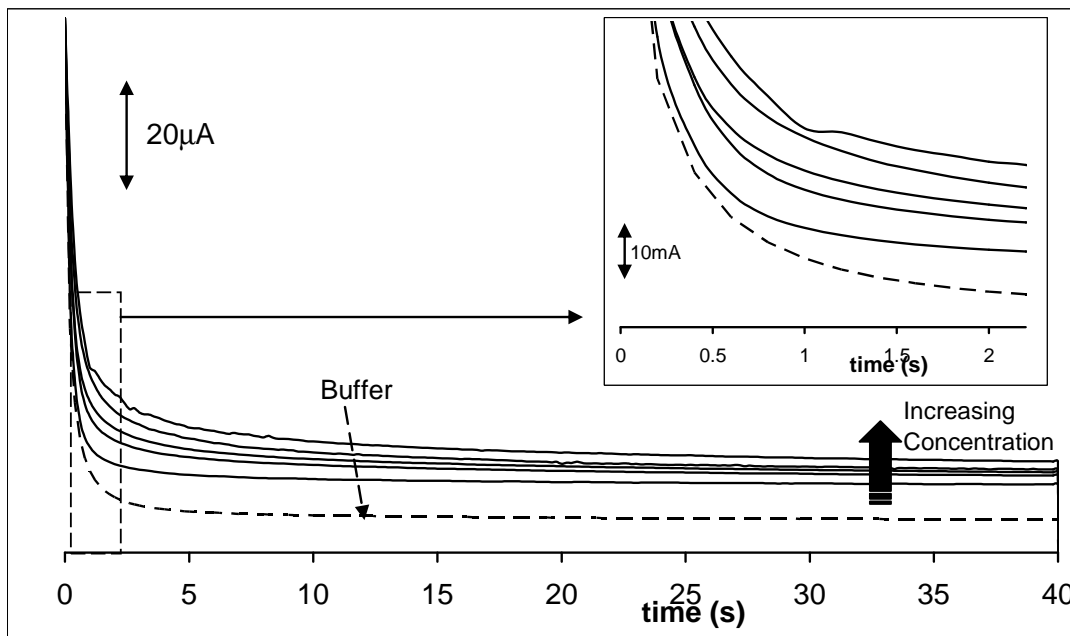
Figure 3.19: A Typical Chronoamperometric profile analysis of DMAET at a BPPGE-SWCNT-CoTAPc$_{(mix)}$ with a potential of 0.6V. Inset showing amplified time region for catalytic rate constant and diffusion coefficient calculations. Concentration: Buffer, 8, 40, 60, 100, 150 µM (inner to outer as shown by arrow).
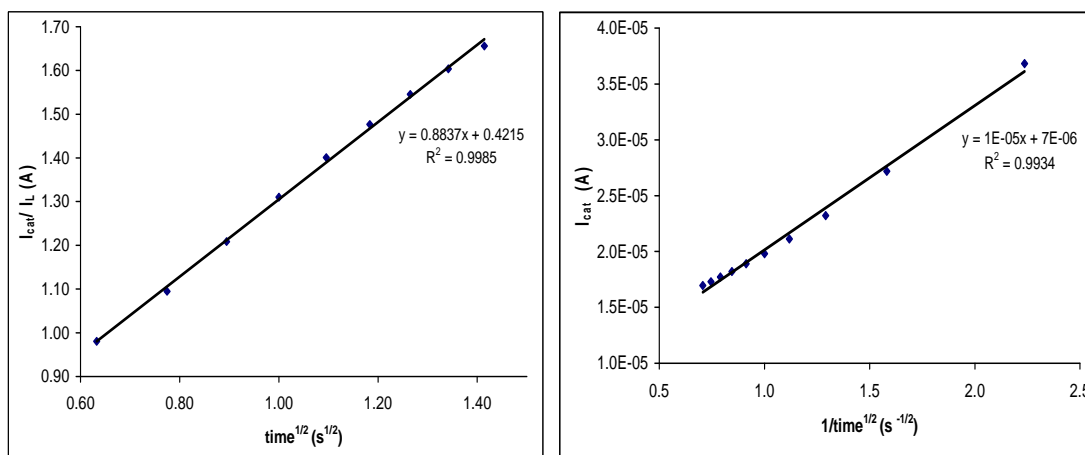
(a)   (b)

Figure 3.20: Plots of (a) I_{cat}/I_L vs. $t^{1/2}$ and (b) I_{cat} vs. $1/t^{1/2}$ resulting from chronoamperometric data of DMAET at a BPPGE-SWCNT-CoTAPc$_{(mix)}$ with a potential of 0.6V (vs. Ag|AgCl)

TABLE 3.3: Summary of the Analytical Parameters at BPPGE-SWCNT-CoTAPc$_{(mix)}$ towards the detection of 1mM DEAET and DMAET solutions.

Modified Electrode	Analytical Parameter	V-Type Nerve Agents	
		DEAET	DMAET
BPPGE-SWCNT-CoTAPc$_{(mix)}$	Ep (mV)	640	730
	Sensitivity (A M^{-1})	6.0×10^{-2}	5.0×10^{-2}
	LOD (μM)	3.0	8.0
	k (M^{-1} s^{-1})	1124	894
	D (cm^2 s^{-1})	2.3×10^{-5}	1.5×10^{-5}

At this juncture, it is important to note that there are no accessible literature at the moment to compare the electrocatalytic parameters obtained here for these two thiol degradation products, the few known reports [3, 30] only dealt with their amperometric detection. Thus, this work is the first to provide detailed electrocatalytic parameters for DEAET and DMAET. This concludes the work on SWCNT-CoTAPc based electrodes.

As already stated the nickel impurity in SWCNT (Figure 3.4 and the subsequent discussion) prompted me to investigate the impact of NiTAPc and nickel powder on the electrocatalytic ability of SWCNT. The next section discusses the results of NiTAPc based electrodes.

3.2 SWCNT-NiTAPc Hybrid Electrode

3.2.1 Modified Basal Plane Pyrolytic Graphite Electrodes

3.2.1.1 Electropolymerization Properties

Unlike in the CoTAPc studies where the electrosorption was observed, electropolymerization process was observed in the attachment of NiTAPc onto BPPGE-SWCNT (Figure 3.21) following established methods for the formation of NiTAPc polymer onto a carbon electrode [133, 134]. Electropolymerization was performed at various scan numbers, between 5 and 40, but 7 Scans proved to be the best as discussed below.
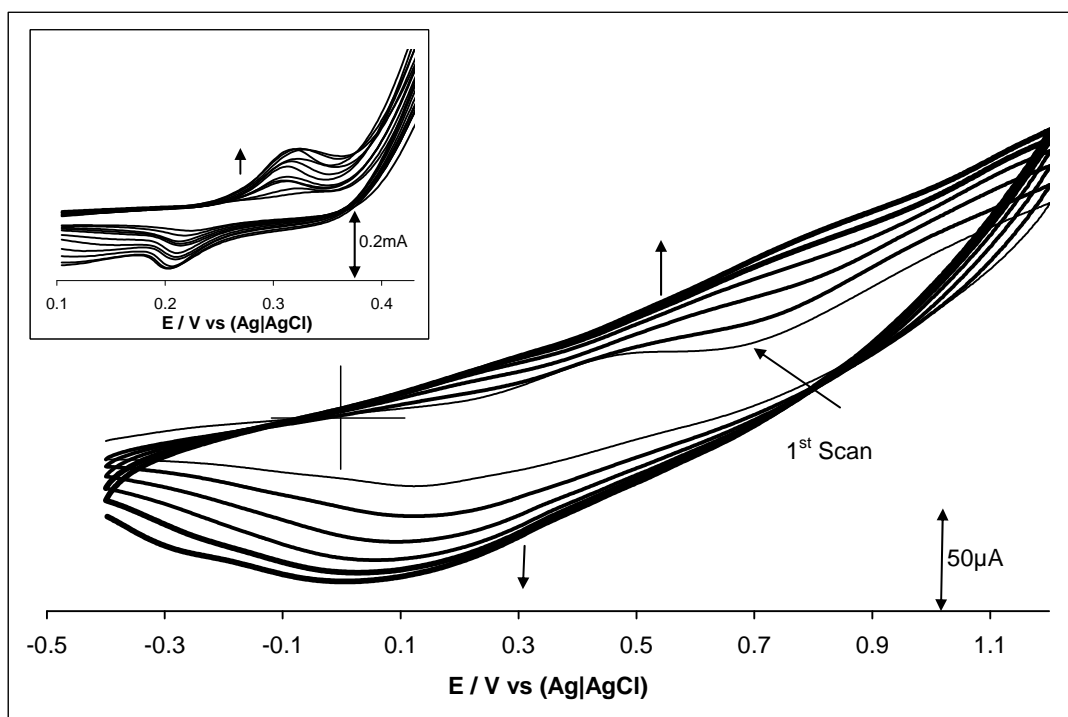
Figure 3.21: Cyclic voltammetric profiles for electropolymerization process (7 scans) of a 5 mM NiTAPc in DMF containing TBABF$_4$ at BPPGE-SWCNT. Inset depicts every fifth scan obtained during conditioning of BPPGE-SWCNT-NiTAPc in 0.1M NaOH.

Electropolymerization of NiTAPc was achieved by 7 repetitive cycles with a BPPGE-SWCNT in a DMF solution containing 5mM of the NiTAPc complex and 0.1 M TBABF$_4$. Figure 3.22 is a typical SEM image of the electropolymeric film formed on the surface of the electrode.
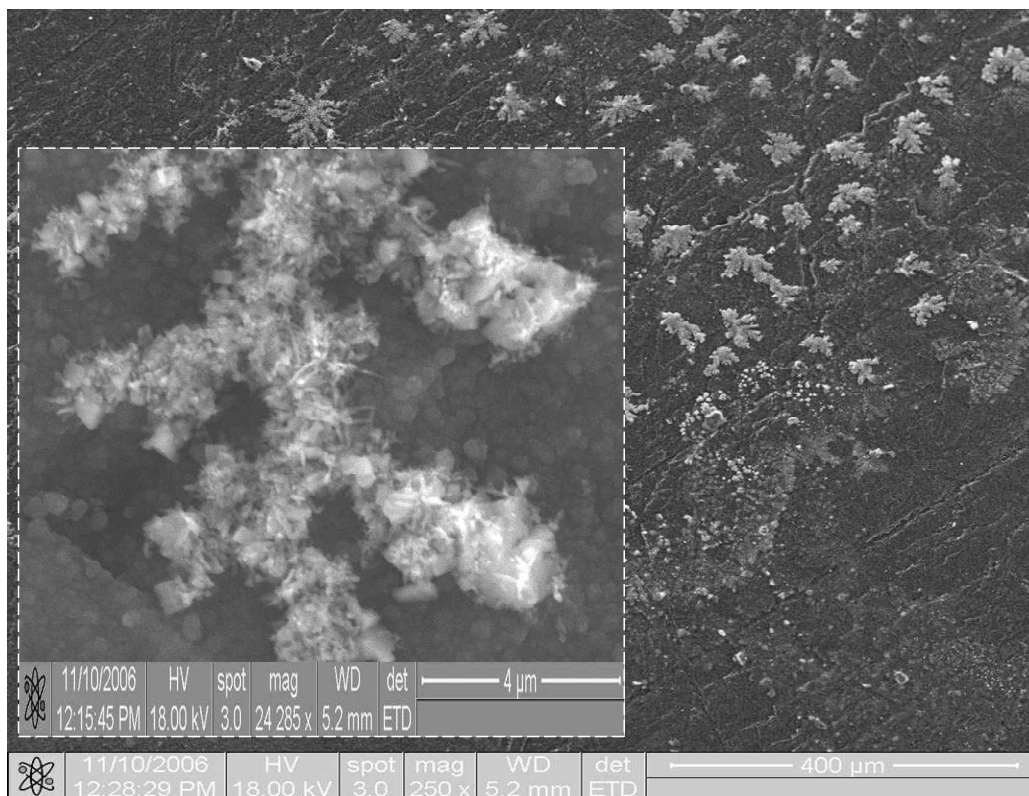
Figure 3.22: SEM image of BPPGE-SWCNT-NiTAPc at 250x magnification. Inset shows the crystalline structure of BPPGE-SWCNT-NiTAPc at increased (24 285x) magnification. Electropolymeric film was obtained by repetitive scanning (7 scans) of a 5 mM NiTAPc in DMF containing TBABF$_4$ at a BPPGE-SWCNT.

The electropolymer was also successfully transformed into the O-Ni-O oxo-bridged derivatives using the known procedure [161-164], BPPGE-SWCNT-*poly*-Ni(OH)TAPc, unfortunately, unlike the BPPGE-SWCNT-*poly*-NiTAPc, the

BPPGE-SWCNT-*poly*-Ni(OH)TAPc peels off from the electrode in aqueous solution, so no further experiment was carried out with this electrode. It is seen from the high SEM magnification (Figure 3.22 inset) that the BPPGE-SWCNT-*poly*-NiTAPc$_7$ gave a dendrite-like microcrystal structure, which can be attributed to the presence of the SWCNT. At a lower magnification (Figure 3.22), it is clear that the BPPGE is not completely covered by these SWCNT-NiTAPc crystals, but are randomly distributed throughout the electrode surface. This behaviour is attributed to the fabrication method; drop-dry coating of SWCNT followed by mild oven-drying encourages aggregation and breaking of the immobilized nanotubes into microscopic pieces. The obtained crystalline NiTAPc electropolymers are concentrated on these microscopic pieces of the immobilized SWCNTs, further confirming the ability of the SWCNT to induce crystallinity on the NiTAPc electropolymer. Although, it has been widely reported that CNTs are capable of inducing crystallinity on polymeric species [165-172], this represents the first report of such observation for an electropolymer and especially for a MPc electropolymer.

3.2.1.1.1 Impact of Scan Number on the Electron Transport

Impedance spectroscopy provides an excellent means of probing the electron transfer properties of modified electrodes [29]. Crystalline structures are efficient intermedia for interchain transport of charge carriers [173]. Therefore, the electron transport features of the films were examined, using a simple electrochemically reversible redox probe, $[Fe(CN)_6]^{3-/4-}$. Figure 3.23 presents

plots of the ΔE_p and k_{app} versus the scan number, indicating the influence of electropolymerization scan numbers on the electron transport of the BPPGE-SWCNT-*poly*-NiTAPc. The k_{app} values were extracted from the electron transfer resistance R_{CT} (Ω) values obtained from the semi-circle of the Nyquist plots using equation 3.13.
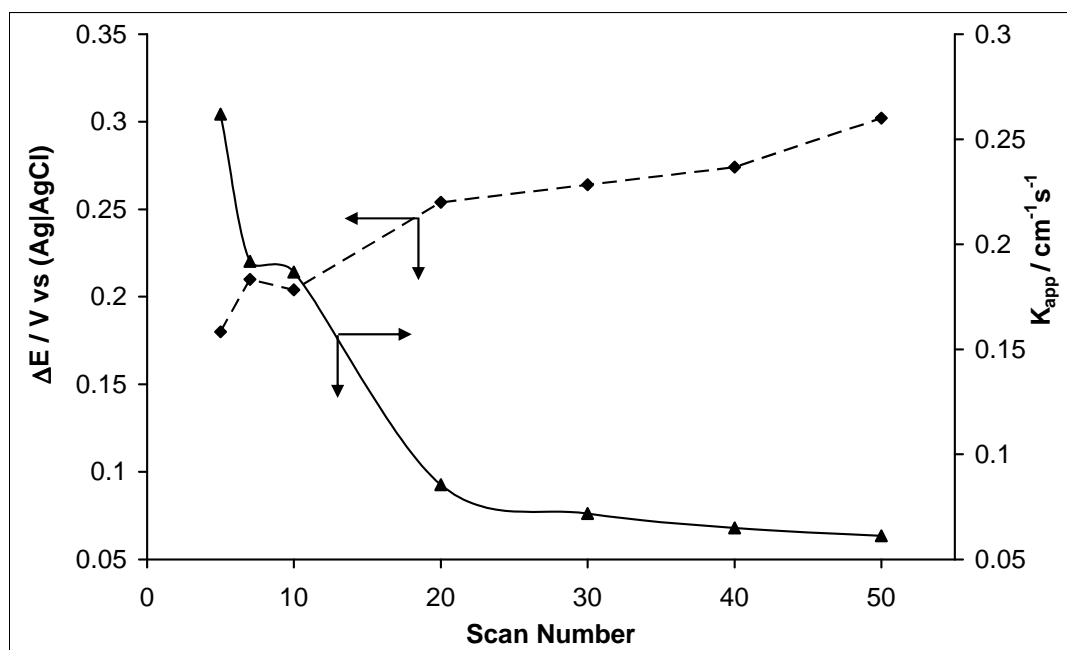
Figure 3.23: Represents plots of the ΔE_p and k_{app} vs. the scan number using the BPPGE-SWCNT-*poly*-NiTAPc in a solution of 1 mM of $K_4Fe(CN)_6$ and 1 mM $K_3Fe(CN)_6$ (1:1) mixture containing 0.1 M KCl.

The plots shows that the CV results agree qualitatively well with the observed EIS data. It is evident from Figure 3.23 that low electropolymerization scans (< 10) gave faster electron transfer kinetics compared to scan numbers greater than 10, meaning that at the conditions employed in this work the best electrode response was observed at low scan numbers of NiTAPc

electropolymers. This result also shows the possibility to control the amount of polymeric species that can be deposited onto the electrode at constant concentration of the MPc.

3.2.1.2   pH Studies

The impact of solution pH on the electron transport kinetics of the BPPGE-SWCNT-*poly*-NiTAPc$_7$ was considered between pH 3.0 and 9.0 of a 1 mM of K$_4$Fe(CN)$_6$/ K$_3$Fe(CN)$_6$ solution. The ΔE_p values increased with increasing pH, indicating the consistent decrease in electron transfer kinetics with increasing pH. This behaviour suggests that the increasing deprotonation of the electropolymeric film leads to the increasing inhibition of the anionic redox probe from penetrating into the electrode surface, hence the loss of Faradaic response. The same trend is seen at the BPPGE-SWCNT-CoTAPc (Figure 3.8) where the potential decreases upon increasing pH. Therefore, this system also supports an equal number of electron and, proton transfer reaction.

3.2.1.3   Comparative Film Capacitances

Comparative CVs of the electrodes at different pH of buffer solutions (0.1 M PBS, pH 3.0 – 10.0) revealed that the cathodic and anodic charges associated with the BPPGE-SWCNT-*poly*-NiTAPc$_7$ are much higher than the charges obtained at the BPPGE-SWCNT, BPPGE-*poly*-NiTAPc$_7$ or BPPGE-*poly*-Ni(OH)TAPc$_7$ electrodes (exemplified in Figure 3.24 for (a) pH 3.0 and (b) pH7.0).

(a)   (b)
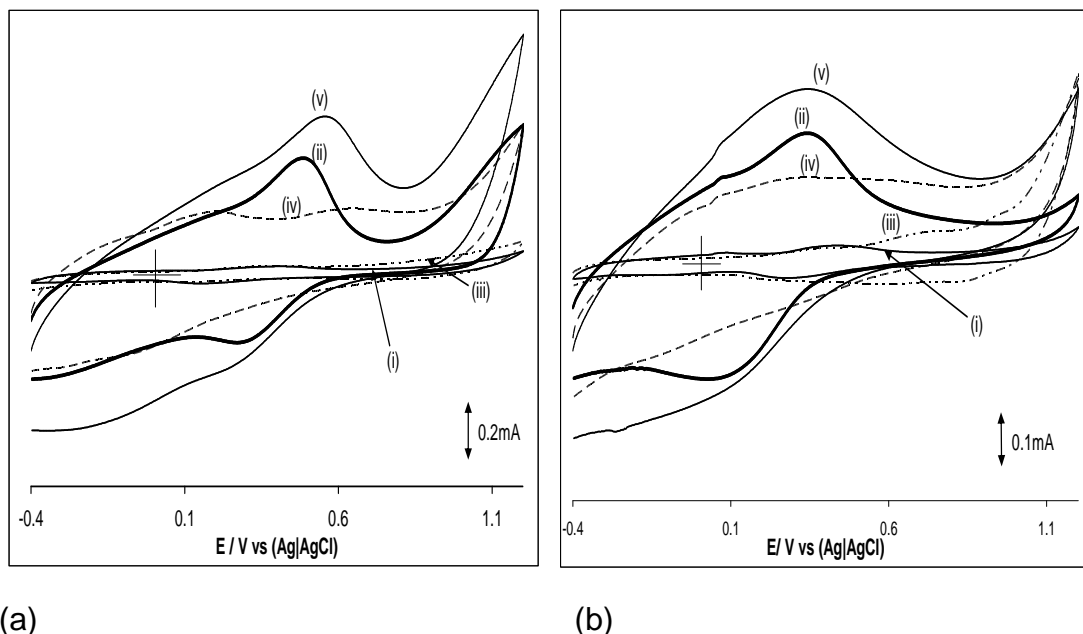
Figure 3.24: Cyclic Voltammograms of the bare BPPGE (i), BPPGE-*poly*-NiTAPc$_7$ (ii), BPPGE-*poly*-Ni(OH)TAPc$_7$ (iii), BPPGE-SWCNT (iv) and BPPGE-SWCNT-*poly*-NiTAPC$_7$ (v) in 0.1 M PBS (a) pH3.0 and (b) pH 7.0.

For example, at pH 3.0, the estimated anodic charges obtained for BPPGE (i), BPPGE-SWCNT (ii), BPPGE-*poly*-NiTAPc$_7$ (iii), BPPGE-*poly*-Ni(OH)TAPc$_7$ (iv) and BPPGE-SWCNT-*poly*-NiTAPc$_7$ (v) are 7.2 x 10^{-4}, 5.7 x 10^{-3}, 1.1 x 10^{-2}, 7.6 x 10^{-4}, 1.4 x 10^{-2} Ccm^{-2}, respectively. The values obtained for the respective electrodes at neutral and alkaline pH conditions were in the same magnitude as for the acidic conditions. This result is consistent with organized electrocrystals, for example, a recent report by Lopez et al., [173] where zinc crystals grown attached to three dimensionally dispersed dendrite backbones efficiently increased interfacial areas and were found to have much higher charges than the corresponding dendritic zinc films of irregular features or electrodes composed with individual crystals.

Insight into the ability of the films to store charges may be obtained from the film capacitance (C_{film} / Fcm^{-2}) estimated in the non-Faradaic regimes (0.93 V vs. Ag|AgCl) using the simple expression [174]:

$$C_{film} = \frac{I_{ch}}{vA} \qquad\qquad \textbf{3.23}$$

where I_{ch} is the charging current, v the scan rate, and A the geometric area of the electrode.

The capacitance at the pH 3.0 was estimated to be 1.1 x 10^{-2} Fcm^{-2} for the BPPGE-SWCNT-*poly*-NiTAPc$_7$ compared to the 7.7 x 10^{-3}, 5.5 x 10^{-3} and 1.8 x 10^{-3} Fcm^{-2} for the BPPGE-SWCNT, BPPGE-*poly*-NiTAPc$_7$ and the BPPGE-*poly*-Ni(OH)TAPc$_7$, respectively. In the pH 7.2 conditions the value for the BPPGE-SWCNT-*poly*-NiTAPc$_7$ was 4.2 x 10^{-3} Fcm^{-2} compared to BPPGE-*poly*-NiTAPc$_7$ (1.7 x 10^{-3} Fcm^{-2}) and BPPGE-*poly*-Ni(OH)TAPc$_7$ (3.2 x 10^{-3} Fcm^{-2}) electrodes without SWCNT. Interestingly, despite the significant decrease (*ca.* 62%) in the capacitance of the BPPGE-SWCNT-*poly*-NiTAPc$_7$ from acidic to the neutral pH, the capacitance of the BPPGE-SWCNT-*poly*-NiTAPc$_7$ is still significantly greater (*ca.* 27 – 50%) than those of the electrode without SWCNT, i.e., BPPGE-*poly*-NiTAPc$_7$ and the BPPGE-*poly*-Ni(OH)TAPc$_7$.

3.2.1.4   Electrochemical Kinetics of the Electropolymerized NiTAPc

The CV evolution at varying rates of BPPGE-SWCNT-*poly*-NiTAPc followed the same trends as the pre-treated BPPPGE-SWCNT-CoTAPc$_{(ads)}$ (Figure 3.9). Therefore, following Laviron's theory [139, 140] for irreversible

electrode reactions, plots of *E*p vs. ln ν (Figure 3.25) at BPPGE-SWCNT-*poly*-NiTAPc yielded $\alpha n = 0.211$ and $k_s = 1.72$ s^{-1} for the cathodic reactions, and $(1-\alpha)n = 0.233$ and $k_s = 221.9$ s^{-1} for the anodic reactions at 25°C. Electrochemical reversibility was better at pH 2.34 solution and therefore electrochemical kinetic studies were carried out in these solutions for BPPGE-SWCNT-*poly*-NiTAPc. At high scan rates, the plots of E_p versus ln ν were linear. The equations of the straight lines for the BPPGE-SWCNT-*poly*-NiTAPc:

$$E_{pa} = 0.1099\ln\nu + 0.8523 \qquad\qquad \textbf{3.24}$$

$$E_{pc} = -0.1216\ln\nu + 0.3071 \qquad\qquad \textbf{3.25}$$
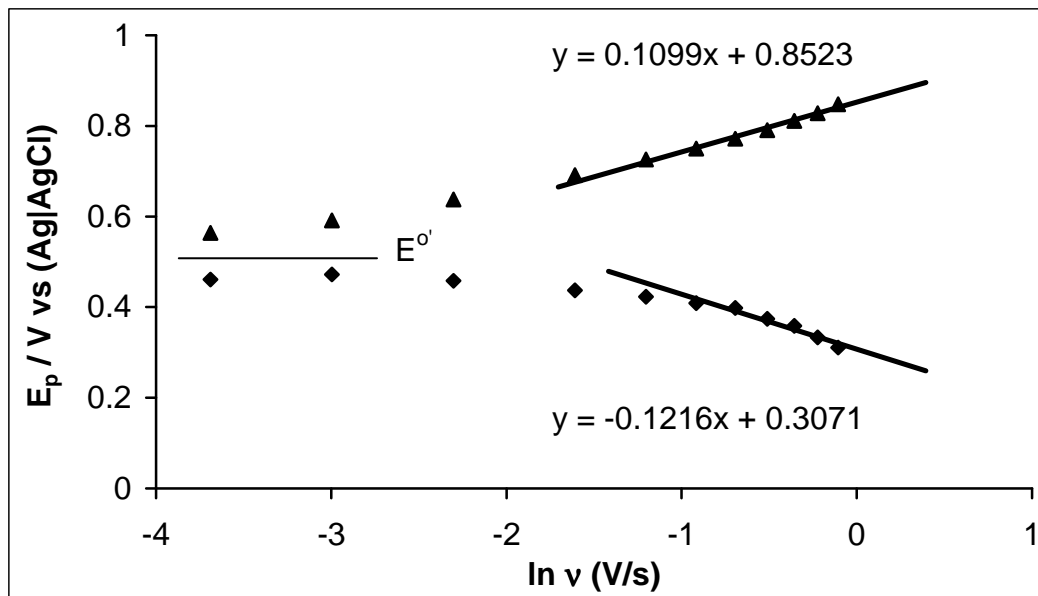
Figure 3.25:   The plots of Ep vs. ln ν for BPPGE-SWCNT-*poly*-NiTAPc in PBS (pH 2.34).

From the calculated values of αn it was possible to estimate that the rate determining step of the reduction process was a single electron transfer reaction (n=1). These values also suggest that the rate-determining steps of the cathodic and anodic reactions are different. The cathodic reaction shows a small k_s value in comparison to the anodic and can be attributed to the weak electron transfer process arising from the complications of the overlapped reactions. Previously mentioned for CoTAPc, the behaviour where one redox wave exhibits higher peak current than its reverse wave is typical for phthalocyanine complexes [141].

3.2.1.5   Electrochemical Impedance Spectroscopy

EIS was employed to examine the electron transport behaviour towards the electrochemistry of the simple redox couple, $[Fe(CN)_6]^{3-}/[Fe(CN)_6]^{4-}$. Figure 3.26 and 3.27 represents typical CVs and their corresponding Nyquist plots respectively for the BPPGE-SWCNT-*poly*-NiTAPc$_7$ and other electrodes.

From the Nyquist plots, the BPPGE and the BPPGE-*poly*-Ni(OH)TAPc$_7$ gave two depressed circles with Warburg lines, the other electrodes exhibited essentially one semicircle with a Warburg line. The most widely accepted explanation for the appearance of depressed circles in Nyquist plots is the occurrence of different electrochemical processes that take place at different RC time constants [29]. Such processes arise because of microscopic roughness or high porosity of the electrodes causing a heterogeneous distribution of the solution resistance and in the double layer capacitance.
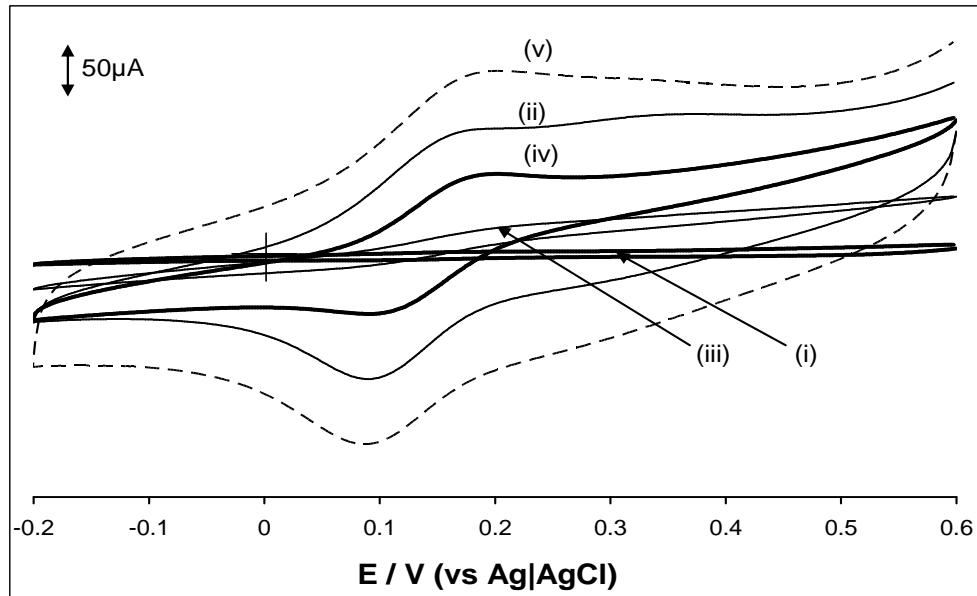
Figure 3.26: (a) Cyclic voltammetric profiles of bare BPPGE (i), BPPGE-*poly*-NiTAPc$_7$ (ii), BPPGE-*poly*-Ni(OH)TAPc$_7$ (iii), BPPGE-SWCNT (iv) and BPPGE-SWCNT-*poly*-NiTAPC$_7$ (v) in K$_4$Fe(CN)$_6$ and K$_3$Fe(CN)$_6$ at 50 mV/s.
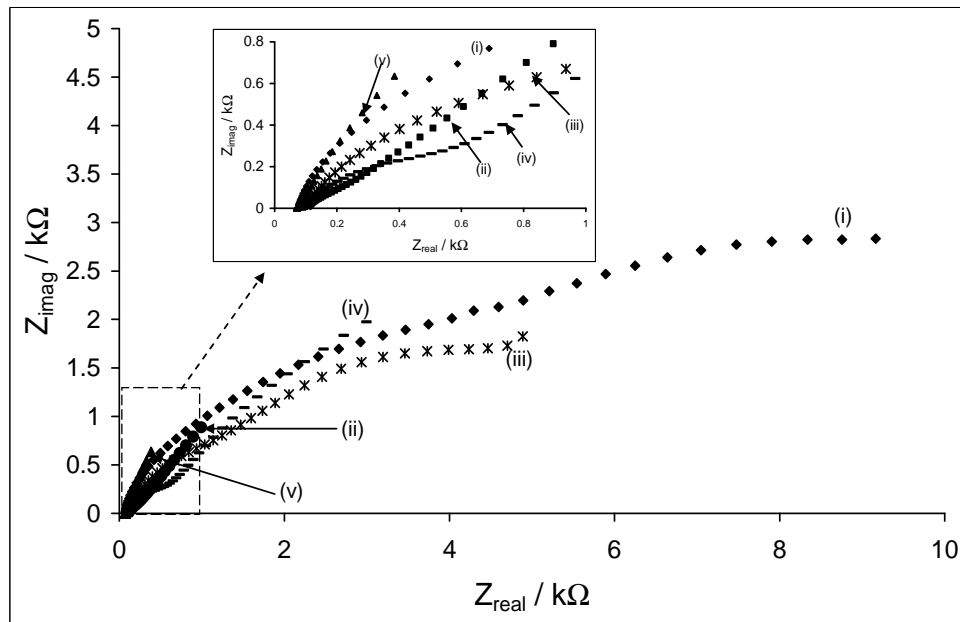
Figure 3.27: Nyquist plots resulting from bare BPPGE (i), BPPGE-*poly*-NiTAPc$_7$ (ii), BPPGE-*poly*-Ni(OH)TAPc$_7$ (iii), BPPGE-SWCNT (iv) and BPPGE-SWCNT-*poly*-NiTAPC$_7$ (v) in K$_4$Fe(CN)$_6$ and K$_3$Fe(CN)$_6$. Scan rate for CV = 50 mV/s. Inset shows the expanded part of the high frequency region.

(a)   (b)
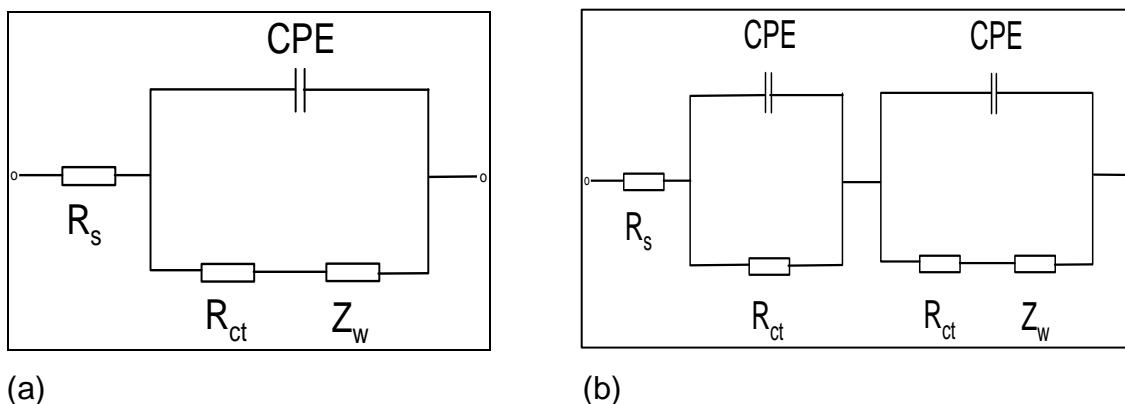
Figure 3.28: The equivalent circuits used to fit the EIS data of the electrodes.

Based on the results, the following equivalent circuits (Figure 3.28) were chosen for fitting the impedance plots of the BPPGE BPPGE-SWCNT-*poly*-NiTAPc$_7$, BPPGE-SWCNT and BPPGE-*poly*-NiTAPc (Figure 3.28 (a))   and BPPGE-*poly*-Ni(OH)TAPc$_7$ (Figure 3.28 (b)). EIS data are summarized in Table 3.4. At the experimental conditions employed in this work, it is clear that electron transport is much faster at the BPPGE-SWCNT-*poly*-NiTAPc$_7$ and slowest at the BPPGE-poly-Ni(OH)TAPc$_7$.

The CPE model for fitting the EIS data was used for reasons mentioned above. The EIS data satisfactorily fitted the chosen equivalent circuits. The high estimated error percentage for the CPE value (17 – 30%) observed in the fitting of the BPPGE, BPPGE-poly-Ni(OH)TAPc and BPPGE-SWCNT is the consequence of the roughness and porosity of these electrodes. As expected for the CPE model, the n values were approximately in the 0.6 – 0.9 range, confirming that the electrodes behave like pseudocapacitors.

TABLE 3.4: Comparative EIS data obtained for the electrodes[a]

Electrode	Electrochemical Impedance Spectral Parameters[a]					
	R_s (Ωcm^2)	CPE (μFcm^{-2})	n	R_{CT} $(k\Omega\ cm^2)$	$10^6\ Z_w$ $(\Omega\ cm^2\ s^{-1/2})$	$10^4\ k_{app}$ $(cm^{-2}\ s^{-1})$
BPPGE	10.05 (7.6)	50.86 (17.3)	0.71 (1.9)	0.864 (5.8)	36.4 (8.0)	3.1 ± 0.2
BPPGE-*poly*-NiTAPc	34.90 (0.2)	229.00 (3.7)	0.87 (0.6)	0.135 (2.3)	186.4 (1.2)	19.7 ± 0.5
BPPGE-*poly*-Ni(OH)TAPc[b]	17.21 (1.1)	11.58 (~35)	0.71 (3.2)	1.097 (~10)	215.3 (1.4)	2.4 ± 2.4
BPPGE-SWCNT	13.25 (3.4)	0.72 (30.2)	0.61 (3.6)	0.130 (10.6)	61.4 (3.3)	20.5 ± 2.2
BPPGE-SWCNT-*poly*-NiTAPc7	14.03 (1.0)	10.51 (9.4)	0.74 (1.4)	0.101 (3.7)	126.8 (1.6)	26.4 ± 1.0

[a] The values in brackets are the estimated errors in percent obtained by fitting the experimental data with the model. [b] Unlike the other electrodes, data were fitted with the equivalent circuit (Figure 3.26 (b)), the k_{app} values were obtained from the R_{CT}.

There are slight variations in the R_{CT} values of BPPGE and SWCNT represented in Tables 3.2 and 3.4. The BPPGE used in these two experiments was cut from different portions of the basal plane pyrolytic graphite slab and the difference in values is a result of the inconsistent surface on the graphite sheet throughout the slab. The contribution of the uneven BPPGEs influences the R_{CT} values. Nevertheless, the general trend of the R_{CT} values remains essentially consistent where: BPPGE-SWCNT-MTAPc < BPPGE-SWCNT < BPPGE-MTAPc < BPPGE.

3.2.2 Electrocatalysis of V-Type Nerve Agents Degradation Products at BPPGE-SWCNT-NiTAPc

Figure 3.29 presents comparative SWV responses of DEAET and DMAET in Figure 3.29 (a) and (b) respectively. In both cases it is clearly observed that BPPGE-SWCNT gave the best electrocatalytic response in terms of current response and less positive peak potential. The electrocatalytic response for both analytes followed the same trend: (iv) BPPGE-SWCNT > (ii) BPPGE-SWCNT-*poly*-NiTAPc > (v) BPPGE-*poly*-NiTAPc > (i) BPPGE confirming the superiority of BPPGE-SWCNT electrode over the other electrodes. The excellent electrocatalytic ability at BPPGE-SWCNT towards the detection of these sulfhydryl degradation products of V-type nerve agents is not surprising, as this electrode performed just as well in the CoTAPc studies above. This however means that the NiTAPc does not in any way assist the SWCNT at BPPGE-SWCNT-*poly*-NiTAPc towards detection of DEAET and DMAET.
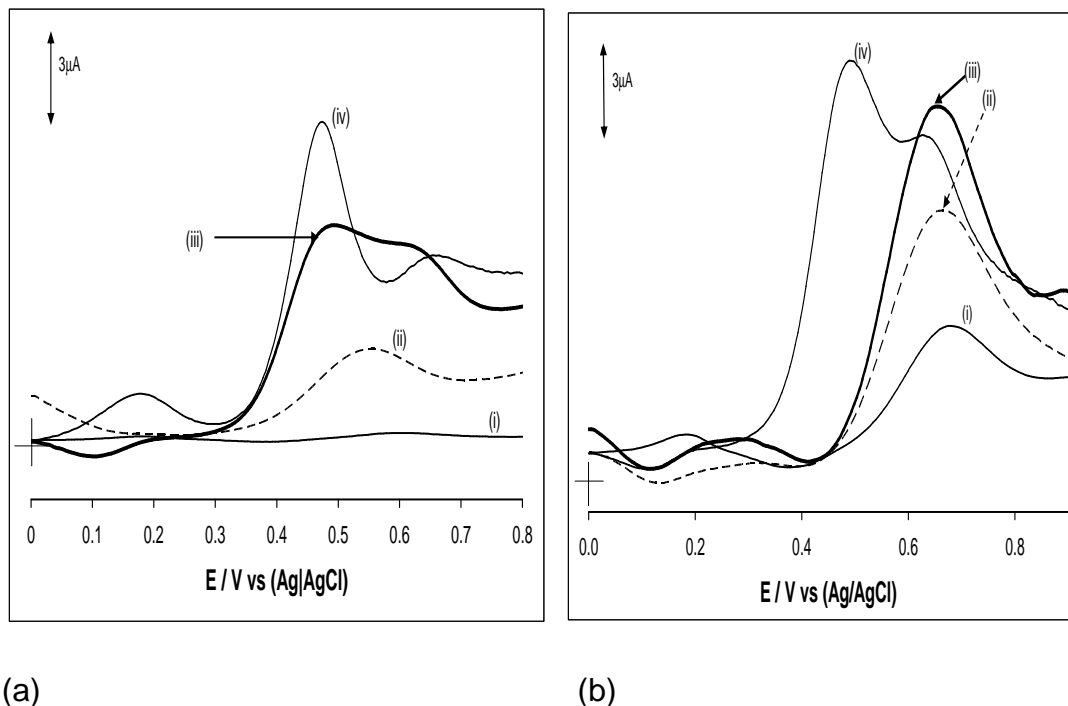
Figure 3.29: SWV profiles illustrating the responses in (a) 10^{-4}M DEAET and (b) 10^{-4}M DMAET solutions of the bare BPPGE (i), BPPGE-*poly*-NiTAPc (ii), BPPGE-SWCNT-*poly*-NiTAPc (iii) and BPPGE-SWCNT (iv).

Nitric Oxide Detection

Although, this is not the main aim of this thesis, the failure of NiTAPc to improve the electrochemical response of DEAET or DMAET prompted me to investigate a well known analyte, nitric oxide (NO), that has been studied with NiTAPc electrode [100]. Figure 3.30 shows the comparative square wave voltammograms for the NO using the different electrodes. The catalytic currents follow the trend: BPPGE-SWCNT-*poly*-NiTAPc$_7$ >> BPPGE-*poly*-Ni(OH)TAPc$_7$ > BPPGE-NiTAPc$_7$ > BPPGE-SWCNT > BPPGE. From the catalytic current responses, it can be implied that SWCNT, by inducing crystalinity onto NiTAPc

electropolymeric film, is able to enhance the electronic communication between *poly*-NiTAPc and the BPPGE.
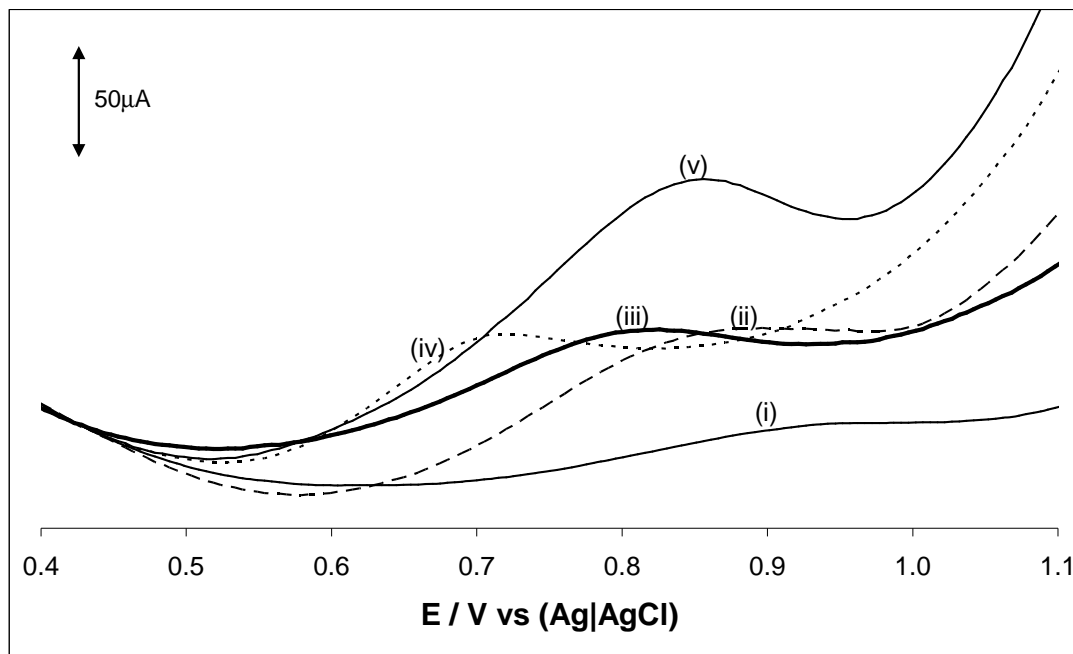
Figure 3.30:   SWV illustrating the responses in 10^{-4}M NO of the bare BPPGE (i), BPPGE-*poly*-NiTAPc$_7$ (ii), BPPGE-*poly*-Ni(OH)TAPc$_7$ (iii), BPPGE-SWCNT (iv) and BPPGE-SWCNT-*poly*-NiTAPC$_7$ (v).

To the best of my knowledge, nickel powder modified BPPGE has never been used in the investigation of V-type nerve agents. This encouraged me to modify the BPPGE with raw nickel to determine conclusively if the nickel impurities found in SWCNT contribute to its electrocatalysis. The next section describes the study with nickel powder modified basal plane pyrolytic graphite electrode (BPPGE-Ni).

3.3 NICKEL POWDER MODIFIED BASAL PLANE PYROLYTIC GRAPHITE ELECTRODE

3.3.1 Particle Size Characterization

Figure 3.31 depicts the particle size distribution of the nickel powder used in this work as determined with the mastersizer instrument. It was found in the range 1.91 – 363.08 µm and the surface weighted mean was 13.19 mm.
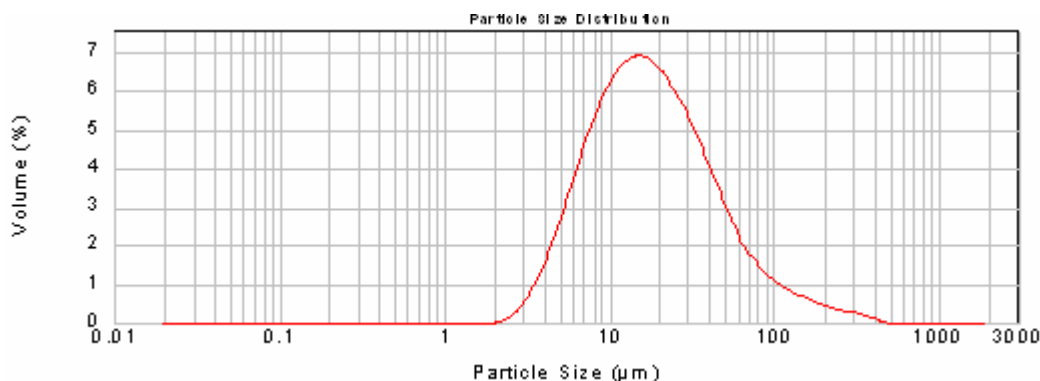
Figure 3.31: Graphical representation of the particle size distribution of nickel powder used in this project.

3.3.2 Cyclic Voltammetric and Impedance Spectroscopic Characterization

Electrochemical impedance spectroscopy technique is employed to investigate the electron transfer properties of the nickel powder modified electrodes [29,142,159,] towards the electrochemistry of the simple redox couple, $[Fe(CN)_6]^{3-}/[Fe(CN)_6]^{4-}$. Figure 3.32 and 3.33 presents the CV profiles and corresponding electrochemical impedance spectral profiles of the, (i) BPPGE, (ii) BPPGE-Ni, (iii) BPPGE-SWCNT, (iv) BPPGE-Ni-SWCNT and (v) nickel disk electrode (Fig. 3.33 only) in a solution of 1 mM of $K_4Fe(CN)_6$ and 1 M $K_3Fe(CN)_6$ (1:1) mixture containing 0.1 M KCl, conducted at the $E_{1/2}$ of the $[Fe(CN)_6]^{3-/4-}$

(0.124 V vs. Ag|AgCl). The well-defined redox couple observed for the BPPGE-Ni (**I**, $E_{1/2}$ = 0.35 V vs. Ag|AgCl) is attributed to the Ni^{II}/Ni^{III} process. The origin of the second couple that occurred around 0.5 V (**II**) cannot be accounted for at this moment but could be due to the one-electron redox process usually occurring with adsorbed nickel species following nickel interaction with the electrolyte [175]. These couples appeared as broad couple in BPPGE-Ni-SWCNT. The CV profile of the nickel disc electrode showed no detectable peak.
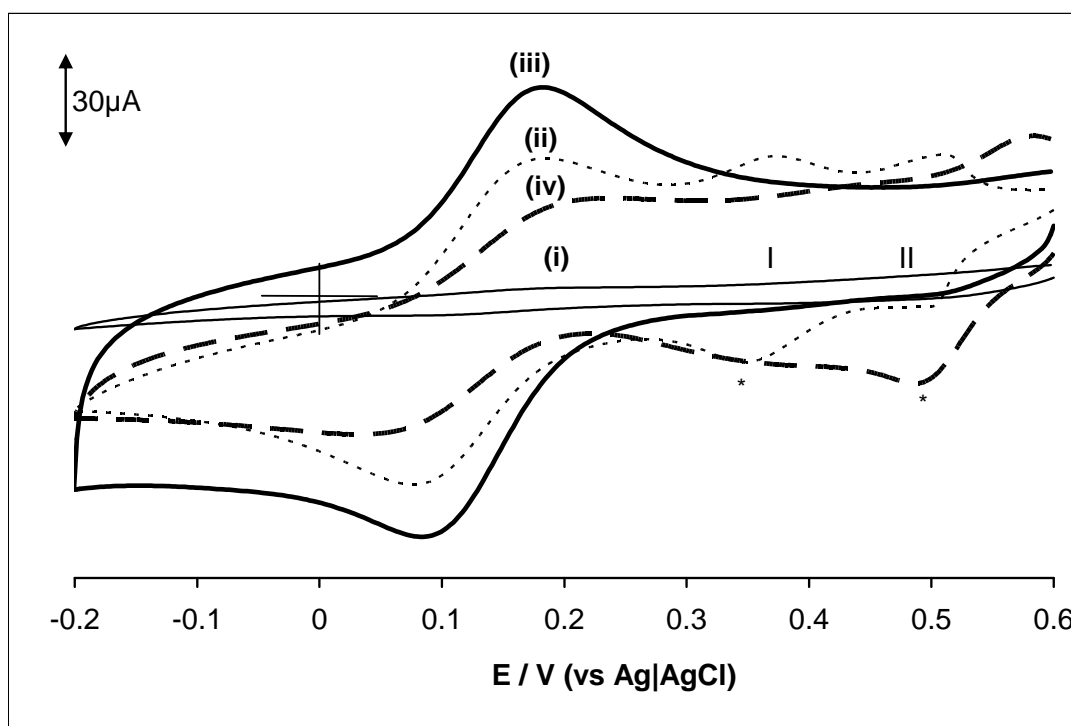
Figure 3.32: CV profiles of $[Fe(CN)_6]^{3-/4-}$ at 50 mV/s of the bare BPPGE (i), BPPGE-Ni (ii), BPPGE-SWCNT (iii) and BPPGE-Ni-SWCNT (iv) in 0.1 M KCl containing equimolar mixture of $K_4Fe(CN)_6$ and $K_3Fe(CN)_6$.

Figure 3.33: Nyquist plots of the bare BPPGE (i), BPPGE-Ni (ii), BPPGE-SWCNT (iii), BPPGE-Ni-SWCNT (iv) and nickel disk electrode (v) in 0.1 M KCl containing equimolar mixture of $K_4Fe(CN)_6$ and $K_3Fe(CN)_6$. Inset presents the Nyquist plots at the high frequency region.

The CPE model was used for reasons mentioned above. Some of the electrodes were best fitted (low percentage errors) by replacing Q with the double layer capacitance (C_{DL}) in the Randles model. The apparent electron transfer constants (k_{app}) were obtained using equation 3.13. It is evident from EIS data (Table 3.5) that at the experimental conditions employed in this work, charge transfer is much faster at the BPPGE-Ni compared to other electrodes. The low R_{CT} and high k_{app} values shown by the BPPGE-Ni over the other electrodes are attributed to the high microscopic surface area of the nickel powder.

TABLE 3.5: Summary of estimated EIS parameters obtained for all electrodes.

Electrode	Impedance Spectral Parameters[a]					
	R_s (Ω cm^2)	CPE (μF cm^{-2})	n	R_{CT} (kΩ cm^2)	10^6 Z_w (Ω cm^2 s$^{-1/2}$)	10^4 k_{app} (cm^{-2} s^{-1})
BPPGE	10.03 (7.63)	0.51 (17.27)	0.71 (1.91)	0.865 (5.77)	36.4 (8.0)	3.08 ±0.18
BPPGE[b]	16.29 (8.65)	5.55 (6.94)	-	0.325 (9.46)	21.79 (8.47)	8.18 ±0.77
Ni-disk electrode	10.75 (1.17)	4.82 (5.44)	0.82 (0.68)	0.220 (1.50)	15.53 (1.86)	12.09±0.70
BPPGE-SWCNT[b]	18.43 (3.44)	16.44 (7.47)	-	0.042 (7.99)	67.12 (3.38)	63.33±5.06
BPPGE-Ni[b]	17.09 (0.93)	132.19 (3.47)	-	0.025 (4.12)	188.79 (1.6)	106.40±2.38
BPPGE-Ni-SWCNT	12.45 (1.38)	11.68 (8.56)	0.81 (1.32)	0.139 (3.43)	104.88 (2.1)	19.14±0.66

[a] The values in brackets are the estimated errors in percent obtained by fitting the experimental data with the model.
[b] The values were obtained by replacing Q with C_{DL} in circuit description.

The comparative Bode plots of phase angle vs. log f (Figure 3.34) showed well-defined symmetrical peaks at different maxima for the different electrodes, corresponding to the different relaxation processes of the electrode/solution interfaces. For example, the BPPGE-Ni/solution relaxation process shifted to 30° at 31.6 Hz upon modification of the BPPGE compared to the bare BPPGE value of ~56° at 501 Hz. In all cases, the phase angles were less than the 90° expected, thus confirming the pseudo-capacitive nature of the electrodes. As mentioned earlier, Z_w and R_s should not be affected by the modification of the electrode surface. Within the limits of errors, the values of R_s in Table 3.5 are not significantly different; they are in the same magnitude, indicating that ohmic resistance of the solutions was not significantly affected by any modification of the electrode surface. As per the reasons mentioned in a recent report by Yang and Li [145] for the fluctuation in Z_w values there is an increase in Z_w between the bare electrodes and the modified electrodes.

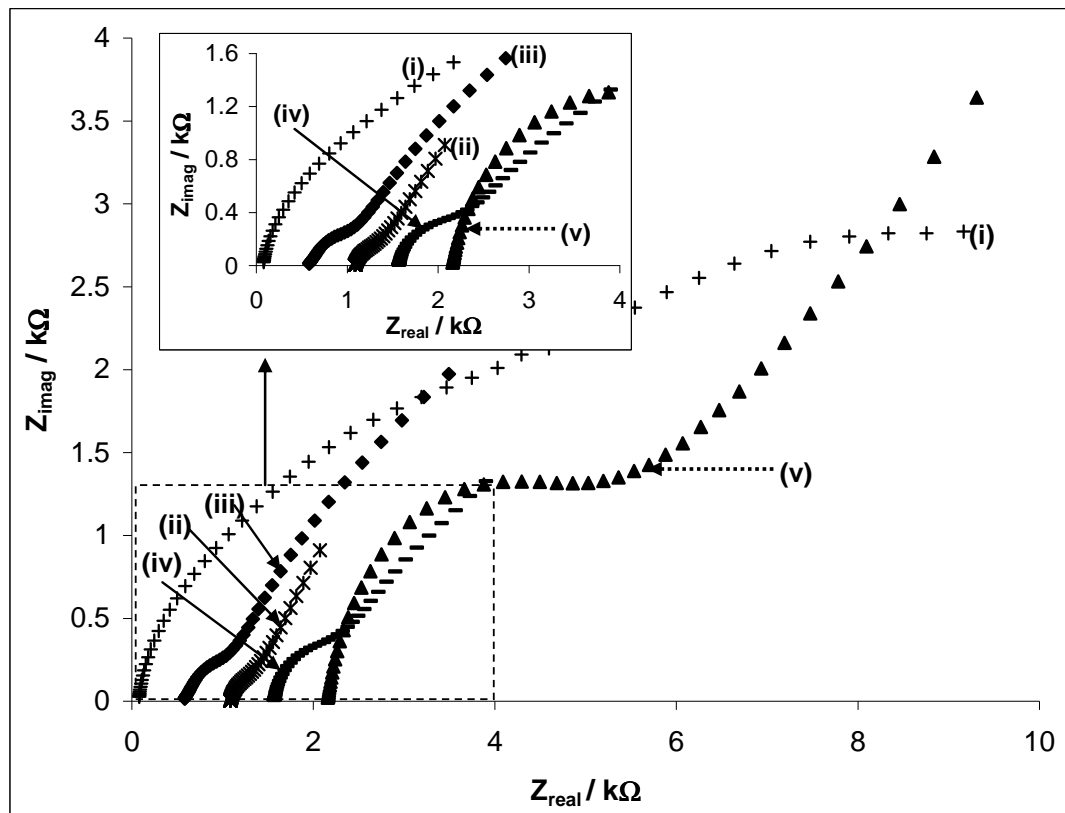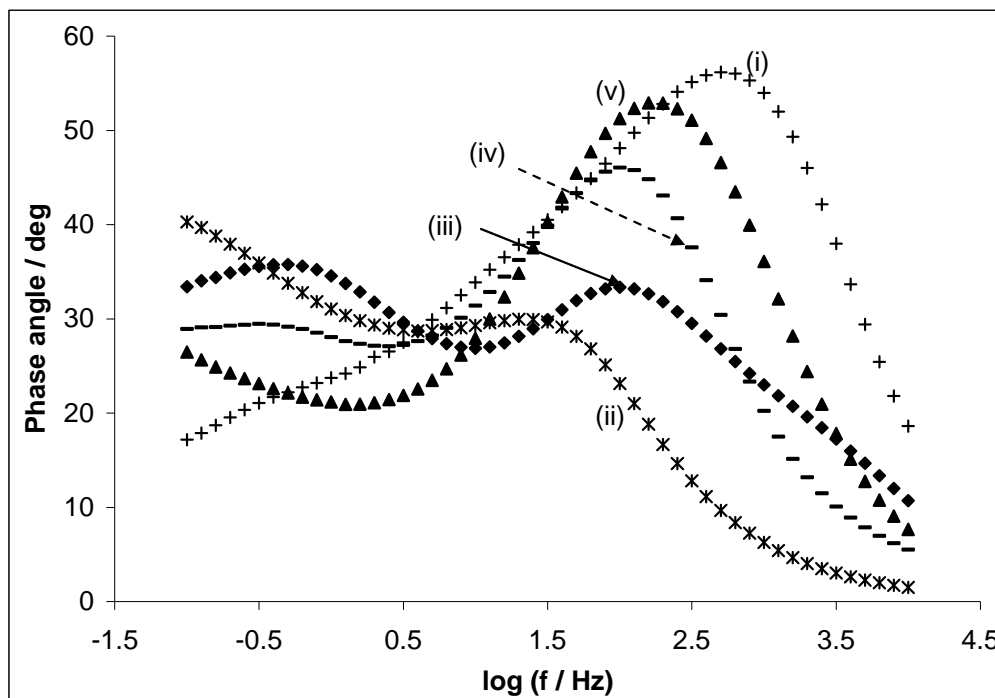**Figure 3.34:** Bode plots of the bare BPPGE (i), BPPGE-Ni (ii), BPPGE-SWCNT (iii) and BPPGE-Ni-SWCNT (iv) and nickel disc electrode (v) in 0.1 M KCl containing equimolar mixture of $K_4Fe(CN)_6$ and $K_3Fe(CN)_6$.

3.3.3 Electrocatalytic Behaviour Towards DEAET and DMAET using Different Electrodes

As mentioned previously, DEAET and DMAET gave the best response at alkaline (pH $\geq$ 9.0) conditions, thus all studies for these analytes were carried out at pH 9.3. Figure 3.35 presents comparative square wave voltammetric responses of the various electrodes towards the detection of DEAET in PBS (pH 9.3). It is clearly observed that BPPGE-Ni gave the best electrocatalytic response in terms of current response and the lowest positive peak potential.
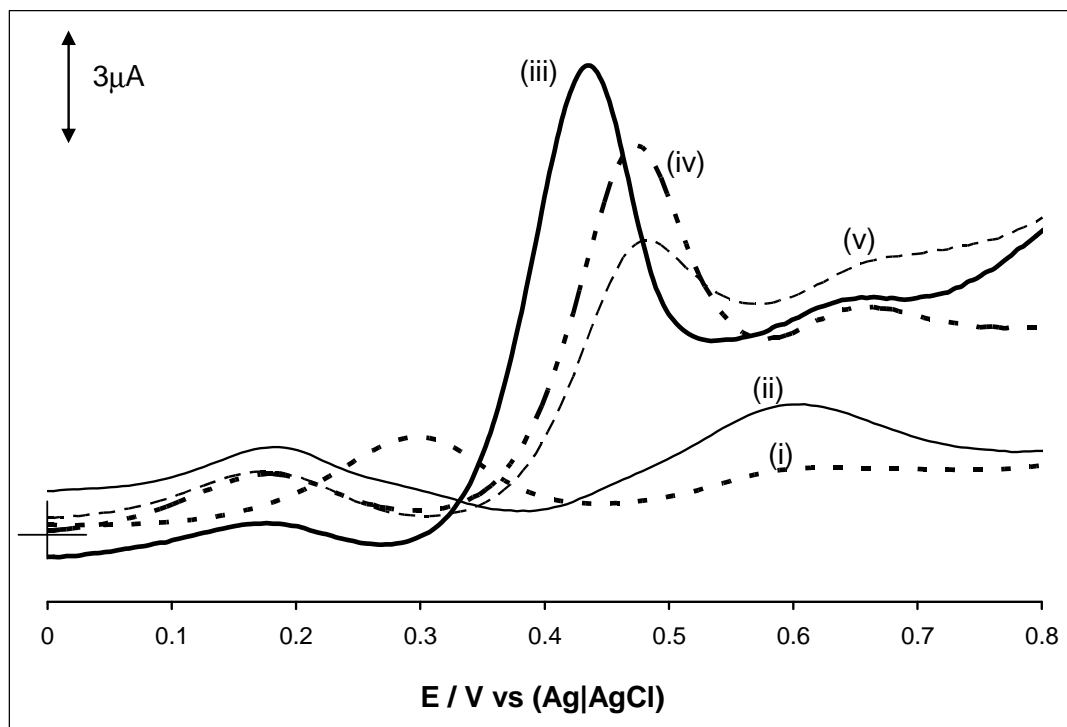
Figure 3.35: SWV illustrating the response of the nickel disc electrode (i), bare BPPGE (ii), BPPGE-Ni (iii), BPPGE-SWCNT (iv) and BPPGE-Ni-SWCNT (v) in 10^{-4} M DEAET in pH 9.3 PBS.

Similar results were obtained for the DMAET. In summary, for both analytes the electrocatalytic response follows the trend: BPPGE-Ni > BPPGE-SWCNT $\approx$ BPPGE-Ni-SWCNT > BPPGE > Ni electrode. The R_{CT} values for the DEAET (at 10^{-4} mol/L) followed same trend: BPPGE-Ni (2.3 kΩ) < BPPGE-SWCNT (3.2 kΩ) < BPPGE-Ni-SWCNT (3.5 kΩ) < BPPGE (4.3 kΩ) $\approx$ Nickel disc electrode (4.3 kΩ). The superiority of BPPGE-Ni electrode over the other electrodes for the detection of these analytes is interesting as this represents the first of such observation for sulfhydryl degradation products of V-type nerve agents. Clearly, the nickel disc electrode showed insignificant current response,

thus suggesting the great impact of the high microscopic surface area of the nickel powder on the catalytic activity of these analytes. The peaks at 0.3 V for the nickel disc electrode and 0.18 V for the other electrodes can be attributed to the redox processes of these electrodes in the electrolytes conditions employed in this study. The mechanistic pathways for Ni powder mediated electrocatalysis for DEAET and DMAET are assumed to involve Ni^{II}/Ni^{III} redox process and possibly follow the same trend as for equations 3.14 – 3.18.

3.3.4 Chronoamperometric Analysis

Chronoamperometric analysis exemplified in Figure 3.37 was employed in the electrocatalytic detection of DEAET and DMAET at the BPPGE-Ni. The diffusion coefficient (D) and the catalytic rate constant (k) were determined using equations 1.9 and 1.10, respectively, at constant concentration of 10^{-4} M and a potential of +410 mV (vs. Ag|AgCl) for both DEAET and DMAET in pH 9.3 PBS. From the slopes of the plots of I_{cat}/I_L vs. $t^{1/2}$ the values of k were found to be 1168 M^{-1} s^{-1} and 1558 M^{-1} s^{-1} for DEAET (Figure 3.38(a)) and DMAET, respectively. The electrocatalytic oxidation of these analytes is slightly faster using BPPGE-Ni rather than SWCNT-CoTAPc films indicative from their larger k values. This research is the first to provide detailed electrocatalytic parameters.
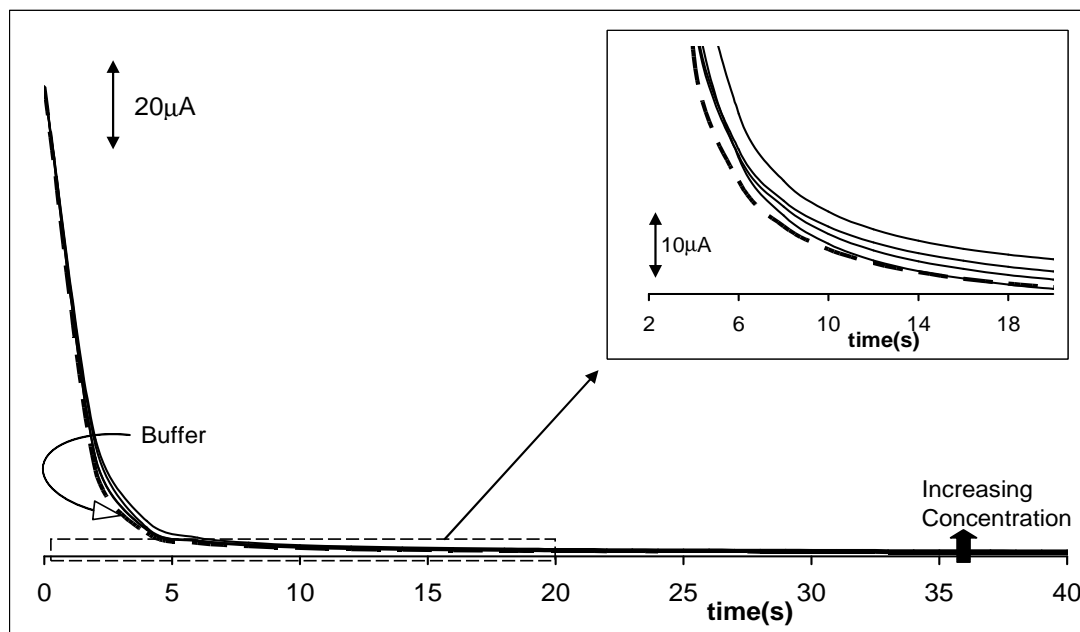
Figure 3.36: A Typical Chronoamperometric profile analysis of DMAET at a BPPGE-Ni with a potential of 0.410 V. Inset showing amplified time region for catalytic rate constant and diffusion coefficient calculations. Concentration: Buffer, 10^{-9}, 10^{-8}, 10^{-7}, 10^{-5}M (inner to outer as shown by arrow).
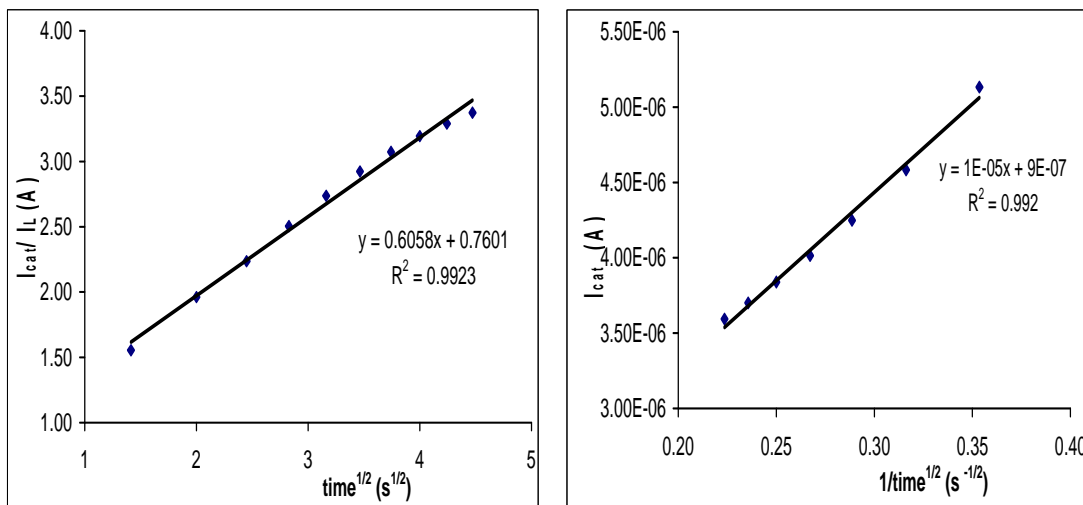
(a)   (b)

Figure 3.37: Plots of (a) I_{cat}/I_L vs. $t^{1/2}$ and (b) I_{cat} vs. $1/t^{1/2}$ resulting from chronoamperometric data of DEAET at a BPPGE-Ni with a potential of 0.410 V (vs. Ag|AgCl).

Table 3.6 presents a comparative analytical data in terms of linear concentration range (LCR), sensitivity (slope) and limits of detection (LoD). All data were obtained with the same electrode, rinsing the electrode before each concentration. When compared to the presently available literature reports on the electrocatalytic detection of these analytes as shown in Table 3.6, it is evident that the results for BPPGE-Ni and BPPGE-SWCNT-CoTAPc are comparable, in terms of detection limit and sensitivity, to the presently available reports on the detection of DMAET and DEAET. Indeed, the BPPGE-Ni proposed here is simpler and less costly to make since it does neither requires the use of enzyme [175], nor cocktails of costly redox-active electropolymers [133, 134], nor the employment of laser-induced fluorescence obtained only after tedious and time-consuming derivatization steps to convert the sulfhydryls to isonindole derivatives by chemical reactions with amino acids and *o*-phthaldialdehyde [103].

TABLE 3.6: Comparative analytical data for sulfhydryl degradation products of the V-type nerve agents, DMAET and DEAET, obtained from different modified electrodes.

V-Type Nerve Agents	Analytical Parameter	Modified Electrode[a]				
		BPPGE-Ni[b]	BPPGE-SWCNT-CoTAPc[c]	SPE- MWCNT-OPH[d]	MCE-EC [e]	GCE-PPy-PQQ[f]
DMAET	Ep	0.41 V	0.73 V	0.8 V	0.5 V	0.38 V
	Electrolyte	pH 9.3 PBS	pH 9.3 PBS	pH 9.45 STB/SDS	pH 7.4 PBS	pH 4 or 9.0 with 0.1M CaCl$_2$
	LCR	10^{-8} -10^{-4} M	8^{-6} – 1.5^{-4} M	Up to 250 µM	~1 – 30 µM	6 – 147 µM
	Sensitivity	2.3 x10^{-2} A/M	5.0x10^{-2} A/M	0.062 µA/mM	52.8 µA/mM	1.18 nA/µM cm^2
	LoD	9.0 µM	8.0 µM	5.0 µM	2.0 µM	4.5 µM
DEAET	Ep	0.41 V	0.64 V	0.8 V	0.5 V	0.38 V
	Electrolyte	pH 9.3 PBS	pH 9.3 PBS	pH 9.45 STB/SDS	pH 7.4 PBS	pH 4 or 9.0 with 0.1M CaCl$_2$
	LCR	10^{-8} -10^{-4} M	8^{-6} – 1.5^{-4} M	Up to 250 µM	~1 – 30 µM	5.8 – 100 µM
	Sensitivity	2.3 x10^{-2} A/M	6.0x10^{-2} A/M	0.036 µA/mM	59.7 µA/mM	1.37 nA/µM cm^2
	LoD	4.0 µM	3.0 µM	8.0 µM	0.8 µM	3.0 µM

[a]All reference electrodes were reported against Ag|AgCl wire with the exception of the GCE-PPy-PQQ which was reported against Ag|AgCl (3M KCl). PBS = Phosphate buffered solution, [b&c]This work; [d][30] ,Screen-printed carbon electrode modified with multi-walled carbon nanotube and organophosphorus hydrolase; [e][31], microchip capillary electrophoresis with electrochemical detection; [f][3], glassy carbon electrode modified with poplypyrrole and pyrroloquinoline quionone. STB = sodium tetraborate; SDS = sodium dodecyl sulphate.

3.3.5 Electrode Stability

Figure 3.38 presents an example of the stability study the BPPGE-Ni electrode, using different scans at constant concentration of DEAET (10^{-4} mol/L) in PBS (pH 9.3).
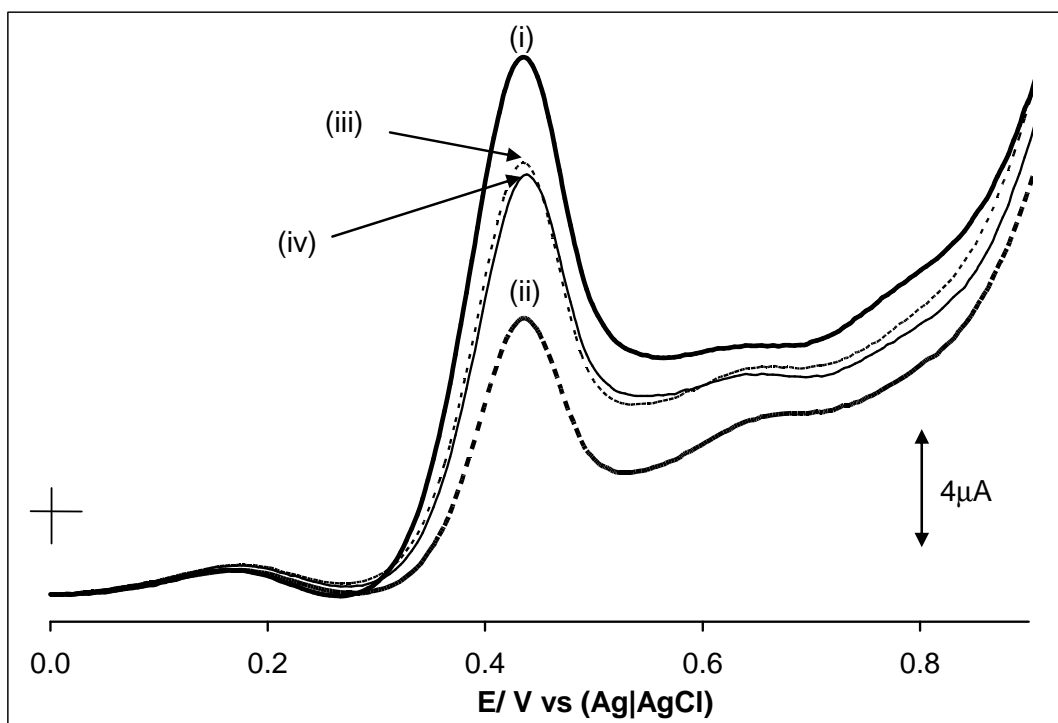
Figure 3.38: SWV illustrating the behaviour of the BPPGE-Ni in 10^{-4} M DEAET during first scan (i), second scan (ii) and after washing in pH 9.3 PBS (iii and iv).

There was a dramatic decrease (*ca.* 50 %) in peak current (ii) after the initial scan (i), which is a typical behaviour for a poisoned electrode. However, on rinsing the electrode in a fresh electrolyte solution (pH 9.3 PBS) and repeating the experiment, about 70% of the initial catalytic current was obtained (iii) indicating partial recovery of the electrode surface. Interestingly, this recovered 70% peak current remained stable after several experiments. This result suggests that the electrodes exhibit satisfactory features of reusability, but could

be more useful for the development of economical, single shot disposable sensors as in screen-printed electrode.

CONCLUSION

AND

RECOMMENDATIONS

CONCLUSION

This thesis essentially describes the electrocatalytic properties of SWCNT and SWCNT functionalized with metallotetraaminophthalocyanine (MTAPc, M = Co and Ni) complexes, and nickel powder on BPPG electrode towards the detection of degradation products of V-type nerve agents. The strong π-π interactions between MTAPc and the SWCNTs are assumed to be responsible for the remarkable electrosorption or electropolymerization processes of MTAPc onto BPPGE-SWCNT surface. The following important results obtained in this work should be emphasised:

(i)   SWCNT clearly enhances both the solution and surface electrochemistry of CoTAPc, which is the first of such observation.

(ii)   The synthesis of SWCNT-CoTAPc by physical attachment produced comparable products to those chemically synthesized, establishing an innovative and cost efficient means of production for this hybrid.

(iii)   BPPGE-SWCNT-CoTAPc$_{(mix)}$ and BPPGE-SWCNT showed comparable electrocatalytic responses towards the detection of sulfhydryl hydrolysis products of V-type nerve agents.

(iv)   BPPGE-SWCNT-CoTAPc showed better peak potential discrimination for the detection of these sulfhydryl analytes than the BPPGE-SWCNT.

(v)   Unlike CoTAPc and nickel powder, NiTAPc did not show detectable catalysis towards DEAET and DMAET.

(vi) Detailed electrocatalytic parameters (rate constants, diffusion coefficients) were provided for the first time for these analytes.

(vii) The results showed excellent analytical data (LCR, LoD, sensitivity) when compared to known electrodes.

(viii) When compared to the distinguished electrodes and detection protocols reported in the literature, BPPGE-Ni exhibits more promising features required for a simple, fast and less expensive electrode for the detection of V-type nerve agents, DMAET and DEAET.

(ix) The nickel impurity in the SWCNT did not show any detectable impact on the electron transfer kinetics or electrocatalytic features which was evident from the electron transfer of the BPPGE-Ni being faster than that of the BPPGE-SWCNT.

(x) SWCNT-confined on the basal plane pyrolytic graphite electrode induces crystallinity on the NiTAPc electropolymeric film and significantly affects the redox properties of the NiTAPc film, notably the sensing of nitric oxide.

(xi) Generally, SWCNT can be integrated to the MTAPc complexes forming potentially useful redox-active hybrids for numerous catalytic and sensing applications.

(xii) Generally to reduce errors of reproducibility the same electrode was used per experiment and the trend of the electrocatalytic current response is consistent for these experiments.

RECOMMENDATIONS

- Similar studies will be conducted using different aminosubstituted metallophthalocyanines and related complexes such as the metalloporphyrins.

- Other analytes and neurotoxins should be investigated using these modified electrodes.

- CNT has two favourable reactive sites (basal plane and edge plane), therefore, future investigations should be conducted using the edge plane pyrolytic graphite electrode (EPPGE) for similar experiments to compare the results of EPPGE and the BPPGE.

REFERENCES

1. E.W. Hooijschuur, A. Hulst, A. de Long, L. de Reuver, S. van Krimpen, B. van Baar, E. Wils, C. Kientz, U.A. Brinkman, *Trends Anal. Chem.* 21 (2002) 116.

2. Y. Yang, *Acc. Chem. Res.* 32 (1999) 109.

3. J. Wang, J. Zima, N. S. Lawrence, M. P. Chatrathi, *Anal. Chem.* 76 (2004) 4721.

4. C.M. Harris, *Anal.Chem.* 74 (2002) 126A.

5. A. E. Kaifer, M. Gómez-Kaifer, *Supramolecular Electrochemistry*, Wiley-VCH, New York, 1999.

6. J. Wang, *Analytical Electrochemistry*, VCH Publishers Inc., New York, 1994.

7. J J.T. Maloy in: P.T. Kissinger and W. R. Heineman (Eds.), *Laboratory Techniques in Electroanalytical Chemistry*, Marcel Dekker Inc., New York, 1996, Chapter 20.

8. K. B. Prater, A. J. Bard, *J. Electrochem. Soc.* 117 (1970) 207.

9. V. J. Puglisi, A. J. Bard, J. *Electrocem. Soc.* 119 (1972) 833.

10. A.J. Bard, L.R. Faulkner, *Electrochemical Methods: Fundamentals and Applications, 2nd ed.*, John Wiley & Sons, Hoboken, NJ, 2001.

11. F. M. Hawkridge in: P. T. Kissinger and W. R. Heineman (Eds.), Laboratory Techniques in *Electroanalytical Chemistry* 2nd ed., Marcel Dekker Inc., New York, 1996.

12. D.B. Hibbert, *Introduction to Electrochemistry*, Macmillan, London, 1993.

13. J. E. B. Randles, *Trans. Faraday Soc.* 44 (1948) 327.

14. P.A. Christenson, A. Hamnet, *Techniques and Mechanisms in Electrochemistry*, 1st ed., Blackie Academic and Professional, London, 1994.

15. R. S. Niccholson, *Anal. Chem.* 37 (1965) 1351.

16. E. R. Brown, R. F. Large in: A. Weissberger and B. Rossiter (Eds.), *Physical Methods of Chemistry. Electrochemical Methods Vol.1-Part IIA*, Wiley-Interscience, New York, 1971.

17. G. C. Barker, I. L. Jenkins, *Analyst* 77 (1952) 685.

18. J. Wang, D.B.Luo, P.A.M. Farias, J.S. Mahmoud, *Anal. Chem.* 57 (1985) 158.

19. J.G. Osteryoung, *Acc. Chem. Res.* 26 (1993) 77.

20. M.H. Pournaghi-Azar, R. Sabzi, *J. Electroanal. Chem.* 543 (2003) 115.

21. P. Santhosh, K.M. Manesh, K.-P. Lee, A.I. Gopalan, *Electroanalysis* 18 (2006) 894.

22. K.M. Manesh, P. Santhosh, A.I. Gopalan, K.-P. Lee, *Electroanalysis* 18 (2006) 1564.

23. M. Sekota, T. Nyokong, *Polyhedron* 16 (1997) 3279.

24. S. Vilakazi, T. Nyokong, *Polyhedron* 19 (2000) 229.

25. J. Limson, T. Nyokong, *Electroanalysis* 9 (1997) 255.

26. K. I. Ozoemena, T. Nyokong, D. Nkosi, I. Chambrier, M. J. Cook, *Electrochim. Acta* 52 (2007) 4132.

27. B. Agboola, T. Nyokong, *Talanta* 72 (2007) 691.

28. M. Isaacs, M.J. Aguirre, A. Toro-Labbé, J. Costamagna, M. Páez, J. H. Zagal, *Electrochim. Acta* 43 (1998) 1821.

29. J. R. Macdonald, W. B. Johnson in: E. Barsoukov, J. R. Macdonald (Eds.), *Impedance Spectroscopy, 2nd ed.*, John Wiley and Sons Inc., 2005.

30. K.A. Joshi, M. Prouza, M. Kum, J. Wang, J. Tang, R. Haddon, W. Chen, A. Mulchandani, *Anal. Chem.* 78 (2006) 331.

31. O.V. Shulga, C. Palmer, *Anal. Bioanal. Chem.* 385 (2006) 1116.

32. S. Krause in: A.J. Bard, M. Stratmann, P.R. Ulwin (Eds.), *Instrumentation and Electroanalytical Chemistry* Vol.3, Wiley-GmbH & Co., 2003.

33. P. Agarwal, M. E. Orazem, L.H. G-Rubio, *J. Electrochem. Soc.* 142 (1995) 4159.

34. M.A.C. Brett, A.M. O. Brett, *Electrochemical Principles, Methods and Applications*, Oxford University Press, New York, 1993.

35. P. Westbroek, G. Priniotakis, P. Kiekens, *Analytical Electrochemistry in Textiles*, Woodhead Publishing Ltd. and CRC Press LLC, Cambridge England, 2005.

36. IUPAC Recommendation, 1997, *Pure and Appl. Chem.* 69 (1997) 1317.

37. R. F. Lane, A. T. Hubbard, *J. Phys. Chem.* 77 (1973) 1401.

38. C. M. Elliot, R. W. Murray, *Anal. Chem.* 48 (1976) 1247.

39. C. R. Martin, C. A. Foss Jr. in: P. T. Kissinger and W. R. Heineman (Eds.), *Laboratory Techniques in Electroanalytical Chemistry* 2nd ed., Marcel Dekker Inc., New York, 1996.

40. A. J. Bard, *J. Chem. Ed.* 60 (1983) 303.

41. J.J. Gooding, D.B. Hibbert, *TrAC* 18 (1999) 52.

42. B. F. Watkins, J. R. Behling, E. Kariv, L. L. Miller, *J. Am. Chem. Soc.* 97 (1975) 3549.

43. L. N. Netzer, J. Sagiv, *J. Am. Chem. Soc.* 105 (1983) 674.

44. Z. Chen, Y. Zhou, *Surface & Coatings Technology* 201 (2006) 2419.

45. C. Deng, M. Li, Q. Xie, M. Liu, Y. Tan, X. Xu, S. Yao, *Anal. Chim. Acta* 557 (2006) 85.

46. N. Diab, J. Oni, W. Schuhmann, *Bioelectrochemistry* 66 (2005) 105.

47. S. Pyun, J-S. Bae, *Journal of Power Sources* 68 (1997) 669.

48. C. Sivakumar, J-N. Nian, H. Teng, *Journal of Power Sources* 144 (2005) 295.

49. E. Mun˜oz, M. A. Heras, A. I. Colina, V. Ruiz, J. Lo´pez-Palacios, *Electrochimica Acta* 52 (2007) 4778.

50. C. E. Banks and R. G. Compton, *Analyst* 131 (2006) 15.

51. N. S. Lawrence, R. P. Deo and J. Wang, *Anal. Chim. Acta* 517 (2004) 131.

52. A. Salimi, R. Hallaj and G.-R. Khayatian, *Electroanalysis* 17 (2005) 873.

53. A.W. Snow and W.R. Barger in A.P.B. Lever and C.C. Leznoff (Eds.), *Phthalocyanines: Properties and Applications Vol 1,* VCH Publishers, New York 1989.

54. M. Musameh, J. Wang, A. Merkoci and Y. Lin, *Electrochem. Commun.* 4 (2002) 743.

55. S. Iijima, *Nature* 354 (1991) 56.

56. S. Iijima and T. Ichihashi, *Nature* 363 (1993) 603.

57. A. Thess, R. Lee, P. Nikolaev, H. Dai, P. Petit, J. Robert, C. Xu, Y. H. Lee, S. G. Kim, A. G. Rinzler, D. T. Colbert, G. E. Scuseria, D. Tomane´k, J.E. Fischer, R.E. Smalley, *Science* 273 (1996) 483.

58. M. J. Yacaman, M. M. Yoshida, L. Rendon, J. G. Santiesteban, *Appl. Phys. Lett.* 62 (1993) 202.

59. C. P. Poole Jr. and F. J. Owens, *Introduction to Nanotechnology*, John Wiley and Sons Inc., Hoboken, New Jersey 2003.

60. T. W. Ebbesen and P.M. Ajayan, *Nature* 358 (1992) 220.

61. Y.-H. Yun, V. Shanov, M.J. Schulz, S. Narasimhadevara, S. Subramaniam, D. Hurd, F.J. Boerio, *Smart Mater. Struct.* 14 (2005) 1526.

62. The Nanotube site: http://nanotube.msu.edu:05/02/07

63. T. Hasobe, S. Fukuzumi, P. V. Kamat, *J. Am. Chem. Soc.* 127 (2005) 11884.

64. J. Kong, N. R. Franklin, C. Zhou, M. G. Chapline, S. Peng, K. Cho, H. Dai, *Science* 287 (2000) 622.

65. W. B. Choi, E. Bae, D. Kang, S. Chae, B.-H. Cheong, J.-H. Ko, E. Lee, W. Park, *Nanotechnology* 15 (2004) 512.

66. K. Tsukagoshi, N. Yoneya, S. Uryu, Y. Aoyagi, A. Kanda, Y. Ootuka, B. W. Alphenaar, *Phys. B: Condens. Matter* 323 (2002) 107.

67. J. A. Rojas-Chapana, M. J. Giersig, *J. Nanosci. Nanotechnol*ogy 6 (2006) 316.

68. S. K. Smart, A. I. Cassady, G. Q. Lu, D. J. Martin, *Carbon* 44 (2006) 1034.

69. A. Bianco, K. Kostarelos, M. Prato, *Curr. Opin. Chem. Biol.* 9 (2005) 674.

70. C. E. Banks, R. R. Moore, T. J. Davies, R. G. Compton, *Chem. Commun.* (2004) 1804.

71. D. H. Robertson, D. W. Brenner, J. W. Mintmire, *Phys. Rev.* B 45 (1992) 12592.

72. G. Che, B. B. Lakshmi, E. R. Fisher, C. R. Martin, *Nature* 393 (1998) 346.

73. B. Gao, A. Kelinhammes, X.P. Tang, C. Bower, Y. Wu, O. Zhou, *Chem. Phys. Lett.* 307 (1999) 153.

74. A. C. Dillon, K. M. Jones, T.A. Bekkendahl, C. H. Kiang, D. S. Bethune, M. J. Heben, *Nature* 386 (1997) 377.

75. A. Bachtold, P. Hadley, T. Nakanishi, C. Dekker, *Science* 294 (2001) 1317.

76. P. C. Collins, M. S. Arnold, P. Avouris, *Science* 292 (2001) 706.

77. G. Hanraham, D. G. Patil, J. Wang, *J. Environ. Monit.* 6 (2004) 657.

78. P. J. Britto, K. S. V. Santhanam, P. M. Ajayan, *Bioelectronics and Bioenergetics* 41 (1996) 121.

79. P. J. Britto, K. S. V. Santhanam, A. Rubio, J. A. Alonso, P. M. Ajayan, *Advanced Mater* 11 (1999) 154.

80. J. J. Davis, R. J. Coles, H. A. O. Hill, *J. Electroanal. Chem.* 440 (1997) 279.

81. J. K. Campbell, Li. Sun and R. M. Crooks, *American Chem. Soc.* 121 (1999) 3779.

82. J. Wang, M. Li, Z. Shi, N. Li, Z. Gu, *Electrochim. Acta* 47 (2001) 651.

83. R.J. Chen, Y. Zhang, D.Wang, H. Dai, *J. Am. Chem. Soc.* 123 (2001) 3838.

84. G. de la Torre, W. Blau, T. Torres, *Nanotechnology* 14 (2003) 765.

85. X. Wang, Y. Liu, W. Qiu, D. Zhu, *J. Mater. Chem.* 12 (2002) 1636.

86. N.B. Mckeown in: *Phthalocyanine Materials: Synthesis, Structure and Function. Chemistry of Solid State Materials*, Cambridge University Press, New York, 1998.

87. A. W. Snow in: C.C. Leznoff and A.B.P. Lever (Eds.), *Phthalocyanines: Properties and Applications*, VCH Publishers, New York, Vols. 1-4, 1993.

88. R. P. Linstead, *J. Chem. Soc.* (1934) 1016.

89. J. M. Robertson and I. Woodward, *J. Chem. Soc.* (1936) 219.

90. R.P.Linstead, *J.Chem. Soc.* (1936) 1195.

91. P. Gregory, J. *Porphrins and Phthalocyanines* 3 (1999) 468.

92. R.P. Linstead, A.R. Lowe, *J.Chem. Soc.* (1934) 1022.

93. M. Hanack, P.Haisch, H. Lehman, *Synthesis* (1993) 387.

94. T. Nyokong, M. J. Stillman in: A.P.B. Lever and C.C. Lensnoff (Eds.),
    Phthalocyanine: Properties and Applications Vol.1, VCH Publishers, New
    York, 1993.

95. M. Thamae and T. Nyokong, *J. Electroanal. Chem.* 470 (1999) 126.

96. E. Ben-Hur and I. Rosenthal, *Int. J. Radiat. Biol.* 47 (1985) 145.

97. D. Phillips, *Pure Appl. Chem.* 67 (1995) 117.

98. Y. Lu, R. G. Reddy, *Electrochim. Acta* 52 (2007) 2562.

99. N. Martz, C. Roth, H. Fueb, *J. Appl. Electrochem.* 35 (2005) 85.

100. K.I. Ozoemena, T. Nyokong, in: C. A Grimes, E.C. Dickey, M.V. Pishko,
     (Eds.), *Encyclopedia of Sensors Vol.3, Chapter E, pp.157 – 200*, American
     Scientific Publishers, California, 2006.

101. P. Vasuvedan, N. Poughat, A.K. Shuklat, *Appl. Organomet. Chem.* (1996)
     591.

102. A. Salimi, C. E. Banks, R. G. Compton, *Analyst* 129 (2004) 225.

103. M.P. Siswana, K.I. Ozoemena, T. Nyokong, *Electrochim. Acta* 52 *(*2006*),*
     114.

104.   X. Lo´pez, M.Be´nard, M-M Rohmer, *Journal of Molecular Structure: THEOCHEM* 777 (2006) 53.

105.   Y.G. Lee, T.-C. Chou, *Electroanalysis* 15 (2003) 1589

106.   D. Giovanelli, N.S. Lawrence, S. J. Wilkins, L. Jiang, T.G. J. Jones, R.G. Compton, *Talanta* 16 (2003) 211.

107.   I. Bianchi, E. Guerrini, S.Trasatti, *Chem. Phys.* 319 (2005)192.

108.   R.P. Deo, N.S. Lawrence, J. Wang, *Analyst* 129 (2004) 1076.

109.   Y.G. Lee, T.-C. Chou, *J. Electrochem. Soc.* 12 (2005) H53.

110.   C.E. Banks, A. Crossley, C. Salter, S.J. Wilkins and R.G. Compton, *Angew. Chem. Intl. Ed.* 45 (2006) 2533.

111.   Y.-L. Li, Kinloch, A. Ian, M.S. P. Shaffer, C. Singh, J. Geng, B.F.G. Johnson, A. H.   Windle, *Chem. Mater.* 16 (2004) 5637.

112.   C.A. Gervasi, P.E. Alvarez, M.V. Fiori Bimbi, M.E. Folquer, *J. Electroanal. Chem.* 601 (2007) 194.

113.   P.E. Alvarez, S.B. Ribotta, M.E. Folquer, C.A. Gervasi, J.R. Vilche, *Corros. Sci.* 44 (2002) 49.

114.   J. B. Hudson, *Surface Science: An Introduction*, John Wiley & Sons, New York, 1998.

115.   M.H. Kibel, in: D. J. O'Connor, B.A. Sexton, R. St. C. Smart, (Eds.), *Surface Analysis Methods in Material Science*, Springer-Verlag, Berlin Heidelberg, Germany, 1993.

116.   I. De´ka´ny, L.G. Nagy, *J. Colloid Interface Sci.* 147 (1991) 119.

117.   X. Jiang, T. Wang, *Applied Surface Science* 252 (2006) 8029.

118.   E. Le Bourhis, G. Patriarche, *Micron* 38 (2007) 377.

119.   C.S. Pande, S. Smith, L.E. Richards, in: G.W. Bailey (Ed.), *Proceedings of 43rd Annual Meeting of Electron Microscopy Society of America*, San Francisco Press Inc., San Francisco, CA, 1985.

120.   J. Liu, G. Rinzler, H. Dai, J.H. Hafner, R.K. Bradley, P.J. Boul, A. Lu, T. Iverson, K. Shelimov, C.B. Huffman, F. Rodrigues-Macias, Y.-S. Shon, T.R. Lee, D.T. Colbert, R.E. Smalley, *Science* 280 (1998) 1253.

121.   B.N. Achar, G.M. Fohlen, J.A. Parker, J. Keshavaya, *Polyhedron* 6 (1987) 1463.

122.   J. Pillay, K. I. Ozoemena (supervisor), BSc. Chem(Hons.) project report, Rhodes University, 2005.

123.   B.A. Boukamp, *Solid State Ionics* 20 (1986) 31.

124.   R.R. Moore, C.E. Banks, R.G. Compton, *Anal. Chem.* 76 (2004) 2677.

125.   Z.-L. Yang, H.-Z Chen, L.Cao, H.-Y. Li, M.Wang, *Mater.Sci.Eng.* B106 (2004) 73.

126.   D.M. Guldi, G.M.A. Rahran, N.Jux, D.Balbinot, U.Hartnagel, N. Tagmatarchi and M.Prato, *J. Am. Chem. Soc.* 127 (2005) 9830.

127.   X. Shi, H. Yang, P. Sun, G. Shao, X. Duan, X. Zhen, *Carbon* (2007), doi: 10.1016/j.carbon.2007.05.006.

128.   A. B. P. Lever, E. R. Milaeva, G. Speier, in: A.P.B. Lever, C.C. Leznoff (Eds.), *Phthalocyanines: Properties and Applications*, vol. 3, VCH Publishers, New York, 1993.

129.   X.-Y. Xiao, S.-G. Sun, *Electrochim. Acta* 45 (2000) 2897.

130. W. Yang, J.J. Gooding, D.B. Hibbert, *J. Electroanal. Chem.* 516 (2001) 10.

131. J.H. Zagal, Coord. *Chem. Rev.* 119 (1992) 89.

132. C.A. Caro, F. Bedioui, J.H. Zagal, *Electrochim. Acta*, 47 (2002) 148.

133. Y.-H. Tse, P. Janda, H. Lam, J.J. Zhang, W.J. Pietro, A.B.P. Lever, J. *Porphyr. Phthalocyanine* 1 (1997) 3.

134. H. Li, T.F. Guarr, *J. Chem. Soc., Chem. Commun.* (1989) 832.

135. A.R. Ozkaya, I. Yilma, O. Bekaroglu, *J. Porphyr. Phthalocya*nine 2 (1998) 483.

136. H. Luo, Z. Shi, N. Li, Z. Gu, Q. Zhuang, *Anal. Chem.* 73 (2001) 915.

137. C. Hu, X. Chen, S. Hu, *J. Electroanal. Chem.* 586 (2006) 77.

138. J. Lim, J. Whitcomb, J. Boyd, J. Varghese, *Journal of Colloid and Interface Science* 305 (2007) 159.

139. E. Laviron, *J. Electroanal. Chem.* 52 (1974) 355.

140. E. Laviron, *J. Electroanal. Chem.* 101 (1979) 19.

141. K.I. Ozoemena, T. Nyokong, *Electrochim. Acta* 51 (2006) 2669.

142. E. Katz, I.Wilner, in: V. M. Mirsky (Ed.), *Ultra thin Electrochemical Chemoand Biosensors Technology and Performance*, Springer-Verlag, NewYork, 2004, p. 68-116 (Chapter 4).

143. D.D. MacDonald, *Electrochim. Acta* 51 (2006) 1376.

144. S. Griveau, J. Pavez, J.H. Zagal, F. Bedoui, *J. Electroanal. Chem.* 497 (2001) 75.

145. L. Yang, Y. Li, Biosens. *Bioelectron.* 20 (2005) 1407.

146. E. Sabatini, I. Rubinstein, *J. Phys. Chem.* 91 (1987) 6663.

147. Y.-C. Yang, L.L. Szafraniec,W.T. Beaudry, D.K. Rohrbaugh, L.R. Procell, J.B. Samuel, *J. Org. Chem.* 61 (1996) 8407.

148. K. Gong, X. Zhu, R. Zhao, S. Xiong, L. Mao, C. Cheng, *Anal. Chem.* 77 (2005) 8158.

149. M.K. Halbert, R.P. Baldwin, *Anal. Chem.* 57 (1985) 591.

150. S. Maree, T. Nyokong, *J. Electroanal. Chem.* 492 (2000) 120.

151. N. Sehlotho, T. Nyokong, *Electrochim. Acta* 51 (2006) 4463.

152. S.M. Golabi, H.R. Zare, *J. Electroanal. Chem.* 465 (1999) 168.

153. J. Zhang, Y.-H. Tse, W.J. Pietro, A.B.P. Lever, *J. Electroanal. Chem.* 406 (1996) 203.

154. J.H. Zagal, M.A. Paez, *Electrochim. Acta* 42 (1997) 3477.

155. L. Niu, T. You, J.Y. Gui, E. Wang, S. Dong, *J. Electroanal. Chem.* l448 (1998) 79.

156. B. Wermeckers, F. Beck, *Electrochim. Acta* 30 (1985) 1491.

157. J.-M. Zen, A.S. Kumar, M.-R. Chang, *Electrochim. Acta* 45 (2000) 1691.

158. J.N. Soderberg, A.C. Co, A.H.C. Sirk, V.I. Birss, *J. Phys. Chem.* B 110 (2006) 10401.

159. P.S. Kumar, V. Lakshminarayanan, *Langmuir* 23 (2007) 1548.

160. S. Majdi, A. Jabbari, H. Heli, A. A. M-Movahedi, *Electrochimica Acta* 52 (2007) 4622.

161. T. Nyokong, S. Vilakazi, *Talanta* 61 (2003) 27.

162. Z. H. Taha, *Talanta* 61 (2003) 3.

163.   C. Wartelle, N.P. Rodrigues, M. Koudelka-Hep, F. Bedioui, *Mater. Sci. Eng.* C26 (2006) 534.

164.   M. Biesaga, K. Pyrzynska, M. Trojanowicz, *Talanta* 51 (2000) 209.

165.   S.-N. Li, Z.-M. Li, M.-B. Yang, Z.-Q. Hu, X.-B. Xu, R. Huang, *Mater. Letts.* 58 (2004) 3967.

166.   S. Tzavalas, V. Drakonakis, D.E. Mouzakis, Dionysis, D. Fischer, V.G. Gregoriou, *Macromolecules* 39 (2006) 9150.

167.   J.Y. Kim, H.S. Park, S.H. Kim, *J. Appl. Polym. Sci.* 103 (2007) 1450.

168.   T.-M. Wu, E.-C. Chen, *Polym. Eng. Sci.* 46 (2006) 1309.

169.   L. Li, C.Y. Li, C. Ni, *J. Am. Chem. Soc.* 128 (2006) 1692.

170.   B.P. Grady, F. Pompeo, R.L. Shambaugh, D.E. Resasco, *J. Phys. Chem.* B. 106 (2002) 5852.

171.   J. Geng, T. Zeng, *J. Am. Chem. Soc.* 128 (2006) 16827.

172.   S.M. Keogh, T.G. Hedderman, M.G. Ruther, F.M. Lyng, E. Gregan, G.F. Farrell, G. Chambers, H.J. Byrne, *J. Phys. Chem.* B109 (2005) 5600.

173.   C.M. López, K.-S. Choi, *Lagmuir* 22 (2006) 10625.

174.   J.Jiang, A. Kucernak, *Synth. Met.* 114 (2000) 209.

175.   R. Rozik, L. Trnková, *J. Electroanal. Chem.* 593 (2006) 247.

APPENDIX A

Peer-Reviewed Articles from this Thesis

1. K.I. Ozoemena, **J. Pillay** and T. Nyokong, "Preferential electrosorption of cobalt (II) tetra-aminophthalocyanine at single-wall carbon nanotubes immobilized on a basal plane pyrolytic graphite electrode", *Electrochem. Commun.* 8 (2006) 1391.

2. **J. Pillay** and K.I. Ozoemena, "Electrochemical properties of surface-confined films of single-walled carbon nanotubes functionalised with cobalt (II) tetra-aminophthalocyanine: Electrocatalysis of sulfhydryl degradation products of V-type nerve agents", *Electrochim. Acta* 52 (2007) 3630.

3. **J. Pillay** and K.I. Ozoemena, "Single-walled carbon nanotube-induced crystallinity on the electropolymeric film of tetra-aminophthalocyaninatonickel (II) complex: Impact on the rate of heterogeneous electron transfer", *Chem. Phys. Lett.* 441 (2007) 72.

4. **J. Pillay** and K.I. Ozoemena, "Efficient electron transport across nickel powder modified basal plane pyrolytic graphite electrode: Sensitive detection of sulfhydryl degradation products of the V-type nerve agents", *Electrochem. Commun.* 2007 in press (doi:10.1016/j.elecom.2007.04.004)

APPENDIX B

Conference Presentations from this Thesis

1. **Jeseelan Pillay** and Kenneth I. Ozoemena, Electrocatalytic and Impedance Spectroscopic Properties of Thin Films of Single-Wall Carbon Nanotubes-Functionalised with Metallophthalocyanine Complexes, 37th International Conference of Coordination Chemistry, Capetown, SOUTH AFRICA, August 13-18, 2006 (Poster Presentation by Mr. Pillay).

2. **Jeseelan Pillay** and Kenneth I. Ozoemena, Electron Transfer At Basal Plane Pyrolytic Graphite Electrodes Modified With Single Wall Carbon Nanotube – Nickel Tetra-Aminophthalocyanine Complex, 38th National Convention of the South African Chemical Institute, Durban, SOUTH AFRICA, December 3-8, 2006 (Oral presentation by Mr. Pillay).

3. Kenneth I. Ozoemena, Msimelelo Siswana, **Jeseelan Pillay**, Tebello Nyokong, Isabelle Fernandes and Michael J. Cook, Unfolding Electrocatalytic Properties of Carbon Nanotube-Metallophthalocyanine (CNT-MPc) Sensing Platforms, 57th Annual Meeting of the International Society of Electrochemistry, Edinburgh, SCOTLAND (UK), August 27 - September 1, 2006 (Oral presentation by Dr. Ozoemena).